

Geochemistry, Geophysics, Geosystems®



RESEARCH ARTICLE

10.1029/2023GC011003

Special Section:

A fresh look at the Caribbean plate geosystems

Active Tectonics, Quaternary Stress Regime Evolution and Seismotectonic Faults in Southern Central Hispaniola: Implications for the Quantitative Seismic Hazard Assessment

J. Escuder-Viruete¹ , F. J. Fernández² , F. Pérez Valera³, and F. McDermott⁴

¹Instituto Geológico y Minero España - CSIC, Madrid, Spain, ²Departamento de Geología, Universidad de Oviedo, Oviedo, Spain, ³Departamento de Ciencias de la Tierra y del Medio Ambiente, Universidad de Alicante, Alicante, Spain, ⁴School of Earth Sciences, University College Dublin, Dublin, Ireland

Key Points:

- Active faults in central southern Hispaniola are controlled by NE-directed shortening
- Quaternary stress regime evolution includes a compressional D1 followed by a strike-slip D2, locally coeval with an extensional D3
- Modeling establishes a very high seismic hazard zone centered in the Ocoa Bay

Supporting Information:

Supporting Information may be found in the online version of this article.

Correspondence to:

J. Escuder-Viruete,
javier.escuder@csic.es

Citation:

Escuder-Viruete, J., Fernández, F. J., Pérez Valera, F., & McDermott, F. (2024). Active tectonics, Quaternary stress regime evolution and seismotectonic faults in southern central Hispaniola: Implications for the quantitative seismic hazard assessment. *Geochemistry, Geophysics, Geosystems*, 25, e2023GC011003. <https://doi.org/10.1029/2023GC011003>

Received 13 APR 2023

Accepted 17 JAN 2024

Author Contributions:

Conceptualization: F. J. Fernández,

F. Pérez Valera

Formal analysis: F. J. Fernández, F. Pérez Valera, F. McDermott

Investigation: F. J. Fernández, F. Pérez Valera, F. McDermott

© 2024 The Authors. *Geochemistry, Geophysics, Geosystems* published by Wiley Periodicals LLC on behalf of American Geophysical Union. This is an open access article under the terms of the [Creative Commons Attribution-NonCommercial-NoDerivs License](https://creativecommons.org/licenses/by/4.0/), which permits use and distribution in any medium, provided the original work is properly cited, the use is non-commercial and no modifications or adaptations are made.

Abstract Present-day convergence between Caribbean and North American plates is accommodated by subduction zones, major active thrusts and strike-slip faults, which are probably the source of the historical large earthquakes on Hispaniola. However, little is known of their geometric and kinematic characteristics, slip rates and seismic activity over time. This information is important to understand the active tectonics in Hispaniola, but it is also crucial to estimate the seismic hazard in the region. Here we show that a relatively constant NE-directed shortening controlled the geometry and kinematics of main active faults in southern central Hispaniola, as well as the evolution of the Quaternary stress regime. This evolution included a pre-Early Pleistocene D1 event of NE-trending compression, which gave rise to the large-scale fold and thrust structure in the Cordillera Central, Peralta Belt, Sierra Martín García and San Juan-Azua basin. This was followed by a near pure strike-slip D2 stress regime, partitioned into the N-S to NE-SW transverse Ocoa-Bonao-La Guácara and Beata Ridge fault zones, as well as subordinate structures in related sub-parallel deformation corridors. Shift to D2 strike-slip deformation was related to indentation of the Beata Ridge in southern Hispaniola from the Early to Middle Pleistocene and continues today. D2 was locally coeval by a more heterogeneous and geographically localized D3 extensional deformation. Defined seismotectonic fault zones divide the region into a set of simplified seismogenic zones as starting point for a seismic hazard modeling. Highest peak ground acceleration values computed in the Ocoa Bay establish a very high seismic hazard.

1. Introduction

The present-day convergence between the Caribbean and North American plates is partially accommodated within Hispaniola Island (Dominican Republic and Haiti). As consequence, this region contains a number of major active faults with lengths of up to several hundred kilometers that stand out as geomorphological and tectonic features (Calais et al., 2016; Hernaiz Huerta & Pérez-Estaún, 2002; Mann et al., 2002; Mann, Draper, & Lewis, 1991) and have been the source of some of the largest earthquakes documented in the past 250 years (Bakun et al., 2012; Calais et al., 2010; Mercier de Lépinay et al., 2011; Prentice et al., 2010). For example, the strike-slip system of the Enriquillo-Plantain Garden Fault Zone (EPGFZ) produced the 12 January 2010 M_w 7.0 Leogâne and 14 August 2012 M_w 7.2 Nippes earthquakes, as well as probably other historical earthquakes in 1770 (estimated M_w 7.5; SISFRANCE-Antilles, 2009) and 1860 (estimated M_w 6.3; Bakun et al., 2012).

The current tectonics in this densely populated and rapidly developing region are broadly understood (e.g., Calais et al., 2016; Corbeau et al., 2016; Escuder-Viruete & Pérez, 2020; Granja Bruña et al., 2014; Hernaiz Huerta & Pérez-Estaún, 2002; Mann et al., 1995, 2002; Pérez-Estaún et al., 2007; Saint Fleur et al., 2019; Wang et al., 2018), with subduction zones, major active thrusts and oblique strike-slip faults identified in several clearly defined zones. However, little is known of detailed geometric and kinematic characteristics, Quaternary offsets and slip rates on these active fault systems, and its seismic activity over time is poorly constrained by geochronological data. This information is essential for understanding the present-day tectonics of Hispaniola, but it is also crucial to establish an inventory of potential seismogenic sources, a seismotectonic zonation model, and an estimate of the seismic hazard in the region.

The focus of this study is threefold: (a) to characterize the active deformation pattern and the main seismotectonic faults in southern central Hispaniola, based on tectonic and geomorphologic field observations, complemented

Methodology: F. J. Fernández, F. Pérez Valera, F. McDermott

with regional gravimetric, magnetic and seismic data analysis; (b) to determine the Quaternary to present-day stress regime evolution by inversion of geologically determined slip vectors on minor and major faults throughout the zone; and (c) to divide the region into a set of simplified seismogenic zones as a starting point for a subsequent quantitative seismic hazard modeling in terms of the peak ground acceleration (PGA).

2. Geological Setting

2.1. From Intra-Oceanic Subduction to Arc-Continent Collision and Subduction Polarity Reversal in the Northern Caribbean Plate

Located on the northern edge of the Caribbean plate, the Hispaniola Island is a tectonic collage produced by the SW-dipping Cretaceous subduction to Eocene oblique collision of the Caribbean intra-oceanic arc with the southern continental margin of North America (Draper et al., 1994; Escuder-Viruete et al., 2013; Escuder-Viruete, Pérez-Estaún, Booth-Rea, & Valverde-Vaquero, 2011; Escuder-Viruete, Pérez-Estaún, Gabites, & Suárez-Rodríguez, 2011; Escuder-Viruete, Suárez, et al., 2016; Mann, Draper, & Lewis, 1991; Pérez-Estaún et al., 2007). The main consequence of the arc-continent collision were the blocking of the suture zone, the transfer of deformation to the back-arc region in southern Hispaniola and subduction polarity reversal, with renewed subduction beginning along a new NE-dipping subduction zone (e.g., Kroehler et al., 2011).

The geodynamic modeling software *GPlates* V2.3 (Müller et al., 2018; www.gplates.org), regional bibliographic data, and observations presented in this paper allows the reconstruction of this relative movement between the Caribbean and North American plates, distinguishing three main stages of evolution from the lower Campanian to the present-day. In the lower Campanian (80 Ma), the Lower Cretaceous Caribbean island-arc is moving to the northeast at a rate of about 4–5 cm/yr (Figure 1a). By this time, the Caribbean arc had overridden the Galapagos hotspot, giving rise to a period of vigorous submarine oceanic plateau volcanism that began as early as 139 Ma and was widespread by 88 Ma, building the Caribbean Large Igneous Province (CLIP). In a SW-dipping subduction zone, the intra-oceanic arc consumed through subduction the large area occupied by the proto-Caribbean oceanic crust in the current central part of the Caribbean, and obliquely collided with the Maya block of the southeastern margin of the North American plate (Mann et al., 2007).

By the middle Eocene (40 Ma) the collision and suturing of the Caribbean island-arc against North America had halted the forward motion of the oceanic arc (Figure 1b). Previous convergence and arc-continent collision caused the extinction of the arc volcanism, the emplacement of supra-subduction zone ophiolites and developed a zone of NE-directed foreland thrusting on the lower plate (Escuder-Viruete et al., 2013; Escuder-Viruete, Suárez, et al., 2016; Mann, Draper, & Lewis, 1991; Pérez-Estaún et al., 2007; Pindell & Kennan, 2009). Because the arc can no longer subduct the more continental crust of North America, convergence was accommodated by back-thrusting and the initiation of a new, NE-dipping subduction zone (Kroehler et al., 2011). In southern Hispaniola, the arc-continent collision in the middle to upper Eocene resulted in a reversal of subduction polarity in the back-arc region, as well as deformation by back-thrusting at the resulting Peralta-Muertos accretionary prism in the upper plate (Dolan et al., 1991; Hernáiz-Huerta & Pérez-Estaún, 2002; Mann, McLaughlin, & Cooper, 1991; Witschard & Dolan, 1990). The new subduction zone separated the Venezuela basin from the upper island-arc crust of central Hispaniola.

Since the lower Miocene, the ENE movement of the Caribbean plate gave rise to the oblique collision/accretion of the northern sector of the Caribbean oceanic plateau of transitional crust with the Peralta accretionary prism, resulting in the formation of the SW-directed Haitian-Neiba fold-and-thrust belt and the San Juan-Azua basins in the foreland (Figure 1c; Dolan et al., 1991; Escuder-Viruete et al., 2023; Granja Bruña et al., 2014; Hernáiz-Huerta & Pérez-Estaún, 2002; Heubeck & Mann, 1991; Mercier de Lépinay, 1987; Pubellier et al., 2000; Witschard & Dolan, 1990). During the Pliocene and until the present-day, convergence gave rise to the accretion of the central sector of the Caribbean oceanic plateau of thickened crust, causing in southern Hispaniola the uplift and folding of the Massif de la Serre-Sierra Bahoruco and the tectonic individualization of the Enriquillo-Cul de Sac basin. The blue star and line in Figure 1c represents the reconstructed location and path of a point of the Sierra Bahoruco as it travels with the Caribbean plate. *GPlates* reconstruction shows that the point started traveling to the NE at a rapid rate of 3–5 cm/yr and changed to a ENE direction in middle Eocene times (45 Ma) with a slow rate of 0.7–2.1 cm/yr. This change coincides with the arc-continent collision in northern Hispaniola and the start of subduction by back-thrusting in the Peralta-Muertos belts of southern Hispaniola.

2.2. Present-Day Geodynamic Configuration of Southern Hispaniola

Oblique collision has also led to the fragmentation of the northern Caribbean plate into several microplates, which are Septentrional (or North Hispaniola), Hispaniola-Puerto Rico and Gonâve (Figure 2; Calais et al., 2016; Mann et al., 1995; Rodríguez-Zurrutero et al., 2019). Microplates are limited by major fault zones that, as reflected by the associated seismicity and modeled displacement rates, accommodate part of the relative movement between them (Benford et al., 2012; Calais et al., 2016; Corbeau et al., 2019; Manaker et al., 2008; Mann et al., 2002; Symithe et al., 2015).

In northern Hispaniola, the Septentrional microplate is a wedge-shaped tectonic forearc sliver, limited offshore to the north by the Northern Hispaniola Fault Zone (NHFZ, or western extension of the Puerto Rico Trench) and onshore to the south by the Septentrional Fault Zone (SFZ; Dolan et al., 1998; Escuder Viruete & Pérez, 2020; Escuder-Viruete et al., 2020; Mann et al., 2002).

The Hispaniola-Puerto Rico microplate is an arc-crust block, limited to the north by the SFZ and to the south by the Muertos Trough (MT). To the west, the boundary between the Hispaniola block and Gonâve microplate is generally placed in the San Juan-Los Pozos fault zone (SJPFZ; e.g., Mann, Draper, & Lewis, 1991, Mann, McLaughlin, & Cooper, 1991). From N to S (Figure 2), the Hispaniola microplate includes the Cordillera Central domain and the Peralta-Muertos deformed belts. The Cordillera Central in the Dominican Republic and its prolongation in the Massif du Nord in Haiti is an Upper Jurassic-Upper Cretaceous basement composed mainly of Pacific-derived oceanic units, structurally limited to the northeast by the Hispaniola fault zone (HFZ) and to the southwest by the SJPFZ (Mann, Draper, & Lewis, 1991, Mann, McLaughlin, & Cooper, 1991). It comprises fragments of oceanic lithosphere, plutono-volcanic complexes related to subduction, and basaltic units related to a mantle-plume magmatism (Escuder-Viruete et al., 2008). It also comprises the Quaternary intramountain basins of Cibao, Jarabacoa, Bonaó, Constanza, Rancho Arriba, and San José de Ocoa (Figure 3).

The Peralta Belt (PB) is a NW-trending and SW-verging fold-and-thrust belt, structurally sandwiched between the San José-Restauración (SJRFZ) and the San Juan-Pozos fault zones (Mann, McLaughlin, & Cooper, 1991). The belt evolved from a back-arc basin for the Caribbean island-arc, with deposition of Campanian to Eocene turbidites (Trois Rivières and Las Palmas Formations), through a transpressive fold-and-thrust belt in the middle Eocene to early Miocene (Dolan et al., 1991; Hernáiz-Huerta et al., 2007a; Mercier de Lépinay, 1987; Ramírez, 1995; Witschard & Dolan, 1990). In the SE sector, the lithostratigraphic units of the PB have been grouped into three thick sedimentary sequences, separated from each other by major unconformities: the Paleocene-Eocene Peralta Group; the middle Eocene-early Miocene Río Ocoa Group; and the middle Miocene-Pleistocene Ingenio Caei Group (Díaz de Neira & Solé Pont, 2002; Dolan et al., 1991; Hernáiz Huerta & Pérez-Estaún, 2002; Hernáiz-Huerta et al., 2007b; Heubeck et al., 1991; Pérez-Valera, 2010).

The MT marks the boundary between the subducting floor of the Caribbean plate and the overlying deformed belt south of eastern Hispaniola and Puerto Rico (Figure 2). The thrust focal mechanism of the 24 June 1984 earthquake (M_w 6.7) indicates subduction along the MT (Byrne et al., 1985). Seismic reflection profiles across the MT image an N-dipping low-angle thrust structure, with folded and faulted sedimentary rocks on top forming an accretionary prism (Dolan et al., 1998; Driscoll & Diebold, 1998; Granja Bruña et al., 2009, 2014; Mauffret & Leroy, 1999). Convergence across the MT probably begins with the end of the arc-continent collision and the onset of back-thrusting. *GPlates* reconstruction shows that the amount of oblique subduction of the Caribbean plate beneath southern Hispaniola at the westernmost Muertos Trench has been about 100 km (Figure 1).

The Gonâve microplate is limited to the north by the Oriente Fault Zone and to the south by the EPGFZ. The nature of the crust of the Gonâve microplate is not well established, having been proposed as a Cretaceous-Eocene remnant arc (Heubeck et al., 1991), back-arc (Mann, Draper, & Lewis, 1991) or the rifted crust of the eastern Cayman continental passive margin (Corbeau et al., 2017, 2019). From the lower Miocene onwards, the oblique collision/accretion processes have formed the Haitian-Neiba belt in the microplate. It consists of a NW-trending and SW-verging fold-and-thrust belt, bounded to the north by the NE-dipping SJPFZ (Hernáiz-Huerta et al., 2007b; Mann et al., 1995; Pubellier et al., 2000; Ramírez, 1995). The thrust bounding the NE Montagnes Noires-Sierra de Neiba thrust sheet was activated during the lower-middle Miocene and the thrust bounding the SW Chaîne des Matheux-southern Sierra de Neiba thrust sheet was developed from the middle-upper Miocene (Pubellier et al., 2000). Tilting and faulting of Quaternary age deposits in the northern margin of the Enriquillo

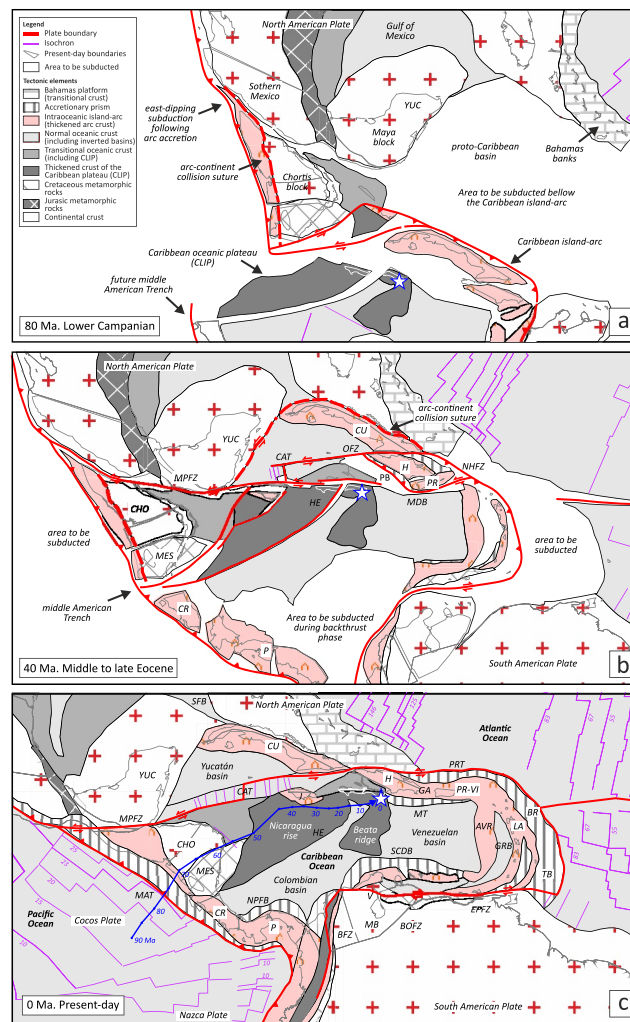


Figure 1. Geodynamic reconstructions made with *Gplates* 2.3.0 software for arc-continent and arc-oceanic plateau collisions in northern and southern Hispaniola, respectively. Different tectonic elements are color coded and described in the key. (a) Reconstruction at 80 Ma (lower Campanian): the large white area in the present-day location of the central Caribbean represents the proto-Caribbean oceanic crust that will be subducted by the NE motion of the intra-oceanic Caribbean island-arc. Dark gray areas represent zones of thickened Caribbean oceanic plateau (CLIP; Caribbean Large Igneous Province). (b) Reconstruction at 40 Ma (middle Eocene): at this time the Caribbean island-arc collided with the southern North American continental margin and is moving eastward. The small white area adjacent to southern Hispaniola will start to subduct due to back-thrusting in the Peralta-Muertos accretionary prism. (c) Present-day: the ENE-directed convergence led to Caribbean plate subduction and Beata Ridge collision in southern central Hispaniola. The blue line represents the path of a point (blue star) on the Sierra Bahoruco in the Caribbean plate since 80 Ma. *Gplates* reconstructions show that the direction of motion of the central Caribbean plate abruptly changes from northeastward to east-northeastward in the middle Eocene. This means that the direction of subduction/collision is highly oblique along the E-W-striking Peralta-Muertos deformed belt in southern Hispaniola. AVR, Aves Ridge; BR, Barbados Prism; BE, Beata Escarpment; BOFZ, Boconó Fault Zone; BOFZ, Bowin Fault Zone; BFZ, Bucaramanga fault zone; CAT, Cayman Trough; CHO, Chortis block; CGFZ, Cerro Golden Fault Zone; CR, Costa Rica; CU, Cuba; EPFZ, El Pilar Fault Zone; EPGFZ, Enriquillo-Platain Garden Fault Zone; GRB, Grenada basin; H, Hispaniola (Dominican Republic and Haiti); HP, Haiti Plateau; HE, Hess Escarpment; HB, Hispaniola Basin; LA, Lesser Antilles; MB, Maracaibo basin; MES, Mesquito terranes; MT, Middle America Trench; MC, Mona Canyon; MP, Mona Passage; MDB, Muertos Deformed Belt; MT, Muertos Trough; MPFZ, Motaguá Polochic fault zone; NHDB, North Hispaniola Deformed Belt; NHFZ, North Hispaniola Fault Zone; NPFZ, Northern Panamá Fold Belt; OFZ, Oriente fault zone; P, Panamá; PB, Peralta Belt; PR, Puerto Rico; PRT, Puerto Rico Trench; SFB, Septentrional Fault Zone; SCDB, South Caribbean Deformed Belt; SFB, South Florida basin; TB, Tobago basin; VDB, Venezuela Deformed Belt; VI, Virgin Islands; YUC, Yucatán block.

basin indicate that the thrust belt is still active (Hernández-Huerta et al., 2007a, 2007b), which is consistent with the seismic activity recorded by Corbeau et al. (2019).

The Beata Ridge is a prominent NE-trending bathymetric high of about 450 km long built on the Caribbean plate (Figure 2a; Granja Bruña et al., 2014; Mauffret & Leroy, 1999; Mauffret et al., 2001). It separates the Haiti basin to the west, from the Venezuelan basin to the east. The width of this structure in the zone of interaction with the Hispaniola-Puerto Rico microplate is about 120 km. The ridge comprises an unusually thick oceanic crust,

essentially made up of mafic igneous rocks (gabbros, dolerites and basalts) of the Cretaceous CLIP (Dürkefälden et al., 2019; Révillon et al., 2000; Sinton et al., 1998). The Cretaceous basement of the Sierra Bahoruco and Hotte-Selle Massifs is made up of submarine volcanic rocks with similar petrological and geochemical characteristics, indicating that the Southern Peninsula of Hispaniola is an emerged fragment of the CLIP (Escuder-Viruete, Joubert, et al., 2016).

Onshore/offshore seismic refraction and wide-angle reflection studies indicate a crustal thickness of 26–32 km in the Sierra Bahoruco, 20–22 km at the Beata Ridge, 10–15 km in the Venezuelan basin and only 5–10 km in the Haitian basin (Kumar et al., 2020; Núñez et al., 2019). The crustal thickness of the Beata Ridge is controlled mainly by NNE to NE-striking faults, such as the Beata Ridge fault zone (BRFZ) that follows its axial trend (Mauffret et al., 2001). According to Granja Bruña et al. (2014), this fault acted in pre-Neogene times as a normal fault. The BRFZ continues to the NE, abruptly limiting the Sierra Bahoruco and Sierra Martín García to the southeast, until it intersects the SJPFZ in the western Ocoa Bay.

The NE-directed collision and impingement of the thickened crust of the Beata Ridge with the Hispaniola microplate in the Neogene gave rise to a recess of the Muertos accretionary prism and the clockwise rotation of fold and thrust structures of the PB east of the Ocoa Bay (Granja Bruña et al., 2014; Hernaiz Huerta & Pérez-Estaún, 2002; Mann, McLaughlin, & Cooper, 1991; Mercier de Lépinay, 1987; Ramírez, 1995). Part of the present-day stress-field induced by the Beata Ridge collision is accommodated by the Ocoa-Bonao-La Guacara Fault Zone (OBFZ) within the Hispaniola microplate (Escuder-Viruete et al., 2023). This fault zone is an active, NNE to NE-striking large-scale fault system that crosses the southern central sector of Hispaniola along more than 250 km (Pérez-Estaún et al., 2007). In the eastern Ocoa Bay, the OBFZ bends the fold and thrust structures of the PB, the SJPFZ and the lower Miocene to Early Pleistocene sedimentary fill of the Azua basin (Figure 2). This fault zone has recently been proposed as the onland transition between oceanic subduction and arc-oceanic plateau collision (Escuder-Viruete et al., 2023).

3. Methodology

3.1. Bathymetric, Gravimetric, and Magnetic Data Sets

Maps shown in this study were created using several topographic and bathymetric data sets: (a) digital elevation models (DEMs) from the Shuttle Radar Topography Mission-30 Plus (<https://www2.jpl.nasa.gov/srtm/>) with a resolution of 30 m (Tozer et al., 2019); (b) DEMs obtained from ALOS Global Digital Surface Model with a resolution of 25 m (Takaku et al., 2020); (c) satellite images from *Google Earth Pro*® (<http://earth.google.com>) with a resolution from 1 km to 10 m; and (d) topographic and bathymetric profiles obtained from the GMRT data-set (available with *GeoMapApp*; www.geomapapp.org; Ryan et al., 2009).

The gravity data are from the compilation by the National Geospatial-Intelligence Agency (<https://www.nga.mil>). This compilation includes data from various campaigns conducted onland between 1939 and 1991 by IFREMER, Royal Astronomical Society, Cambridge University, Lamont-Doherty Geological Observatory and Woods Hole Oceanographic Institution. This compilation contains 3,012 stations with a resolution of ± 2 mGal and a density reduction of 2.67 g/cm^3 .

The magnetic data come from the magnetic and radiometric flight carried out between 1995 and 1997 by the Compagnie Générale de Géophysique (CGG) in the onland territory of the Dominican Republic, with 500 m of separation of lines and a nominal height of 120 m, in the context of the SYSMIN Program of the EU of *Cartografía geotemática de la República Dominicana* (García Lobón & Rey Moral, 2004). Data were gridded at 250 m and several procedures were followed to ensure data quality, such as micro-levelling and filtering of frequencies greater than Nyquist.

3.2. Regional Analysis of Potential Field Data

In this work, lithological, structural, gravimetric and magnetic data were analyzed together to constrain the crustal structure underlying southern central Hispaniola, to establish the distribution of different crustal blocks with specific geophysical properties at the surface and to identify their tectonic boundaries (even when they are hidden by a recent sedimentary cover). The analysis of the potential field data was carried out with the *Geosoft Oasis Montaj*® software. Gravity data has been gridded using a minimum curvature algorithm, resulting a grid cell size of 250×250 m.

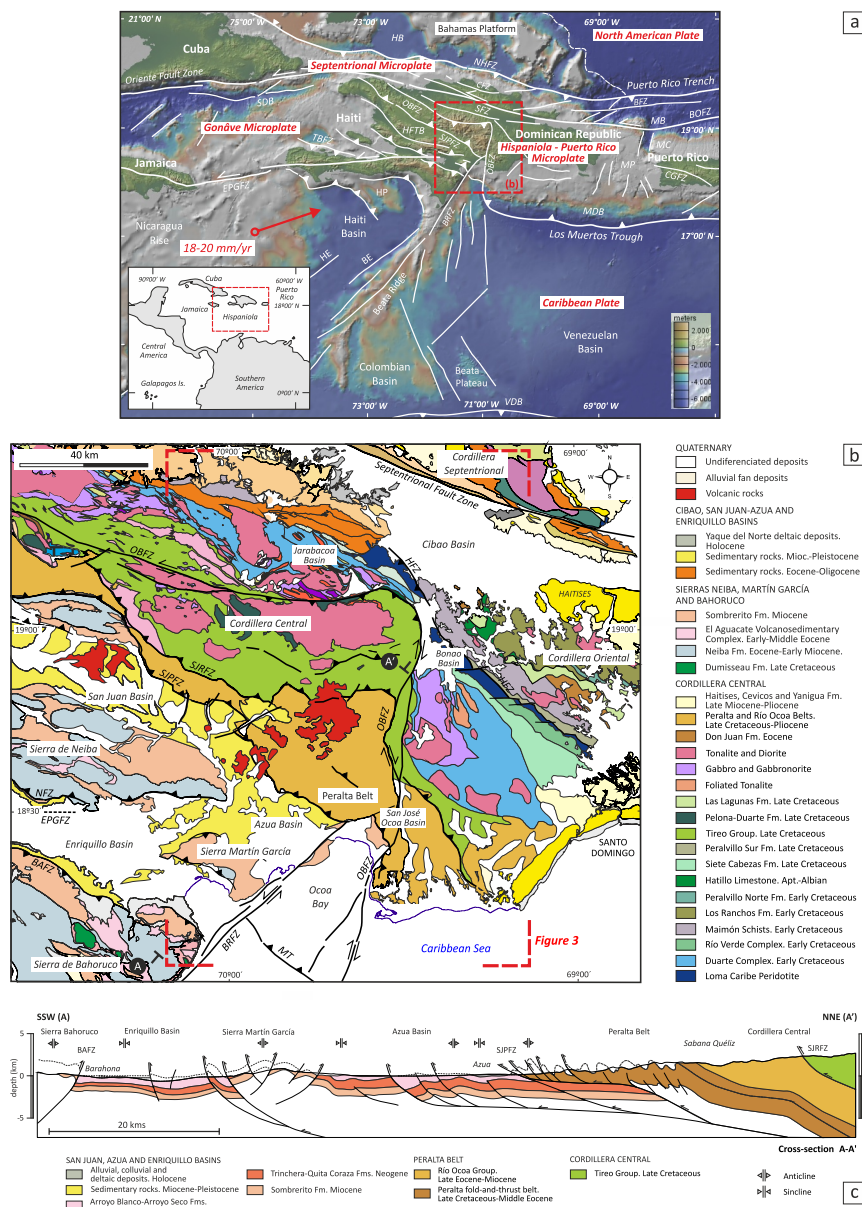


Figure 2. (a) Map of the northeastern margin of the Caribbean Plate showing the location of plate and microplate boundaries, as well as the main tectonic structures. The red arrow defines the movement vector of 18–20 mm/a in the direction N070°E of the Caribbean Plate with respect to the North American Plate (mod. Mann et al., 2002). Relief in color scale has been made from the GMRT synthesis data set (Ryan et al., 2009) with *GeoMapApp* (www.geomapapp.org). The discontinuous red rectangle defines the situation of the study area in the Dominican Republic. (b) Schematic geologic map of southern Hispaniola (mod. from the SYSMIN Project; Pérez-Estaún et al., 2007). The discontinuous red line marks location of Figure 3. (c) Geological cross-section of the study area. The location is shown in (b). Abbreviations as in Figure 1, in addition: CFZ, Camú fault zone; HFTB, Haitian fold-and-thrust belt; OBFZ, Ocoa-Bonao-La Guacara fault zone; SFZ, Septentrional fault zone; SJPFZ, San Juan-Los Pozos fault zone; TBFZ, Trois Baies fault zone.

Magnetic grids were calculated from raw data provided by CGG. Qualitative interpretation of the magnetic data has been made using a reduction technique to the pole of the total magnetic field. This reduction to the pole was calculated assuming a local inclination of 48°N and declination of 10°W. This process removes the inclination effect of the total magnetic field by transforming the anomaly into the vertical component of the field produced as if the source were at the North magnetic pole -90° inclination. The inclination and declination used in the reduction to the pole were calculated from the International Geomagnetic Reference Field subroutine in *Oasis Montaj*® based on the latitude and longitude. Gravimetric and magnetic grids were interpreted on variations in

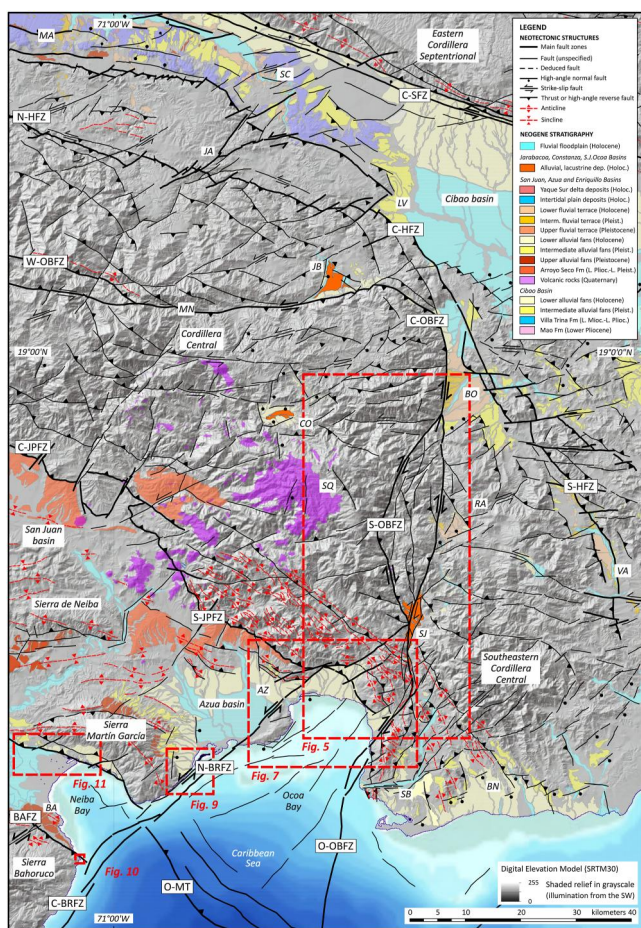


Figure 3. Neotectonic map of southern central Hispaniola. Shaded relief in grayscale has been made from the GMRT synthesis data set (Ryan et al., 2009) with *GeoMapApp* (www.geomapp.org). The neotectonic structures and late Neogene and Quaternary lithostratigraphic units compiled in the map result from integrating new field data with the geologic map obtained by the SYSMIN Project in the Dominican Republic (Pérez-Estaún et al., 2007). The main neotectonic structures are: Offshore (O-OBFZ) and Southern (S-OBFZ) segments of the Ocoa-Bonao-La Guacara fault zone; Central (C-SFZ) segment of the Septentrional fault zone; Southern (S-HFZ), Central (C-HFZ) and Northern (N-HFZ) segments of Hispaniola fault zone; Southern (S-JPFZ) and Central (C-JPFZ) segments of the San Juan-Los Pozos fault zone; and Northern (N-BRFZ) and Central (C-BRFZ) segments of the Beata Ridge fault Zone. Other relevant structures are the Bahoruco fault zone (BAFZ) and the Ocoa segment of the Muertos Trust (O-MT). Abbreviations as in Figure 1, in addition: AZ, Azua; BA, Barahona; BN, Baní; BO, Bonao; CO, Constanza; JA, Jánico; JB, Jarabacoa; LV, La Vega; MA, Mao; MN, Manabao; RA, Rancho Arriba; SB, Sabana Buey; SC, Santiago de los Caballeros; SJ, San José de Ocoa; SQ, Sábana Quéliz; VA, Villa Altigracia.

amplitude, wavelength character, lineament distribution, texture, and structural discontinuities. More details of the methodology of acquisition and analysis of the potential field data are included in García Lobón and Rey Moral (2004), García-Lobón and Ayala (2007), and Ayala et al. (2017).

3.3. Seismicity

Compilation of an earthquake catalog allowed us to determine the spatial and temporal distribution of earthquakes, their relationships with the main active fault zones, and the characterization of the seismotectonic structures in terms of their seismic parameters. For southern central Hispaniola, the catalog was compiled by collecting and analyzing historical data (Bakun et al., 2012; Bertil et al., 2010; Flores et al., 2011; McCann et al., 2011; SISFRANCE-Antilles, 2009; ten Brink et al., 2011; and references herein) and instrumental/experimental data (Alvarez et al., 1999; Russo & Villaseñor, 1995; Tanner & Shepherd, 1997; Terrier-Sedan & Bertil, 2021; ISC 2014; RSPR-Puerto Rico catalogue, and USGC-NEIC catalogue). Access the local network, constituted by the *Instituto Sismológico de la Universidad Autónoma de Santo Domingo* (ISU; uasd.edu.do), the *Observatorio Sismológico Politécnico Loyola* (OSPL; ospl.ipl.edu.do) and the *Projet Ayiti-Seismes* performed by Laboratoire Mixte International CARIBACT (ayiti.unice.fr/ayiti-seismes; BME, UEH/FDS/URGéo, ENS, and Géoazur partnership), enabled information on earthquakes in ghost areas of the global seismic network to be obtained. Following Bertil et al. (2010, 2015), the catalogue was revised for data quality, duplication, and foreshocks or aftershocks, and then homogenized the magnitudes using the moment magnitude scale (M_w). The most contemporary sources describing the historical earthquakes were investigated to establish the focal characteristics of each seismic event.

Due to the high uncertainty related to the magnitude and location of historical earthquakes, the earthquakes in the catalogue were classified into three groups following Terrier-Sedan and Bertil (2021): historical data before 1750 of unreliable magnitude and location; historical data between 1750 and 1960 of intermediate quality; and instrumental data after 1960 generally of high quality. More than 12 epicenters of earthquakes of magnitude at least M_w 6.0 are located in the study area, or the immediate surroundings, including the earthquakes of 1562 (destroyed La Vega and Santiago de los Caballeros), 1615 (destroyed Santo Domingo), 1684 (affected Azua and Santo Domingo), 1691 (destroyed Azua, affected Santo Domingo), 1751 (destroyed Azua) and 1911 (affected San Juan). The catalogue of earthquakes and focal mechanisms compiled for southern central Hispaniola is included in Figure S1 of Supporting Information S1.

3.4. U-Th Geochronology

Fossil coral reefs provide a snapshot of the ocean environment and sea level during their growth. As uranium is incorporated into the coral calcium carbonate skeleton during its growth, the U-Th geochronology method is

appropriate for dating geological and oceanographic events in the Quaternary (e.g., Hibbert et al., 2016). To limit the effects of element mobility during diagenesis and/or any chemical alteration, coral samples were collected in apparently unaltered sectors on top of fossil wave-cut platforms and paleo-cliffs of the topographically lower terraces, as well as on the sides of small narrow gorges cut through the higher terraces. Fragments of corals that preserve the pristine growth structure were selected in the field. Subsequently, thin sections of these fragments were examined under the petrographic microscope to characterize the crystalline habit, the mineralogy as indicated by staining for carbonate minerals, and the degree of neomorphism. Coral fragments with an excellent

preservation of the original skeleton and primary pore spaces void of cement and sediment were selected. Fragments were ground and the resulting powder analyzed by X-ray diffraction analysis at the IGME Laboratories in Madrid. Samples selected for U-Th dating yielded more than 95% aragonite during diffraction analysis. This test eliminated most samples of the topographically higher coral reef terraces.

U-series measurements were carried out using a high-resolution multi-collector inductively coupled plasma mass spectrometer (ThermoFisher Neptune® multi-collector equipped with an Aridus® desolvation nebulizer) at the National Center for Isotope Geochemistry, University College Dublin. Samples were spiked with a mixed ^{229}Th - ^{233}U - ^{236}U spike and were slowly dissolved in 7M HNO_3 . Following overnight sample-spike equilibration, U and Th fractions were separated using anion ion-exchange columns using standard methods (Fankhauser et al., 2016). $^{238}\text{U}/^{236}\text{U}$ and $^{233}\text{U}/^{236}\text{U}$ isotope ratios were measured simultaneously using Faraday collectors, and the lower intensity of the ^{234}U ion beam was measured using a Faraday collector equipped with a low-noise $10^{13}\ \Omega$ resistor. A mass-fractionation correction was applied to the measured uranium and thorium isotope ratios based on the certified near-unity $^{233}\text{U}/^{236}\text{U}$ ratio of the mixed spike (sufficient uranium carry over into the thorium fraction permitted this for all thorium analyses). For thorium, $^{230}\text{Th}/^{232}\text{Th}$ and $^{230}\text{Th}/^{223}\text{Th}$ ratios were measured separately from the uranium runs, using the $10^{13}\ \Omega$ equipped Faraday collector in the axial position for ^{223}Th . A detrital (inherited initial non-radiogenic ^{230}Th) correction was applied to all U-Th analyses, assuming that the inherited component had a ($^{230}\text{Th}/^{232}\text{Th}$) ratio of 0.8 ± 0.4 (parentheses denote activity ratios). Whilst the choice of ($^{230}\text{Th}/^{232}\text{Th}$) for the detrital component is somewhat arbitrary, the calculated ages for all are quite insensitive to this correction (Table S2). All ages were calculated using the following decay constants ($\lambda^{234}\text{U} = 2.826\text{E}-6$, $\lambda^{230}\text{Th} = 9.1577\text{E}-6$, $\lambda^{238}\text{U} = 1.551\text{E}-10$ and $\lambda^{232}\text{Th} = 4.9475\text{E}-11$; Cheng et al., 2000; Jaffey et al., 1971). Laboratory blanks for ^{238}U and ^{232}Th were typically in the 1–10 pg range, and no blank corrections were applied.

3.5. Fault-Slip Data Analysis

Stress or strain can be evaluated using brittle fault-slip data inversion methods (Angelier, 1994). It involves collecting faults data such as plane orientations, fault striae directions and sense of slip from kinematic indicators at the outcrop scale. The methodology of fault-slip data inversion to determine stress fields and to demonstrate temporal and spatial changes in the late Cenozoic stress states has been used in many active tectonic areas around the world over the past three decades (Angelier, 1994; Célérier et al., 2012; Twiss & Unruh, 1998; and references therein). It consists of obtaining from a population of fault-slip data the principal stress axes that best fit the reduced stress tensor at a given measurement site. Inversion results include the orientation (azimuth and plunge) of the principal stress axes ($\sigma_1 > \sigma_2 > \sigma_3$) of a reduced stress tensor as well as the stress ratio $R = (\sigma_2 - \sigma_3 / \sigma_1 - \sigma_3)$, a parameter describing relative stress magnitudes. The stress tensor provides information on the stress regime, that is, compressional (with σ_3 vertical), strike-slip (with σ_2 vertical), transpressional (σ_2 or σ_3 vertical and σ_2 close to σ_3 in magnitude), or extensional (with σ_1 vertical).

Several inversion methods have been proposed in the literature (see reviews by Célérier et al. (2012)). Using multiple methods, hence different algorithms, increases the accuracy of the results by reducing the effect of systematic errors. In this study, the fault-slip data analysis and principal stress axes calculation were first performed with the kinematic right-dihedra method (RDM; Angelier, 1994), which shows the distribution of the percentage of compression or extension dihedra in stereographic projection. Next, fault-slip data were inverted with two independent methods: direct inversion (DIM) and numeric dynamic analysis. All inversion methods were performed with *TectonicsFP* v1.7.9 software of Reiter and Acs (2000) and Ortner et al. (2002). Statistically stable stress tensors were obtained from 10 to 30 fault-slip data measured in each structural site, which have dimensions between 5 and 50 m in length and/or width. A further explanation of the fault-slip data acquisition and analysis is included in Text S3 of Supporting Information S1.

The main goal of the fault-slip data analysis was to characterize the Quaternary to present-day stress regime evolution in southern central Hispaniola. Unfortunately, it is generally challenging to date the striations more precisely than by simply recording that they are younger than the rocks deformed by the faults. For this reason, we include results obtained from fault-slip data measured in igneous and sedimentary rocks of upper Cretaceous to Late Pleistocene age, which were constrained with geochronological data from faulted Middle to Late Pleistocene coral reef terraces and alluvial fan deposits.

On occasions, more than one set of striae are present on a fault plane at the same measurement site, which were formed by different stress tensors. For example, reverse dip-slip and oblique reverse striations caused by an NE-

Table 1
Characteristics of Neotectonic Structures in Southern Central Hispaniola

Deformative event	Main structures	Stress regime	Age
D1	NW to WNW-striking folds and thrusts. Large-scale structure of the Cordillera Central and Peralta belt	Compression. NE-trending σ_1 axis	Lower Miocene to Early Pleistocene
D2	N-S to NE-SW strike-slip faults and fault segment. Transverse structures related to Ocoa-Bonao-La Guácara and Beata Ridge fault zones. ENE to E-striking left-lateral strike-slip faults. Transverse structures in the NW sector	Near pure strike-slip. NE-trending σ_1 axis	Early-Middle Pleistocene to Holocene
D3	Extensional faults. D3a, NE to NNE striking faults in the Cordillera Central sector; D3b, WNW to W striking faults in the Ocoa Bay sector. Alignment of the Quaternary emissive centers	D3a, NW-directed pure extension; D3b, N to NNE-directed extension	Late Pleistocene-Holocene

trending compression are crosscut by low-pitch angle striations resulting from a NE-trending σ_1 strike-slip stress regime. The discrimination of striae belonging to each fault set was conducted by numerical checking of compatibility with an inversion method and geological arguments. Fault crosscutting relationships, the overprinting of several striations in the same fault plane and the absolute age of the faulted rocks have also been used as geological criteria to date faults and thus discriminate paleostress tensors and tectonic events.

4. Neotectonics of Southern Central Hispaniola

4.1. Large-Scale Structures

The geology of southern central Hispaniola consists of five main elements: (a) an Upper Jurassic to Upper Cretaceous igneous and metamorphic basement of the Cordillera Central domain; (b) a group of latest Cretaceous-lower Eocene sedimentary rocks of the Peralta fold-and-thrust belt, that locally unconformable overlie the basement; (c) an unconformable cover of folded and faulted middle Eocene to lower Miocene sedimentary rocks of the Rio Ocoa Group; (d) a sequence of slightly faulted and tilted Neogene sediments of the San Juan-Azua and Enriquillo basins; and (e) an unconformable cover of Quaternary alluvial, fluvial and shallow marine deposits. The spatial distribution of these elements is included in the geological map and cross-sections of Figure 2.

The neotectonic structures of southern central Hispaniola are compiled in the map of Figure 3, which results from integrating of new field data with the geologic map obtained by the SYSMIN Project in the Dominican Republic (Pérez-Estaún et al., 2007). This map covers the eastern half of the Cordillera Central, the Sierra Martín García, the southeastern part of the San Juan basin and the whole Azua basin including the Baní pediment. This fieldwork area was selected because contains the main active structures of the arc-plateau collision in the southern Dominican Republic.

The neotectonic structures of this area show three main trends: NW to WNW-striking folds and thrusts; N to NE-striking right-lateral strike-slip faults; and ENE to E-striking left-lateral strike-slip faults. Combined detailed structural analysis, fault-slip data inversion, and geochronology show that these structures were generated during three main tectonic events (Table 1). The NW to WNW-trending D1 structures are parallel to the structural grain of the Cordillera Central, as the folds and thrusts of the PB. Located in the southern and eastern parts of the study area, the N-S to NE-SW transverse D2 structures are the strike-slip fault segments of the Ocoa-Bonao-La Guácara and Beata Ridge fault zones, as well as second-order structural elements of the related sub-parallel deformation corridors. The ENE to E-striking faults are also transverse D2 structures concentrated in the northwestern sector of the studied area, which also deform the boundary with the Cibao basin. The previous structures appear locally cut by two families of D3 extensional faults, which have a different trend depending on their geographic location: WNW to W in the Ocoa Bay sector; and NE in the Cordillera Central sector.

The Ocoa-Bonao-La Guácara fault zone represents the structural transition between the Muertos oceanic accretionary prism and the Beata Ridge-Peralta Belt collision zone (Figure 3; Escuder-Viruet et al., 2023). This fault runs along a N to NNE-striking band, 2–12 km wide and 120 km long, extending from the western termination of the MT in the south to the Cibao basin in the north. Northward, the fault zone connects to the HFZ

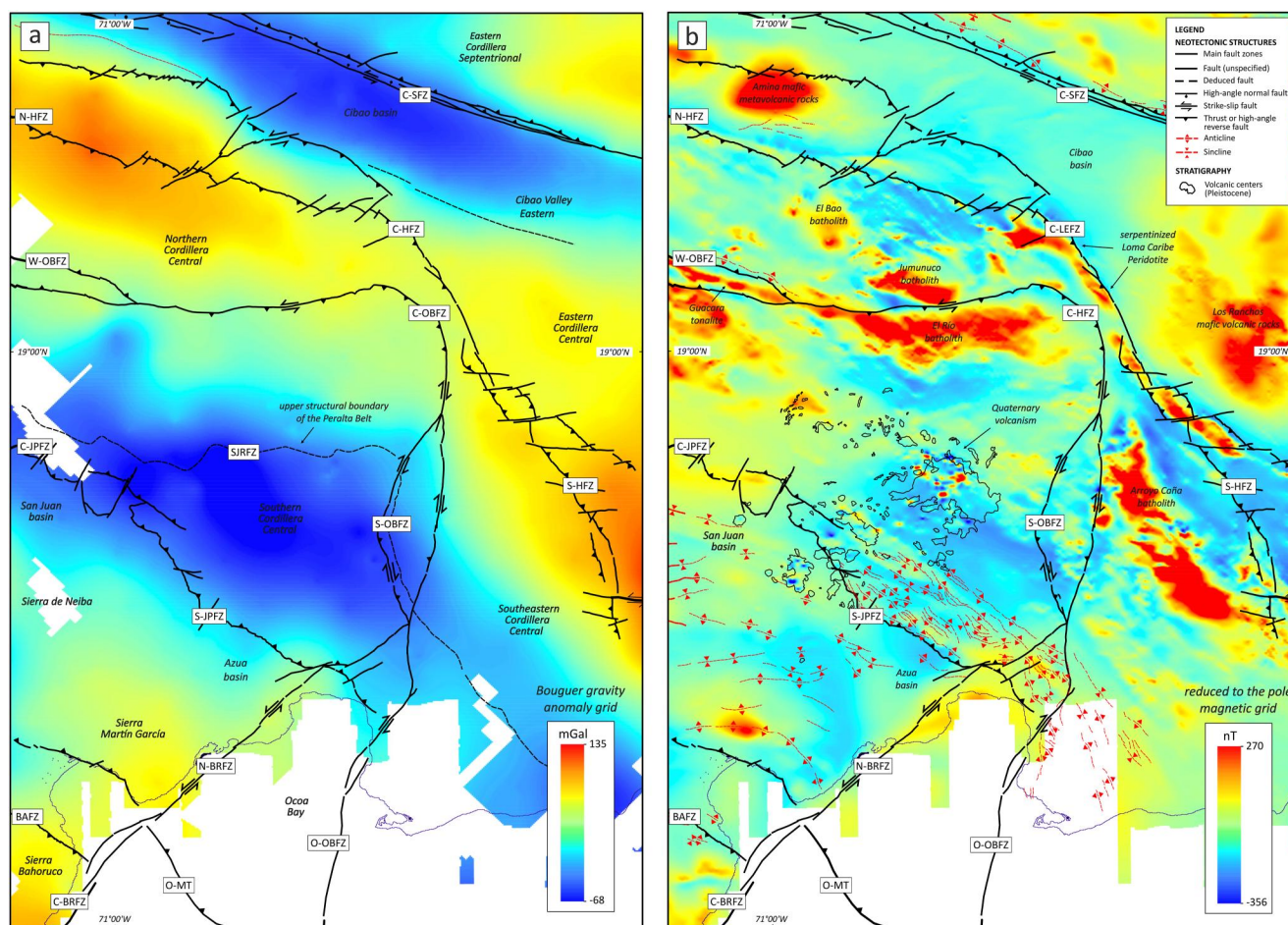


Figure 4. (a) Bouguer gravity anomaly map of southern central Hispaniola showing major tectonic features delineated by sharp gravity gradients (source of gravity data: <https://www.nga.mil>). Areas of exposed or shallow igneous and metamorphic basement of Cretaceous age in the northern Cordillera Central and Sierra Bahoruco show higher anomalies (red to yellow tones), whereas areas with high sediment accumulation in the Cibao, San Juan and Azua basins are expressed by low anomalies (dark to light blue tones). (b) Reduced to the pole magnetic pole map showing major lithologic and tectonic features of southern central Hispaniola (mod. from García Lobón and Rey Moral (2004) and Ayala et al. (2017)). The reduction to the pole of the whole magnetic field improves the spatial position of anomalies that help to define areas with long and short wavelengths, regional trends and tectonic boundaries between magnetic provinces. See explanation in the text.

and changes its trend, curving from N-S to W-E over a distance of ~30 km. Based on discontinuities in its trace (such as step-overs, relays and bends), the fault zone comprises four major segments which are, from south to north (Figure 3): Offshore (O-OBFZ), Southern (S-OBFZ), Central (C-OBFZ) and Western (W-OBFZ). These active segments are variably oblique with respect to the regional convergence direction and, therefore, they exhibit strike-slip, oblique reverse and thrust fault movements. Along the eastern margin of Ocoa Bay, the O-OBFZ segment produces offshore a clockwise rotation of the folded sediments of the Muertos accretionary prism, and bends and deforms onshore the fold and thrust structures of the PB, the SJPFZ, the sedimentary fill of the Azua basin and the Late Pleistocene to Holocene alluvial fans (Escuder-Viruet et al., 2023).

The BRFZ is part of the Beata Ridge. Mauffret and Leroy (1999) and Mauffret et al. (2001) suggested that the BRFZ is a recent major NE-striking right-lateral strike-slip fault that limits the Beata Ridge to the west and would continue to the NE along the Beata Ridge summit and the eastern termination of the Sierra Bahoruco. On the basis of swath bathymetry and offshore seismic reflection data (Granja Bruña et al., 2014), the northern part of the BRFZ can be divided in two fault segments which are, from south to north (Figure 3): Central (C-BRFZ) and Northern (N-BRFZ). The N-BRFZ segment shows a constant NE-SW trend along 55 km, parallel to the east coast of the Sierra Bahoruco and Martín García and extends onland through the Azua Basin. The linearity of the fault segment indicates that it is a nearly vertical structure that accommodates a predominantly strike-slip displacement. Field data obtained in onland sub-parallel faults (see below) indicate a left-lateral strike-slip displacement

characterizes the N-BRFZ. This fault segment cuts the post-middle Miocene macrostructure of NW-trending folds in the Sierra Bahoruco and Martín García, as well as the post-Early Pleistocene folds and thrusts that deform the Arroyo Seco Formation in the Azua Basin. This segment connects at its northern end with the OBFZ.

4.2. Regional Gravimetric Data

The regional pattern of the Bouguer anomaly reflects the main lithological and structural characteristics of southern central Hispaniola (Figure 4), even though the distribution of the stations of gravity data is sparse and the used grid cell size is 250×250 m. Areas with positive anomalies ranging from 40 to 134 mGal (yellow and orange tones) are present in the northern and eastern sectors of the Cordillera Central, the northern sector of Sierra Bahoruco, Sierra Martín García and the western Ocoa Bay, as well as the eastern Cordillera Septentrional. These anomalies have a general NW-SE to WNW-ESE trend and are interpreted as areas of variably thickened island arc crust of mafic to intermediate composition, with average densities around 2.95 g/cm^3 (Ayala et al., 2017). Varying textures of the gravity field within these areas include smooth parallel lineaments associated with bands of foliated amphibolites, elongated gabbro-dioritic batholiths and CLIP-related basaltic units of the Upper Cretaceous basement. In contrast, long wavelength gravity anomalies between -60 and 14 mGal (dark and light blue tones) characterize the Cibao basin, the southern sector of the Cordillera Central (PB) and the San Juan-Azua basin. These areas comprise siliclastic and carbonate rocks of the late Cenozoic sedimentary cover, with average densities around 2.55 g/cm^3 (Ayala et al., 2017). These negative anomalies present a smooth texture and are elongated in the NW-SE to WNW-ESE direction, subparallel to the positive anomalies of the Cretaceous basement.

Therefore, the regional gravity field defines an alternance of NW to WNW-striking long wavelength anomalies, reflecting the contrast between the high-density Cretaceous igneous and metamorphic basement of the northern Cordillera Central and the low-density Cenozoic sedimentary rocks of the southern Cordillera Central, Cibao and San Juan-Azua basins (Figure 4). The positive gravity anomaly of the Cordillera Central is disturbed by intermediate anomalies between 20 and 50 mGal (light green tones), along the arcuate trace of the Ocoa-Bonao-La Guacara fault zone. This pattern seems to reflect a NE-directed thick-skinned thrust structure in the basement, composed of tonalitic batholiths and intermediate volcanic rocks of the Tiroo Group, over the Cibao and Bonao sedimentary basins.

The northern boundary of the Cibao Basin is linear and defined by a steep gradient in the gravity field toward the positive anomaly of the eastern Cordillera Septentrional, coinciding with the surface trace of the Septentrional fault zone. The southern limit of the Cibao basin with the Cordillera Central is also marked by a strong gradient and coincide with the northern branch of the HFZ. In turn, the southern boundary of the San Juan-Azua basin is marked by a transition toward a NE-striking long wavelength positive gravity anomaly, which suggests the existence of high-density basaltic rocks of the CLIP forming the basement of the Sierra Bahoruco, the Sierra Martín García and the Ocoa Bay.

4.3. Regional Magnetic Data

The large-scale structure of southern central Hispaniola can be deduced by the orientation of the regional magnetic field in NW to WNW-trending subparallel bands, which are often characterized by a distinctive textural pattern (Ayala et al., 2017). In the reduced to the pole grid (Figure 4a), short-wavelength magnetic signatures generally correspond to areas where the magnetic sources in the basement are located close to the surface. These areas are characterized by a pattern of NW to WNW-trending sub-parallel anomalies, related to the late Cretaceous regional structure of amphibolites, gabbro-tonalitic batholiths and ridges of basalts in the Cordillera Central. The strong ferromagnetic character of the gabbros produces positive anomalies between 100 and 250 nT, which delineate the intrusive contact of the Arroyo Caña, Jumunuco, and El Río batholiths. In the eastern Cordillera Central, the HFZ defines a strong NW-trending positive magnetic anomaly between 150 and 270 nT, separating the Loma Caribe Peridotite outcrops and the mafic volcanic rocks of the Los Ranchos Formation. This strong anomaly is related to the titanomagnetite growth during serpentinization by tectonic exhumation and surficial alteration of the peridotites in the late Cenozoic. A part of the southern Cordillera Central is characterized by scattered short-wavelength anomalies, roughly elongated along a NE-SW trend and related to the extrusion of mafic to intermediate calc-alkaline to alkaline volcanic rocks during the Quaternary.

By contrast, long-wavelength magnetic signatures correspond to areas where the magnetic source is located farther from the surface, or where the magnetic rock intensity in the basement is weak. In the reduced to the pole grid (Figure 4b), the Cibao and San Juan-Azua sedimentary basins generally display long-wavelength negative magnetic anomalies between -10 and -350 nT. These negative anomalies are related to the 1 to 5 km-thick overburden of paramagnetic sediments that fill these basins and reduces the basement magnetic intensity. In turn, the pattern of NW-striking negative magnetic anomalies that characterize the southern sector of the Cordillera Central is associated with the fold and thrust structure of the PB sedimentary rocks. Nevertheless, the sedimentary carbonate massifs of the Sierra Bahoruco, Sierra Martín García, and coastal sectors of the Ocoa Bay shows long-wavelengths of relatively high magnetic intensity between 0 and 100 nT, suggesting a magnetic source that is shallower than the surrounding areas. A possible explanation for this high magnetic intensity is that the basement in these areas comprises magnetite-rich basalts typical of the late Cretaceous CLIP.

In general, the main magnetic discontinuities in the reduced to the pole magnetic grid correlate well with the large-scale fault zones and the regional macrostructure of southern central Hispaniola (Figure 4b). These discontinuities juxtapose areas of long and short-wavelength magnetic anomalies and define tectonic blocks bounded by the segments of the Septentrional, Hispaniola, Ocoa-Bonao-La Guácara and Beata Ridge fault zones (Figure 4b). In detail, low magnetic values mark the surface trace of the main fault zones, suggesting that the deformed fault rocks are partially demagnetized. The reduced to the pole magnetic grid also shows the truncation and displacement of the NW to WNW-striking D1 structures in the Cordillera Central by the transverse D2 strike-slip fault system of the Ocoa-Bonao-La Guácara fault zone.

4.4. Late Neogene and Quaternary Lithostratigraphy

In southern central Hispaniola, neotectonic activity is recorded by the sedimentary fill of the San Juan-Azua and Enriquillo basins, and by the growing of a system of coral reef terraces overlain by alluvial fans. The San Juan-Azua and Enriquillo basins have been defined as syn-tectonic flexural basins limited to the NE by SW-verging thrust systems, although the Enriquillo basin is also limited by opposite-vergence thrusts directed to the NE (Díaz de Neira, 2004; Hernáiz Huerta & Pérez-Estaún, 2002; Hernáiz-Huerta et al., 2007a; Mann et al., 1995; Mann, McLaughlin, & Cooper, 1991). These basins form the southeastern extension of the Plateau Central and Cul-de-Sac basins in Haiti (Pubellier et al., 2000). The basins are filled by a ~ 4 km-thick upward shallowing and coarsening mega-sequence composed of Miocene to Early Pleistocene marine sediments (Díaz de Neira & Solé Pont, 2002; McLaughlin et al., 1991; Pérez-Valera, 2010).

The megasequence includes initial sedimentation on a regionally extensive open marine carbonate platform in the lower to middle Miocene (Sombrerito Formation). The deposition of turbiditic-type clastic sediments in a deep marine environment occurred in the middle to upper Miocene (Trinchera Formation) and in a shallow-water platform in the lower Pliocene (Quita Coraza Formation). The regressive character of sedimentation gave rise in the Pliocene to shallow-marine clastic and coral reef deposits (Arroyo Blanco Formation) and, in the Enriquillo basin, the deposition of halite and gypsum evaporites (Angostura Formation), and fine-grained clastic sediments of a bay with excess salinity (Las Salinas Formation). The change to continental deposition took place in the late Pliocene-Early Pleistocene in the Azua basin, with the sedimentation of coarse-grained clastic sediments (Arroyo Seco Formation), and in the Early-Middle Pleistocene in the Enriquillo basin, with an upward change from reef limestones and supralittoral marls to alluvial-fan breccias and conglomerates (Jimaní Formation).

From the uppermost Pliocene, tectonic indentation of the southern margin of Hispaniola by northeastward displacement of the Beata Ridge (Hernaiz Huerta & Pérez-Estaún, 2002; Heubeck & Mann, 1991; Mann, McLaughlin, & Cooper, 1991; Ramírez, 1995), destroyed the foreland configuration developed in the southern margin, uplift and erosion of the Cordillera Central and emergence of the Azua and Enriquillo basins. After a sedimentary hiatus, uplift is recorded by the formation and progressive elevation of coral reef terraces in the southernmost coastal area during the Middle to Late Pleistocene. These coral terraces were probably organized in a staircase marine terrace system, which has only been partially preserved by later erosion and tectonics (see below).

Continued uplift and erosion were also accompanied by syn-tectonic sedimentation of coarse-grained alluvial fan systems directed toward Ocoa Bay (Díaz de Neira, 2000; Pérez-Valera, 2010). Recently, three alluvial fans systems developed at different topographic levels have been distinguished on the southern slope of the Cordillera Central during the Late Pleistocene to the Holocene (Figure 3; Escuder-Viruete et al., 2023). The upper alluvial fan system forms small relict plateaus inclined toward the S and SE, over the surface of the intermediate alluvial

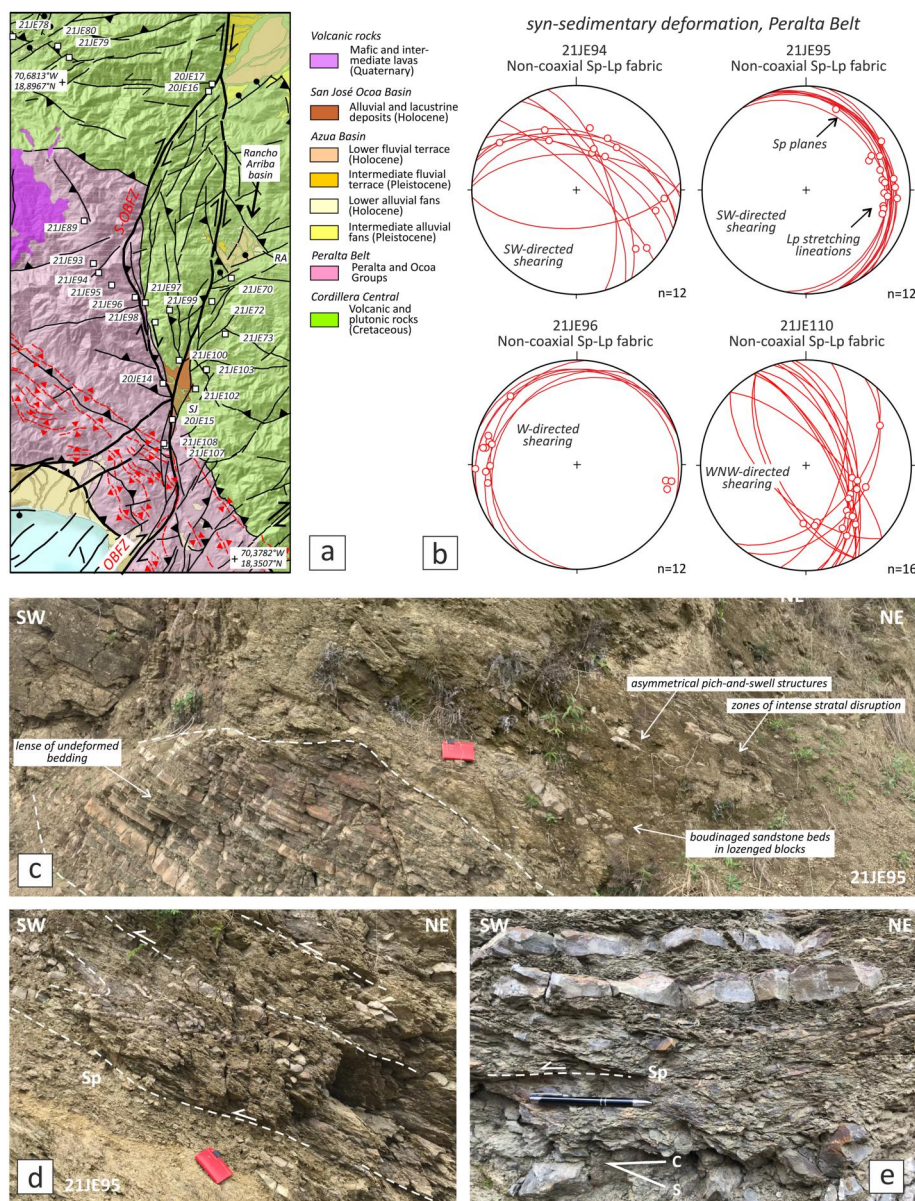


Figure 5. Structural analysis of the Peralta Belt (PB). (a) Structural map of the eastern PB in southern central Hispaniola (see location in Figure 3), showing the tectonic domains, main Quaternary lithostratigraphic units, neotectonic structures, and sites of fault-slip data measurements. OBFZ, Ocoa-Bonao-La Guacara fault zone; SJ, San José de Ocoa intramountain basin; RA, Rancho Arriba intramountain basin. (b) Stereoplots of the non-coaxial Sp-Lp fabric produced by syn-sedimentary deformation during the upper Eocene in the Peralta and Ocoa Groups. (c) Field aspect of the syn-sedimentary deformation developed heterogeneously in the turbidites of the Ocoa Group, characterized by boudinage of sandstone beds, tight to isoclinal folds with rootless limbs, and a pervasive scaly clay fabric (Sp) in mudstone interbeds. (d) Zone of stratal disruption in the Ocoa Group, characterized by boudinage of sandstone beds, tight to isoclinal folds with rootless limbs, and a pervasive scaly clay fabric (Sp) in mudstone interbeds. (e) Detail of the boudinaged sandstone beds and the S-C structures in the mudstones.

fan system. The intermediate alluvial fan system forms a more extensive and better-preserved deposit, which connects the foot of the Cordillera Central relief with the southern coast. The current lower alluvial fan system is spatially restricted to the Sabana Buey valley and small coastal plains of southwestern Baní (Figure 3). Its incision in the intermediate alluvial fans implies a change in the geometry of the drainage network, which has been attributed to fluvial capture processes (Díaz de Neira, 2000; Pérez-Valera, 2010), triggered by the activity of the OBFZ (Escuder-Viruete et al., 2023).

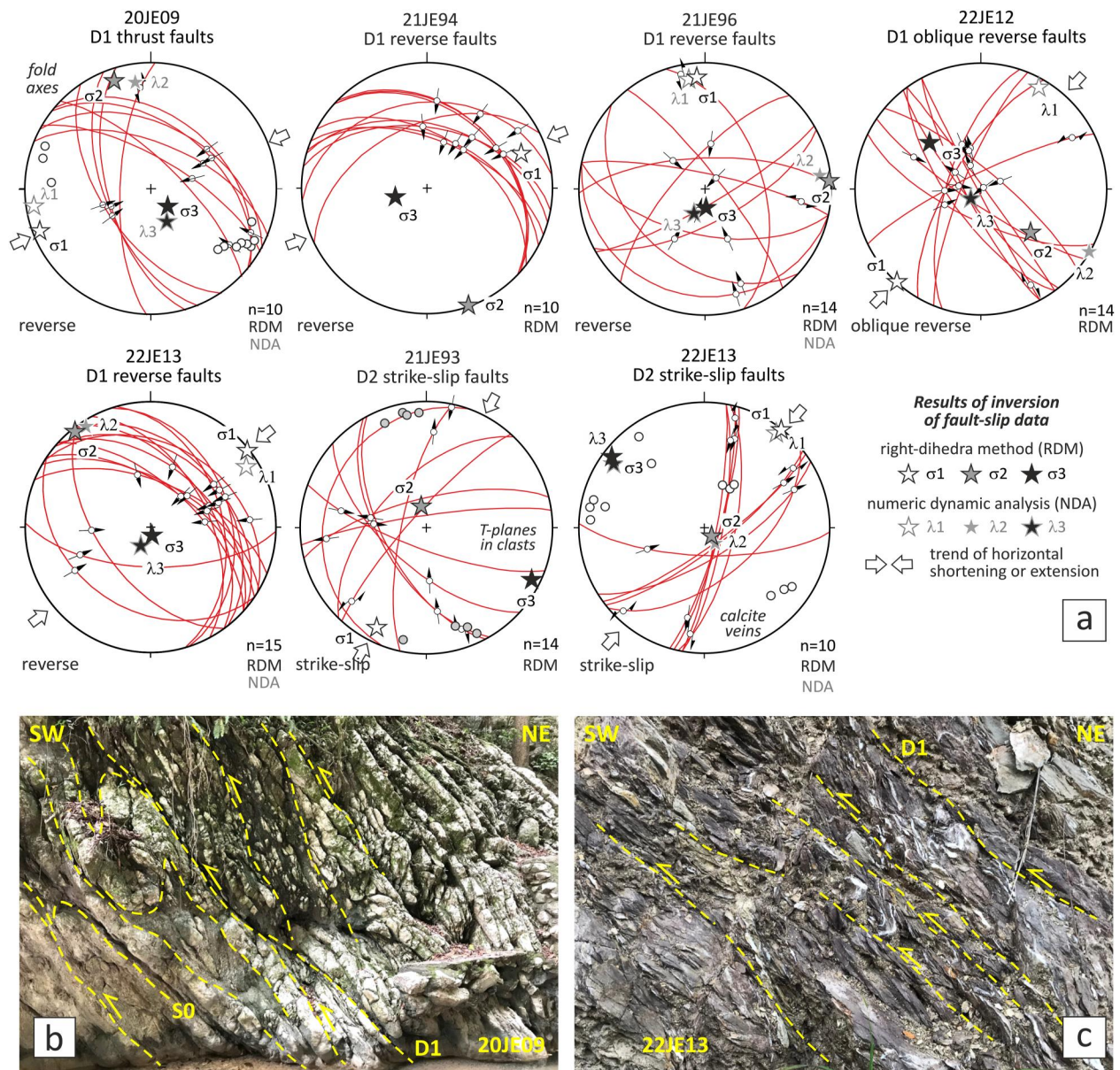


Figure 6. Structural analysis of the Peralta Belt. (a) Stereoplots of the principal stress axes obtained from inversion of fault-slip data. *n*, number of data. Inversion methods: PTM, P-T Method; RDM, Right Dihedra Method; DIM, Direct Inversion Method; and NDA, Numerical Dynamic Analysis Method. (b) Asymmetric D1 folds of SW vergence, associated with mid-dip angle reverse faults, developed in the limestones of the lower Miocene Sobrerito Formation. (c) D1 reverse faults cutting the block-in-matrix fabric (Sp) and calcite veins in the Peralta Group.

5. Fault-Slip Data Inversion and Late Cenozoic Stress Regimes

This work calculated stress tensors from a population of 562 fault-slip data, measured in 32 sites covering an area of approximately $100 \times 50 \text{ km}^2$ in southern central Hispaniola. Geological characteristics of these sites are reported in Table S4. Stress inversion of the fault-slip data yields 44 stress tensors and their respective plots are shown in Figures 5–14. The orientation of their maximum horizontal stress, stress regime, kinematic type of faults and the immersion method used in each site, which are generally consistent with each other, are included in Table S5.

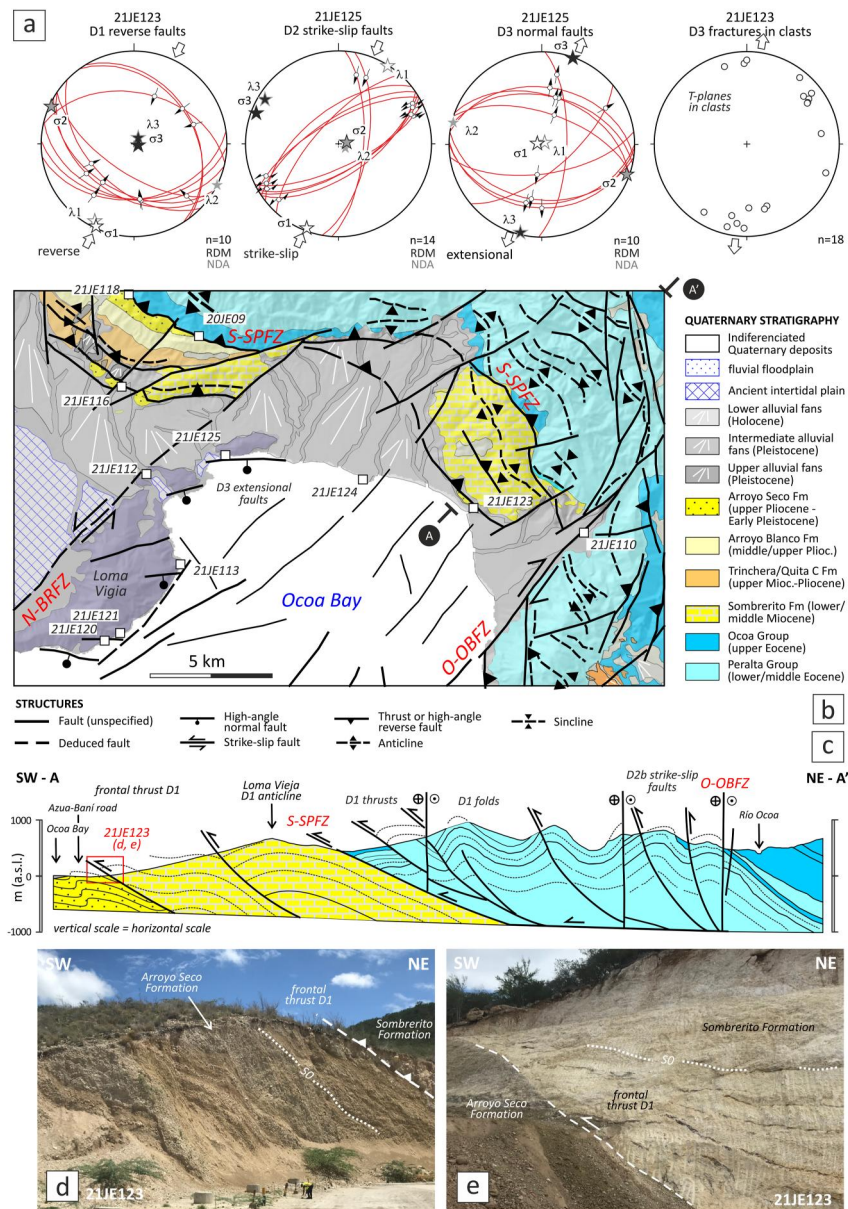


Figure 7. Structural analysis of the Peralta Belt (PB). (a) Stereoplots of the principal stress-axes obtained from inversion of fault-slip data. (b) Structural map of the northern Ocoa Bay in southern central Hispaniola (see location in Figure 3), showing main lithostratigraphic units, neotectonic structures, and sites of fault-slip data measurements. (c) Geological cross-section of the frontal part of the PB. (d and e) Field aspect of the Loma Vieja frontal thrust (site 21JE123, see location in the cross-section), where the lower to middle Miocene limestones of the Sombrerito Formation overthrust the conglomerates of the late Pliocene to lower Pleistocene Arroyo Seco Formation. Acronyms as in Figure 3.

5.1. Fault-Slip Data Inversion in the Peralta Belt

Sites 21JE94, 21JE95 and 21JE96 are located along the highway between San José de Ocoa and Nizao, within the PB (Figure 5). Both the mudstone-rich siliciclastic rocks of the lower Eocene Peralta Group and the turbiditic sediments and conglomerates of the late Eocene Ocoa Group exhibit 1 to 100 m-thick zones of intense stratal disruption, which were interpreted by Witschard and Dolan (1990) as thrust surfaces formed during the late Eocene in the Peralta accretionary prism. Disrupted zones are mesoscopically characterized by boudinaged sandstone beds and pich-and-swell structures defining lozenged blocks. Mudstone interbeds and argillaceous cataclastic bands have a WNW to NW-striking pervasive scaly clay fabric (Sp) and occasionally contain tight to isoclinal folds with rootless limbs (Figure 5). The planar fabric (Sp) often contains a N to NE-trending calcite

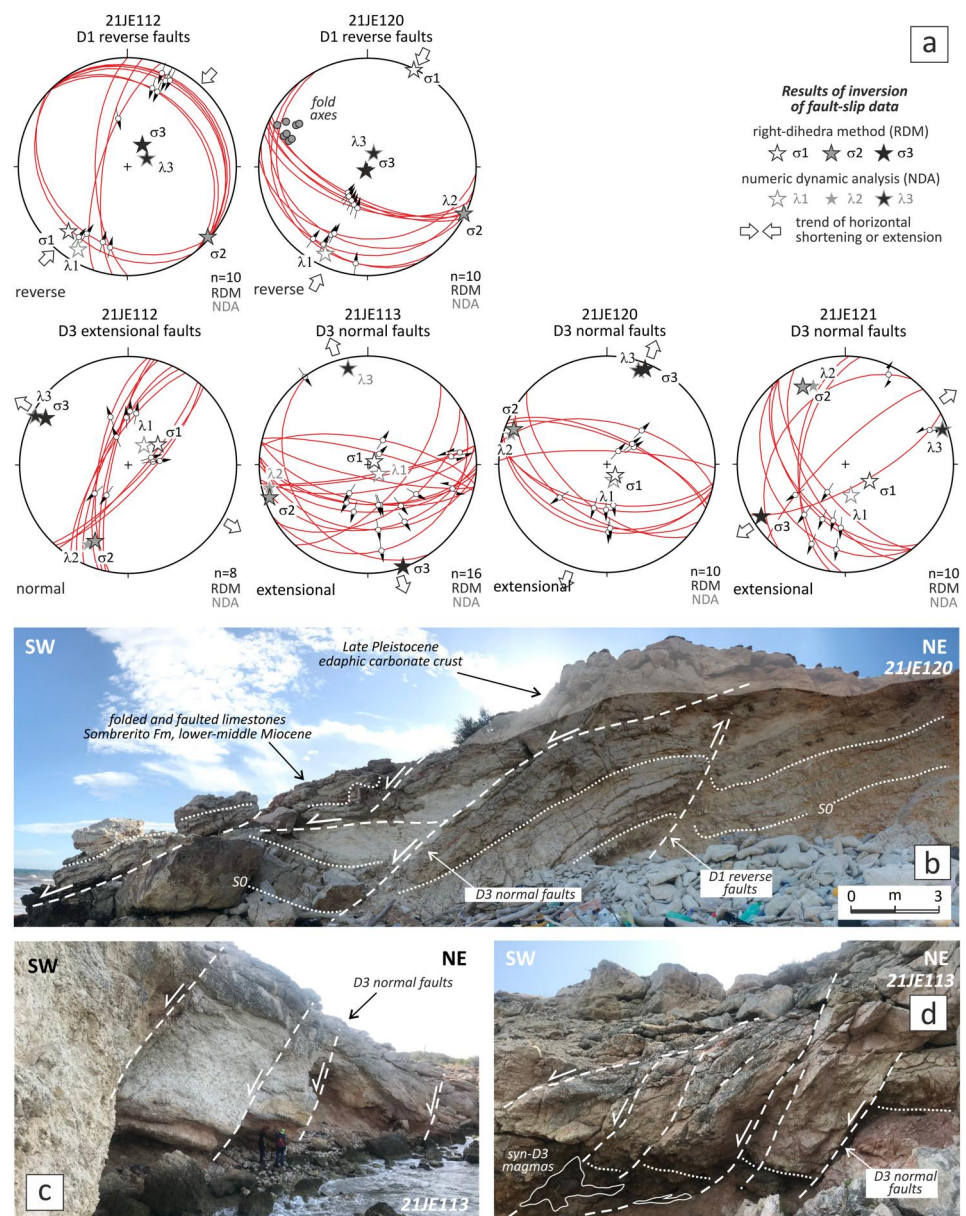


Figure 8. Structural analysis in the Loma Vigia sector of the Ocoa Bay. (a) Stereoplots of the principal stress axes obtained from inversion of fault-slip data. (b) D1 fold and reverse fault truncated by D3 normal faults, dragging the limestone layers in the hanging-wall block to the SW (site 21JE120). (c and d) Limestone beds of the Sombrito Formation displaced by a system of ENE to E-striking normal faults along whose planes intrude locally mafic magmas (site 21JE113).

stretching lineation (L_p) subparallel to the fold axes. In this Sp - L_p fabric, kinematic indicators such as the asymmetry of the boudins or the S - C structures establish a general top-to-the W and SW shear sense. All these structures are typical of a block-in-matrix fabric of a mélangé, essentially produced by syn-sedimentary deformation during the Late Eocene (see below). Stratally disrupted zones in the Ocoa Group rocks are cut by WNW-striking D1 thrust surfaces that typically dip 5° – 30° more deeply than the Sp fabric, when they are restored to the original horizontal position. Both the block-in-matrix fabric and the thrusts are cut by NNW to NE-striking strike-slip faults D2 and by high-dip angle normal faults D3 (Figure 6).

The inversion of fault-slip data collected in several localidades throughout the PB enables the separation of populations related to three distinct stress regimes (Figure 6). The first population is represented by variably oblique reverse slip vectors in NW-striking and NE-dipping faults (sites 20JE09, 21JE94, 22JE12 in Yayas de

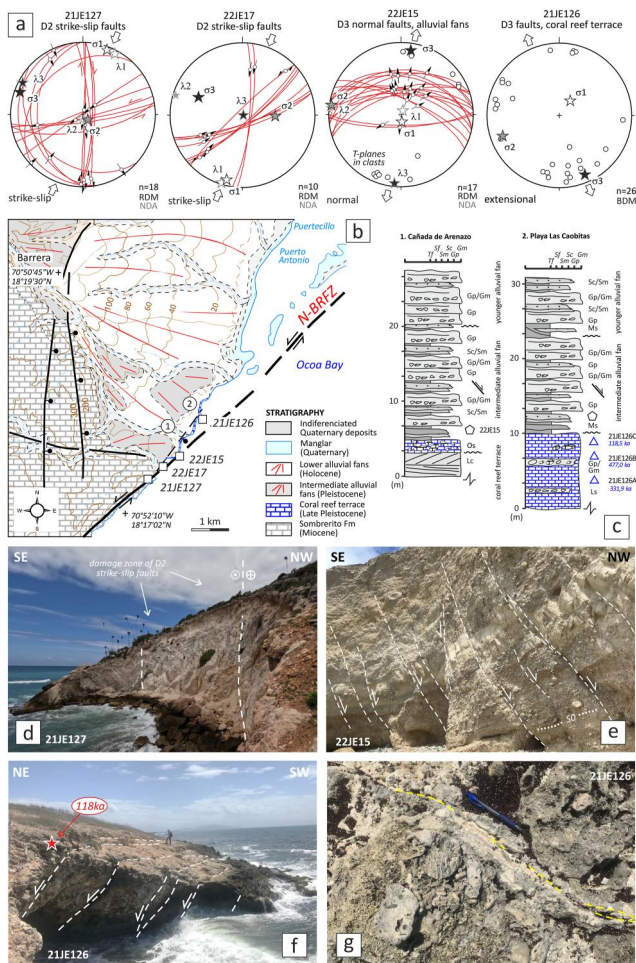


Figure 9. Structural analysis in the Sierra Martín García. (a) Stereoplots of the principal stress axes obtained from inversion of fault-slip data. (b) Structural map of the eastern Sierra Martín García in southern central Hispaniola (see location in Figure 3), showing main lithostratigraphic units, neotectonic structures, and sites of fault-slip data measurements. (c) Stratigraphic logs in Cañada Arenazo and Playa Caobita sites. (d) Aspect of the bands of fault-gouge and fine crush breccia several tens of meters thick associated with the strike-slip D2 deformation. View width is 40 m. (e) D3 normal faults deforming the alluvial fans deposits of Late Pleistocene to Holocene age? View width is 18 m. (f) Coral-reef terrace of Late Pleistocene boundary age (MIS 5c) deformed by D3 normal faults. (g) Field appearance of the calcite fill in the planes of the D3 extensional faults that deform the coral terrace. Gm, matrix-supported, muddy-sandy conglomerate; Gp, clast-supported, sandy conglomerate; Sc, medium-to-thick bedded coarse-grained sandstone and microconglomerates; Sm, thin-bedded, medium-to-fine-grained sandstone; Sf, fine-grained sandstone, siltstone and laminated mudstone; Ms, massive varicolored mudstone; Ls, coral reef limestone.

Viajama, and 22JE13 in Tabera Arriba). It corresponds to a compressional stress regime D1 characterized by a NE-SW to ENE-WSW trending σ_1 . The second population contains strike-slip to oblique reverse left-lateral slip vectors in NE-striking subvertical faults (sites 22JE13 and 21JE93). It is related to a near pure strike-slip stress regime D2 characterized by a NNE to NE-trending σ_1 . The third population includes normal vectors along dip-slip and oblique normal striae in NE-striking high-angle faults (site 21JE96), and corresponds to an extensional stress regime D3 with a N136°E trending σ_3 (Figure 13).

Sites 21JE123 and 21JE125 are located in the southernmost outcrops of the PB, on the road Azua-Bañí in the northern sector of the Ocoa Bay (Figure 7). In this sector, the macrostructure in the PB consists of a fold system of the lower to middle Eocene limestones of the Peralta Group and the upper Eocene turbidites with olistoliths of the Ocoa Group, related to a D1 deformation in a fold-and-thrust belt of NW-SE trend and SW-directed vergence. Toward the SE, the NW-trending D1 folds and thrusts of the PB turn progressively toward a N-S trend and are cut and displaced by the O-OBFZ right-lateral D2 strike-slip fault. In the geological cross-section of Figure 7, the Eocene rocks of the PB overthrust through the SJPFZ the lower to middle Miocene limestones of the Sobrerito Formation, and the assemblage overthrust in turn the conglomerates of the upper Pliocene to Early Pleistocene Arroyo Seco Formation. Therefore, D1 thrusting continued in this sector until the Early Pleistocene times.

Site 21JE123 is located along the Loma Vieja frontal thrust, which corresponds to the thrust ramp associated with the NNW to NW-trending D1 Loma Vieja anticline (Figure 7). The related D1 structures in the limestones of the Sobrerito Formation consist of SW-verging asymmetric folds, associated with mid-dip angle faults inclined to the NE and SW, subparallel to the Loma Vieja thrust. The mesoscopic S-C structures and other kinematic indicators imprinted on the fault planes establish a top-to-the-SW reverse movement. Predominant dip-slip striae in reverse fault planes define a population compatible with a thrust faulting stress regime and a N204°E trending compressional axis (Figure 7). On the other hand, the orientation of calcite veins and T-planes in clasts of the conglomerates of the Arroyo Seco Fm establish a consistent NNE trend of D3 subhorizontal extension.

Site 21JE125 is located at the northwest end of the Ocoa Bay, 3.5 km southeast of the town of Azua, on the southern flank of a W-trending D1 anticline build-up in the limestones of the Sobrerito Formation (Figure 7). The anticline is affected by a system of high-dip angle (>60°) strike-slip faults D2 composed by NE-striking left-lateral strike-slip faults and anti-thetic N-striking right-lateral strike-slip faults. The assemblage is truncated by E to WNW-trending D3 normal faults, exhibiting a high-dip angle toward the N and S. Fault-slip measurements define two contrasting subsets (Figure 7). The first subset includes striations with a low-pitch angle in NE-striking strike-slip faults. Normal and oblique normal dip-slip vectors in

WNW-striking and NE and SW-dipping conjugate faults represent the second subset. The first population corresponds to a purely strike-slip stress regime D2 with a N200°E trending σ_1 and the second population to an extensional stress regime D3 characterized by a N020°E trending σ_3 .

5.2. Fault-Slip Data Inversion in the Ocoa Bay

The limestone outcrops of the Sobrerito Fm located on the eastern coast of Loma Vigía, about 6 km southeast of Azua (Figure 7) exhibit folds, reverse faults and thrusts related to D1 deformation. In the 21JE112 site, these D1

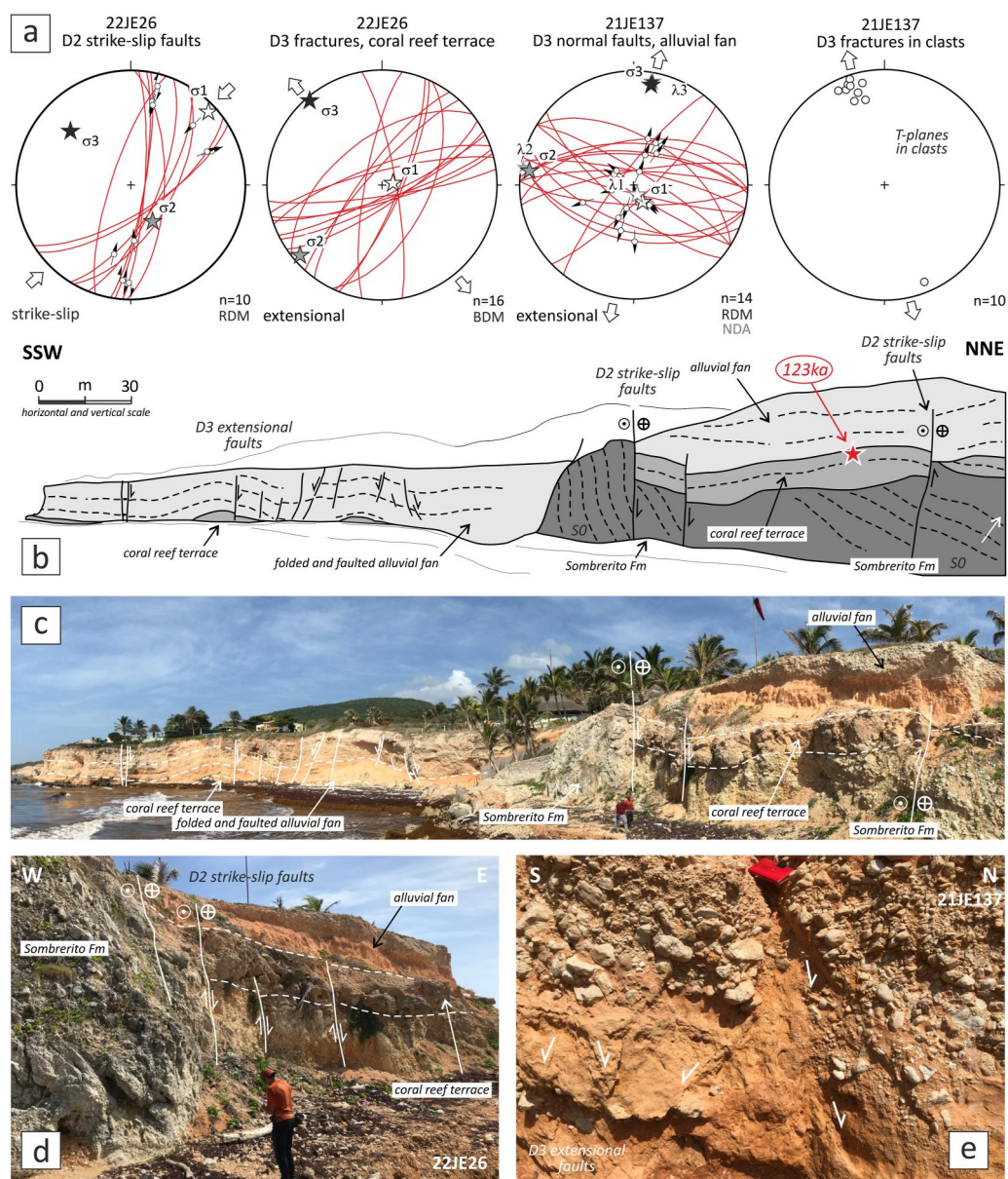


Figure 10. Structural analysis in northeast Sierra Bahoruco. (a) Stereoplots of the principal stress axes obtained from inversion of fault-slip data. (b) Geological cross-section of the Playa Azul site (see location in Figure 3). (c) Panoramic view of the geological cross-section outcrop. (d) Field relationships of the limestones of the Sombrerito Formation, coral-reef terrace of Middle to Late Pleistocene boundary age (MIS 5e stage) and gravels and red mudstones of the alluvial fan faulted by D2 strike-slip faults. (e) Field aspect of the gravels and red mudstones of the alluvial fan faulted by D3 extensional faults.

structures consist of NW to WNW-trending and SW-verging asymmetric folds, associated with low to mid-dip angle reverse faults inclined to the NE, subparallel to the SJPFZ. The mesoscopic S-C structures and other kinematic indicators imprinted on these fault planes establish a top-to-the-SW reverse movement. Striae on the fault planes define a reverse slip consistent with a thrust faulting stress regime and a N222°E trending compressional axis (Figure 8). In the 21JE120 site, several WNW-striking and NE-verging asymmetric anticlines correspond to the folds associated with a D1 back-thrust (Figure 8). Slip measurements on the limbs of a decimeter-scale anticline define a population of WNW-striking and SW-dipping reverse faults. This population corresponds to a purely compressional stress regime with a N026°E trending σ_1 .

Throughout the Loma Vigía sector, D1 structures appear truncated by NW to W-trending D3 normal faults, which exhibit mid to high-dip angles toward the NE and SW (Figure 8). For instance, the SW limb of a D1 anticline is cut by a D3 normal fault, causing the dragging of the limestone layers in the hanging-wall block (site 21JE120), or the stratification appears displaced by a system of ENE to E-striking normal faults with associated intrusion of mafic magmas (site 21JE113). In general, dip-slip striae in these fault planes define normal faults populations compatible with extensional stress regimes D3, characterized by a SSW to SW trending σ_3 (Figure 8).

5.3. Fault-Slip Data Inversion in the Eastern Sierra Martín García

In the limestone outcrops of the Sombrerito Formation located on the southeast coast of the Sierra Martín García, the D1 structures are strongly obliterated by the D2 deformation. This deformation has given rise to fault zones with a general NE-SW direction and several kilometers in length, parallel to the trace of the BRZF, which runs offshore about 1.5 km to the SE. Fault zones are marked by the development of bands of fault-gouge and fine crush breccia several tens of meters thick (Figure 9). Individual fault planes are very steep (dip $>70^\circ$) and have low-pitch angle ($<20^\circ$) striations that indicate a dominant strike-slip displacement.

At the Playa Caobita (site 21JE126), the Miocene limestones appear to be unconformably overlain by a ~ 50 -m-thick Quaternary sequence composed from bottom to top of (Figure 9): reef limestones of a basal fossil coral terrace; poorly consolidated conglomerates of an intermediate alluvial fan, that includes reworked corals and cobbles at the base; and gravels and sands rich in limestone cobbles of a younger alluvial fan. A gastropod *Strombus* sp. collected at the highest stratigraphic levels of the coral terrace has provided a U-Th age of 118.47 ± 0.52 ka (21JE126C), so its growth took place in the interglacial marine oxygen isotope stage (MIS) 5e, in the Middle to Late Pleistocene boundary. Two specimens of coral *Diploria* sp. collected toward the basal and intermediate levels of the terrace have provided U-Th ages of 476.99 ± 23.6 ka (21JE126B) and 331.92 ± 4.51 ka (21JE126A), respectively. These ages indicate growth of the coral terrace during MIS 9c and 11 stages in the Middle Pleistocene, although a reworking of the corals is not ruled out because the terrace intercalates clastic levels.

Observations made in outcrops along the coast indicate that D2 strike-slip faults cut both reef terrace limestones and intermediate alluvial fan conglomerates. These relationships establish a Late Pleistocene age at least for the D2 deformation. On the other hand, the whole sequence of the coral terrace and the overlying alluvial fans is tilted $10\text{--}18^\circ$ toward the SE and appear deformed by a system of E to ENE-striking D3 normal faults, which exhibits a high-dip angle ($>60^\circ$) toward the N and S (Figure 9). Therefore, the D3 deformation has taken place in the Late Pleistocene to Holocene. Fault-slip data measurements allow discrimination of a first population characterized by striations with a low-pitch angle in subvertical fault planes and a second population of normal dip-slip vectors in high-dipping faults. These populations represent two successive stress regimes: the first corresponds to a near strike-slip stress regime D2 with a $N020^\circ E$ trending σ_1 (21JE127); and the second matches with a near purely extensional regime D3 with a $N008^\circ E$ trending σ_3 (22JE15; Figure 9).

5.4. Fault-Slip Data Inversion in the Northeast Sierra Bahoruco

The northwestern end of the Sierra Bahoruco shows a very sharp NE-SW trending coastline, subparallel to the trace of the central segment of the BRZF, which runs offshore about 2.5 km to the SE (Figure 3). Swath bathymetry and seismic reflection data suggest that fault segment constitutes the active boundary between the 1,500 m elevated mountains of the Sierra Bahoruco to the NW and the $-2,500$ m submerged slope of the Dominican sub-basin to the SE (Granja Bruña et al., 2014; Mauffret & Leroy, 1999).

Sites 21JE137 and 22JE26 are located in Playa Azul, about 6 km southeast of Barahona (Figure 10). Along the coast, the limestone outcrops of the Sombrerito Formation define the northern limb of a D1 thrusting anticline of WNW trend and kilometric scale, which constitutes the internal structure of the Sierra Bahoruco in this sector. Limestones are strongly karstified and are unconformably overlain by a fossil coral reef 6 to 10 m-thick that defines a discontinuous morphological terrace along the coast. A *Diploria* sp. collected in the stratigraphically highest levels of the coral terrace has provided a U-Th age of 123.23 ± 0.70 ka (22JE26B), so its growth took place in the MIS 5e. The assemblage is also unconformably overlain by the poorly consolidated conglomerates and red clays of a >20 -m-thick alluvial fan (Figure 10).

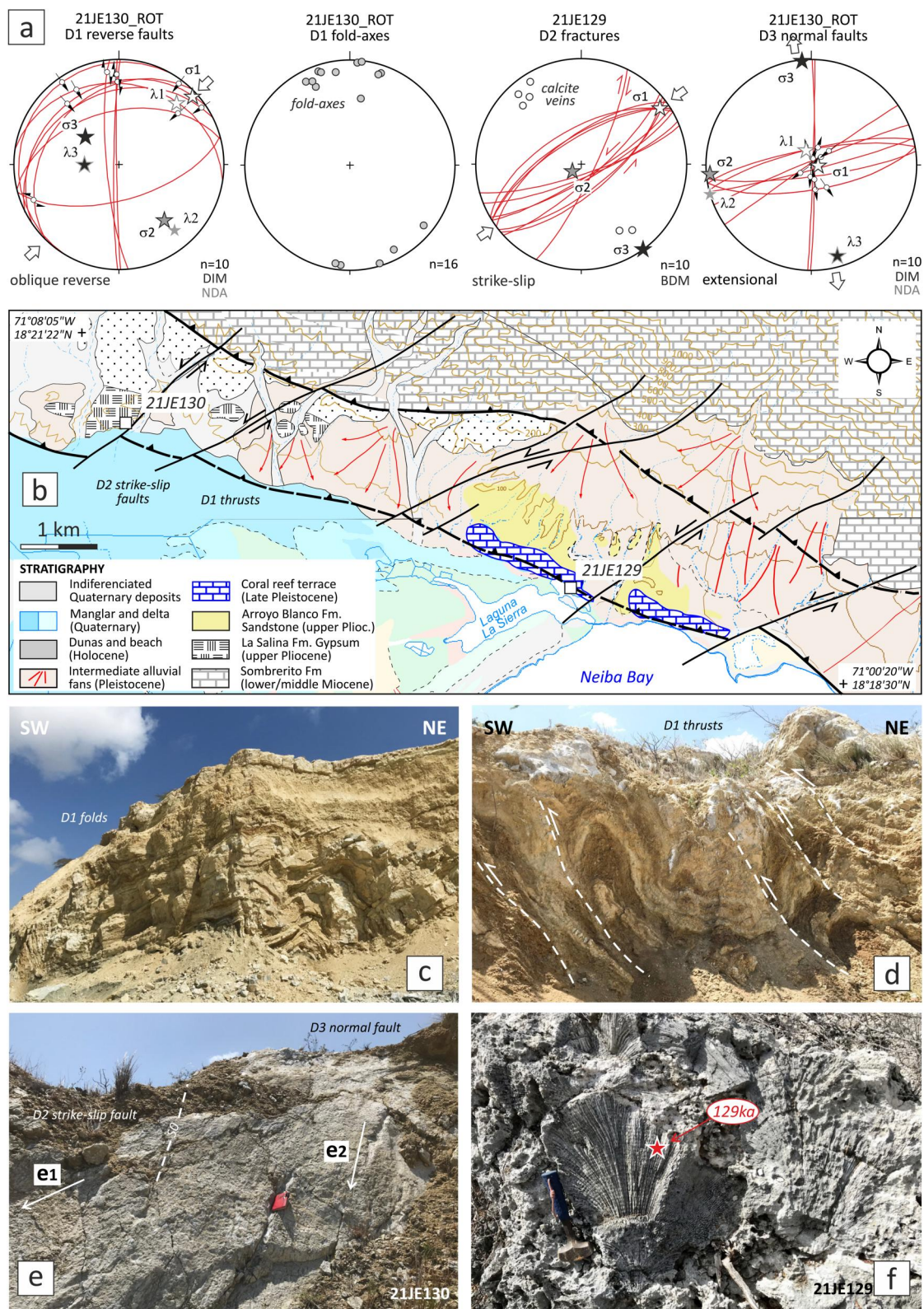


Figure 11.

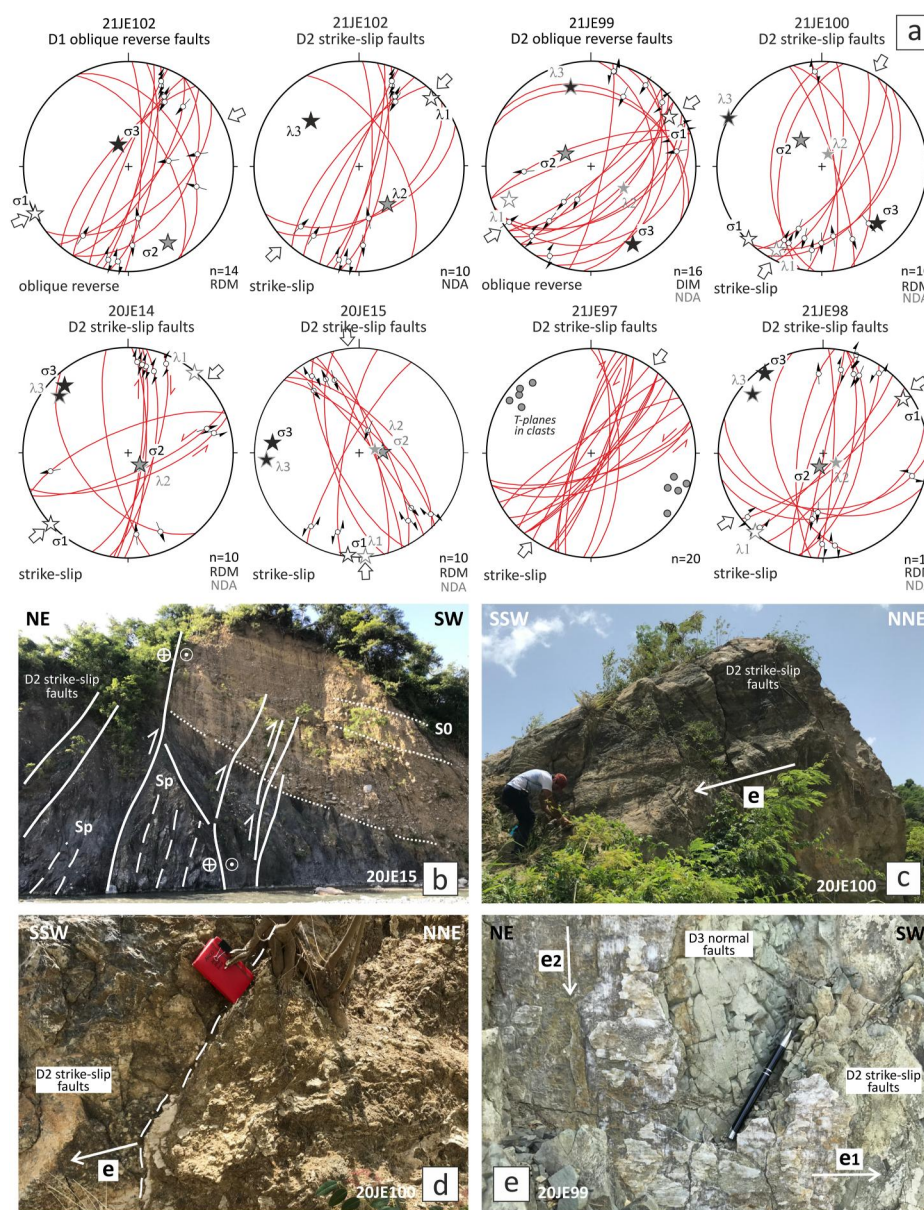


Figure 12. Structural analysis in the San José de Ocoa basin. (a) Stereoplots of the principal stress axes obtained from inversion of fault-slip data. (b) Folded and faulted mudstones of the Numero Formation juxtaposed to tilted and faulted San José de Ocoa basin deposits through subvertical oblique reverse right-lateral D2 faults of the eastern branch of the S-OBZF segment. (c) Low-pitch angle striations developed in subvertical fault planes subparallel to the S-OBZF segment deforming the volcanic rocks of the Tiroo Group. (d) Brecciated damage fault zone with low-pitch angle striations developed in subvertical D2 fault planes sub-parallel to the S-OBZF segment. (e) Field overlapping relationships between low-pitch angle strike-slip striations deformed by dip-slip normal striations in the same fault plane, establishing a temporal order between D2 and D3 deformations.

Figure 11. Structural analysis in the Sierra Martín García. (a) Stereoplots of the principal stress axes obtained from inversion of fault-slip data. (b) Structural map of the southwestern Sierra Martín García (see location in Figure 3), showing main lithostratigraphic units, neotectonic structures, and sites of fault-slip data measurements. (c) WNW-trending and SW-verging asymmetric D1 folds developed in the marls and gypsum beds of the upper Pliocene La Salina Formation. (d) SW-verging asymmetric D1 folds associated with mid-dip angle reverse faults inclined to the NE developed in the gypsum deposits. The asymmetry of D1 folds and mesoscopic S-C structures establish a top-to-the-SW reverse movement. (e) Field relationships of superposition of D3 normal fault striations (e2) over D2 strike-slip striations (e1) deforming stratified gypsum beds (S0). (f) Accumulation of *Diploria* sp. forming the reef-platform facies of a coral terrace grown during the MIS 5e stage that fossilizes the D1 frontal thrust of the Sierra Martín García.

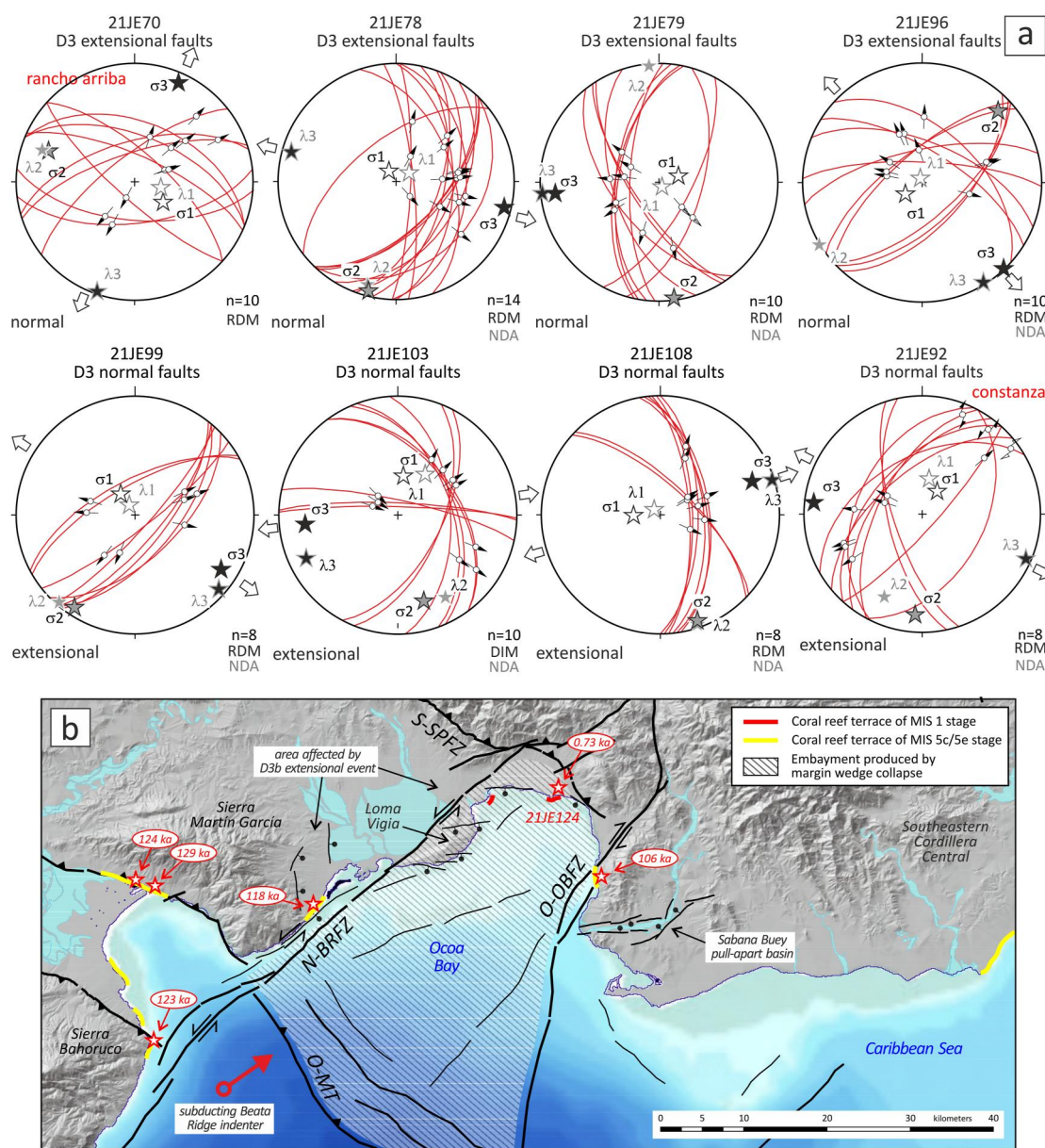


Figure 13. Structural analysis of the extensional D3 deformation in the Cordillera Central. (a) Stereoplots of the principal stress-axes obtained from inversion of fault-slip data. (b) Map of distribution of fossil coral reef terraces of the MIS 5e/5c and 1 stages, as well as the area affected by the D3b extensional event. See explanation in text. Shaded relief as in Figure 3.

Both the karstified limestones and the overlying coral terrace and clastic deposits are faulted and tilted by a system of N to NE-striking D2 strike-slip faults, subparallel to the trace of the BRFZ (see cross section in Figure 10). Fault planes are generally very steep (dip >65°) and the striae show left- and right-lateral conjugate motion with a low reverse component (pitch <25°). Fault-slip data inversion reveals a strike-slip D2 stress-field with a N046°E trending σ_1 stress axis (Figure 10). Therefore, the central Beata Ridge fault segment has been active for at least the Late Pleistocene. In turn, the internal structure in the alluvial fan deposit defines a system of open anticlines and synclines of WNW-ESE trend and decametric to hectometric wavelength, which appears faulted on the flanks by WNW to W-trending D3 normal faults. These folds are interpreted as roll-over structures related to the D3 extensional faulting. Striations measured in decametric-scale fault planes and T-planes open in clasts are compatible with an extensional D3 regime, characterized by a N010°E trending σ_3 (Figure 10).

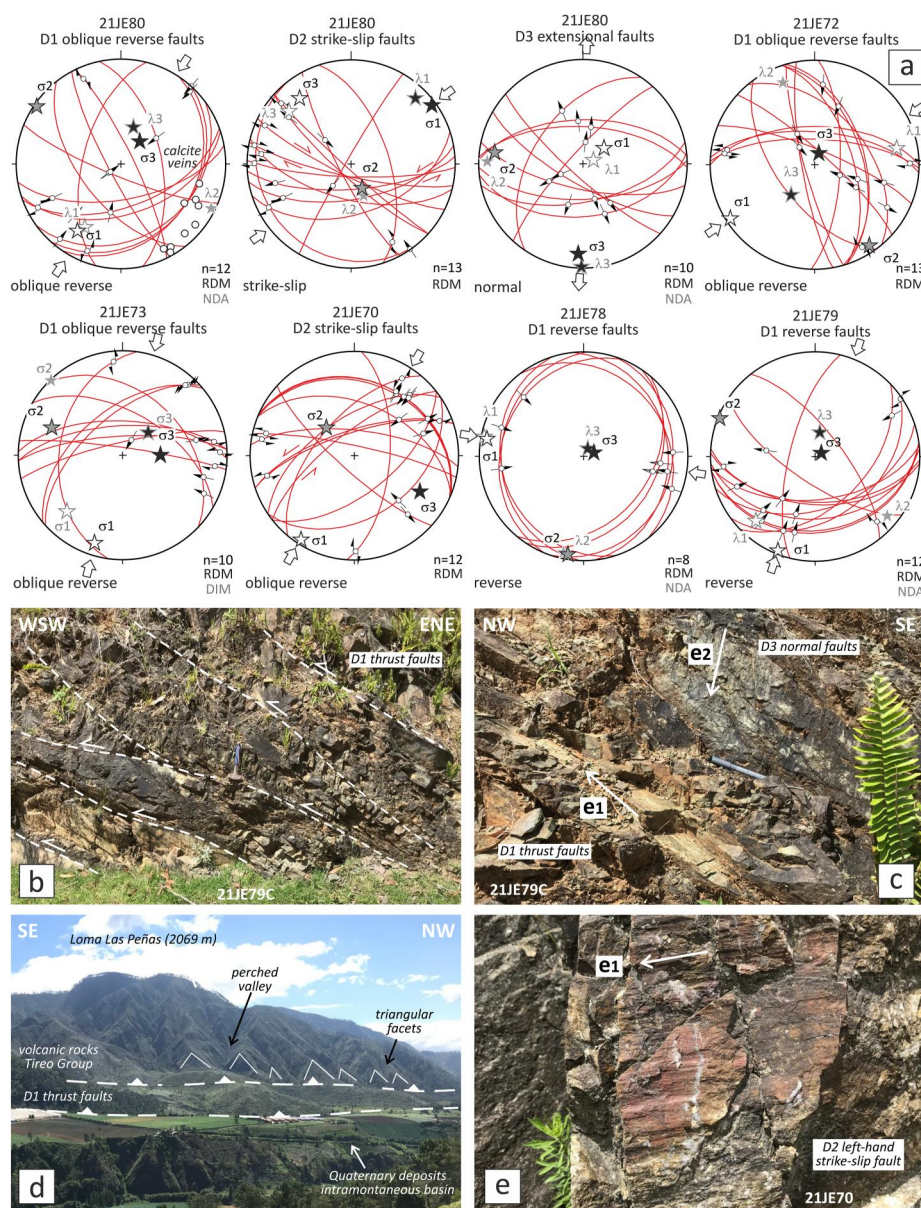


Figure 14. Structural analysis in the Cordillera Central. (a) Stereoplots of the principal stress-axes obtained from inversion of fault-slip data. (b) Late Cretaceous green tuffs of the Tiroo Group imbricated by WSW-directed D1 thrusts. (c) Detail of D3 extensional faults overlapping D1 thrusts in the green tuffs. (d) Panoramic view of Constanza mountainous area showing a D1 macrostructure of NW-striking thrusts built up on late Cretaceous volcano-plutonic rocks overthrusting the sedimentary fill of a Quaternary intramontaneous basin. Note the development of perched valleys and triangular facets in the hanging-wall block. (e) Detail of the striae associated to the development of a D2 sinistral strike-slip fault in late Cretaceous tonalitic rocks.

5.5. Fault-Slip Data Inversion in the Southwestern Sierra Martín García

In the southwestern sector of the Sierra Martín García, the limestones of the Miocene Sombrero Formation overthrust the sandstones, marls and gypsum of the upper Pliocene La Salina Formation, and the ensemble regionally overthrusts the continental conglomerates and mudstones of the upper Pliocene to Early Pleistocene Arroyo Seco Formation. These WNW-trending structures constitute the SW-directed D1 frontal thrust, which juxtaposes the anticline macrostructure of the Sierra Martín García to the poorly consolidated alluvial, floodplain and deltaic Quaternary deposits of the Enriquillo basin (Figure 3).

Site 21JE130 is located in the hanging-wall block, about 300 m northward of the frontal thrust, where the gypsum and marl beds of the La Salina Formation exhibit structures related to D1 deformation (Figure 11). These structures consist of WNW-trending and SW-verging asymmetric folds, associated with mid-dip angle reverse faults inclined to the NE, subparallel to the basal thrust. The asymmetry of D1 folds and mesoscopic S-C structures establish a top-to-the-SW reverse movement. Oblique reverse striae measured in the reverse fault planes define a fault population compatible with a D1 thrust faulting stress regime and a N047°E trending compressional axis (Figure 11). In the site 21JE129, the D1 frontal thrust is locally fossilized by a coral reef terrace, where a *Strombus* sp. collected near its stratigraphic base has provided a U-Th age of 124.65 ± 0.85 ka. A *Diploria* sp. also collected in the same basal levels has given a similar U-Th age of 128.89 ka (Figure 11), thus the coral terrace grew in the MIS 5e stage.

Both the D1 thrust-related folds and the coral terrace are affected by a system of high-dip ($>60^\circ$) strike-slip faults D2. This fault system comprises NE to ENE-striking left-lateral strike-slip faults filled by subvertical calcite veins and antithetical N to NNE-striking right-lateral strike-slip faults, establishing a strike-slip stress D2 regime characterized by a NE-trending σ_1 axis (Figure 11). Therefore, the thrust-related D1 deformation reaches the Middle Pleistocene and the strike-slip-related D2 deformation continues after the Middle to Late Pleistocene boundary. Finally, a set of E to ENE-trending and high-dip angle D3 normal faults locally truncate the assemblage. Normal dip-slip striae measured in these fault planes cutting the gypsum beds are compatible to an extensional regime with a N355°E trending σ_3 axis (Figure 11).

5.6. Fault-Slip Data Inversion in the San José de Ocoa Basin

The southern segment of the Ocoa-Bonao-La Guácara fault zone is a roughly 50 km-long, N-striking right-lateral strike-slip fault system, that cuts at a high-angle and clockwise rotate the NW-SE trending folds and thrusts of the PB and the structure of the late Cretaceous basement of the Cordillera Central (Figures 3 and 5). The segment is geometrically characterized by separating the fault trace into two branches south of San José de Ocoa town, giving rise to a right-hand releasing-bend and the San José de Ocoa pull-apart sedimentary basin (Escuder-Viruet et al., 2023). Both branches rejoin about 35 km northward into the C-OBFZ segment in the Bonao basin.

Site 21JE102 is located near the eastern branch of the S-OBFZ segment, in the town of Naranjal, 2.5 km east of San José de Ocoa (Figure 5). At outcrop scale, N to NNE-striking right-lateral D2 strike-slip faults cut D1 thrust surfaces inclined to the NE, defined by sheared bands of mudstones in the upper Eocene Ocoa Formation, characterized by a SW-directed penetrative S-C fabric. Fault-slip measurements define two contrasting subsets (Figure 12): the first subset is reverse to oblique reverse and is associated to striations with a high-pitch angle in NW-striking fault planes; the second subset has oblique reverse and strike-slip vectors in conjugate right- and left-lateral faults. The first population corresponds to a compressional stress regime D1 with a N243°E trending σ_1 and the second population establishes a purely strike-slip stress regime D2 characterized by a N047°E trending σ_1 .

Site 21JE100 is also located along the eastern strand of the S-OBFZ segment, 2 km north of San José de Ocoa, on the road to Constanza (Figure 5). The fault segment tectonically juxtaposes the folded and faulted volcanic rocks of the Tiroo Group and the gravels and sands of the Quaternary fill of the San José de Ocoa basin. Volcanic rocks have developed hectometer-scale subvertical fault planes sub-parallel to the S-OBFZ, characterized by a 5 m-wide brecciated damage zone and striations with a low-pitch angle (Figure 12). These striae define a vector population compatible with a D2 strike-slip stress regime and a N226°E trending compressional axis. South of San José de Ocoa town, the eastern strand juxtaposes the folded and faulted mudstones of the Numero Fm and the gravels and sands of the basin through a subvertical D2 fault system that also tilts westward the Quaternary deposits. Striations measured in NNW-striking oblique reverse right-lateral faults of the 20JE15 site are compatible with a D2 strike-slip regime and a N186°E σ_1 axis (Figure 12).

The D2 strike-slip deformation is also very penetrative along the western branch of the S-OBFZ segment, which is morphologically marked by an east facing 200 m-high scarp. This strand juxtaposes the folded and faulted rocks of the PB to the W with poorly consolidated gravels and sands that fill the San José de Ocoa basin to the E (Figure 5). In several sites (20JE14, 21JE97, 21JE98 and 21JE99), striations measured on metric to decametric-scale faults subparallel to the S-OBFZ segment define a population of pure strike-slip to oblique reverse slip vectors, compatible with a D2 strike-slip regime and a predominant NE trending σ_1 stress axis (Figure 12). The subvertical orientation of calcite veins and T-planes in clasts of the Quaternary conglomerates consistently establishes a WNW to NW trend of subhorizontal extension.

However, the effects of D3 extensional deformation are limited in this sector and geographically localized to the right-hand releasing-bend that forms the San José de Ocoa basin. Site 21JE99 is located between the two branches of the S-OBFZ segment, where the mafic to intermediate tuffs of the Tiroo Group are in tectonic contact with the well-bedded limestones of Maastrichtian age. Slip measurements show two different populations: oblique reverse right-lateral and dip-slip reverse vectors (Figure 12); and oblique normal vectors (Figure 13). The overlap relationships between striae establish that these two populations represent two successive stress fields: the first corresponds to a transpressional D2 stress regime with a N270°E trending σ_1 ; and the second corresponds to a more purely extensional D3 regime characterized by a N121°E trending σ_3 . Also related to local D3 extensional tectonics, NW to N-striking normal faults have also been observed at sites 21JE103 and 21JE108 (Figure 5). Dip-slip striations measured on these fault planes establish an extensional D3 regime characterized by a W-trending σ_3 (Figure 13).

5.7. Fault-Slip Data Inversion in the Cordillera Central

The Cordillera Central is characterized by the development of crustal shortening structures, topographic uplift and exposure of the late Cretaceous volcano-plutonic basement in the core of large-scale WNW to NW-trending D1 anticlines (Figure 3). In the Constanza-Sabana Quéliz area, the macrostructure consists of D1 folds and thrusts of WNW-ESE trend and usually SW-directed vergence, built up in a sequence composed by Cenomanian limestones and siliceous-rich sediments, Turonian to early Campanian mafic tuffs of the Constanza Formation, late Campanian mudstones of the El Convento Formation and Maastrichtian shallow-water platform limestones, as well as plutonic rocks (Escuder-Viruet et al., 2008). This macrostructure is locally cut and displaced by a system of high-dip angle strike-slip D2 faults, which includes NW to NNE-striking right-lateral strike-slip faults and conjugate NE to ESE-striking left-lateral strike-slip faults. NE to E-trending D3 normal faults locally truncated the assemblage exhibiting a high-dip angle toward the NW and SE.

This deformative sequence is well recorded at the 21JE80 site, located ~10 km east of the Constanza town in the Tiroo river valley (Figure 5). Fault-slip data measurements and cross-cutting relationships show three contrasting subpopulations (Figure 14): reverse and oblique reverse left-lateral faults; subvertical faults with low-pitch angle striations; and normal and oblique normal right-lateral faults. These subsets represent three successive stress regimes: the first corresponds to a compressional stress regime D1 characterized by a N213°E trending σ_1 ; the second adjusts to a near strike-slip stress regime D2 with a N321°E trending σ_1 ; and the third matches with a purely extensional regime D3 with a N183°E trending σ_3 (Figure 14).

Field observations at various points in the Cordillera Central show that D3 extensional faults overlap D1 thrusts. For example, the various kinematic types of faults that deform green mafic tuffs at sites 21JE78 and 21JE79, where the fault-slip data inversion enables the separation of populations related to two distinct stress regimes (Figures 13 and 14). The first population is represented by dip-slip to variably oblique reverse slip vectors in low to mid-dip faults; the second population includes normal slip vectors along dip-slip striae in predominantly NNE to NE-striking high-dip faults. Both fault types define a NE-SW to W-E compressional D1 regime and a NW-SE extensional D3 regime, respectively.

A similar deformative sequence is recognized in the southeastern Cordillera Central, located east of the S-OBFZ segment (Figure 3). In this sector, the S-OBFZ exhibits a fresh N-S scarp and represents the boundary between the >2,000 m elevated mountains of the Cordillera Central to the W and the 650 m elevated Rancho Arriba valley to the E. Along this morphological step, the fault zone produces triangular facets, perched valleys, and dextral offsets of streams that testify its recent activity. Deformation related to this segment produced the local clockwise rotation of the D1 fold and thrust structure and the formation of the Rancho Arriba intramountain basin, which is filled by the Quaternary alluvial fans fed by the erosion of the surrounding relief.

Site 21JE70 is located at the Rancho Arriba basin southern bound. The basin exhibits an ENE-WSW elongated rectangular shape controlled by a southern active master fault (Figure 5). Fault-slip measurements on hornblende-bearing tonalities of the Arroyo Caña batholith define two contrasting subsets (Figures 13 and 14): oblique reverse to strike-slip vectors in NE to ENE-striking faults; and oblique normal slip vectors in conjugate ENE and WSW-striking high-angle faults. The first set corresponds to a strike-slip stress regime D2 with a N022°E trending σ_1 and the second set establishes a near pure extensional stress regime D3 characterized by a N023°E trending σ_3 , related to the formation of the basin. Observations carried out in the volcanic rocks of the Tiroo Group at sites 21JE72 and

21JE73 allow us to establish similar temporal relationships: younger NE to E-striking D3 normal faults cut older D2 strike-slip and D1 reverse faults. Striations measured in decametric-scale fault planes subparallel to the NW to WNW-trending regional macrostructure in these sites are compatible with a compressional D1 regime, characterized by a general NNE to NE-trending σ_1 (Figure 14).

The NW-SE to W-E directed D3 extensional tectonics has also been detected in other sites located close to the OBFZ. Site 21JE99 is located between the two branches of the S-OBFZ segment, north of San José de Ocoa town (Figure 5), where Maastrichtian limestones exhibit a penetrative brecciation associated with decametric-scale NE-striking fault surfaces, dipping a high-angle to the NW and SE. Slip measurements establish an oblique normal left-lateral movement on these planes and their inversion establishes an extensional D3 regime characterized by a N121°E trending σ_3 (Figure 13). Site 21JE103 is located ~1.5 km east of the S-OBFZ (Figure 5), where decametric-scale fault planes measured in basalts of the Tiroo Group contain striations of an oblique normal kinematics in NW to NE-trending and E-dipping faults. Inversion of these fault-slip data yields an extensional stress regime characterized by a N256°E trending σ_3 (Figure 13). Finally, slip measurements in N- to NNW-striking fault planes at site 21JE108 (Figure 5) indicates a predominance of dip-slip normal vectors, compatible with a purely extensional regime with a N069°E trending σ_3 (Figure 13).

6. Discussion

6.1. Relations Between Neotectonics and Quaternary Sedimentation in Southern Central Hispaniola

Several researchers have previously described the uplift, folding and thrusting of the Cordillera Central basement and the PB during the lower Miocene to upper Pliocene time interval (Heubeck & Mann, 1991; Mann, Draper, & Lewis, 1991; Mann, McLaughlin, & Cooper, 1991; Pubellier et al., 2000; Ramírez, 1995). The style of this D1 deformation consisted of a SW-directed fold-and-thrust belt, which was developed above a basal detachment horizon following a forward propagating sequence (Heubeck & Mann, 1991; Hernaiz Huerta & Pérez-Estaún, 2002; this work). D1 is superimposed on a deformation produced during the upper Eocene in the Peralta accretionary prism (Witschard & Dolan, 1990). Data obtained in this study indicate that a large part of this deformation is syn-sedimentary and characterized by the formation of a block-in-matrix fabric typical of a heterogeneous mélange. Syn-sedimentary deformation was very probably produced by submarine gravitational processes, triggered by instability in the basin slope and/or tectonics (e.g., Alonso et al., 2014; Escuder-Viruete & Baumgartner, 2014; Suárez Rodríguez et al., 2017).

In this tectonic context, the San Juan-Azua basin constitutes the foreland flexural basin developed in front of the SW-directed Peralta fold-and-thrust belt, and bounded to the NE by SW-directed thrusts (Hernaiz Huerta & Pérez-Estaún, 2002; Díaz de Neira, 2004; this work). These basins were filled by shelf marine, turbiditic, and continental sediments giving rise to a 4-km thick, shallowing and coarsening upward regressive megasequence of lower Miocene to Lower Pleistocene age. D1 deformation propagated to the Azua basin sediments and continued until Early to Middle Pleistocene times, which is the age of the Arroyo Seco Formation deformed in the footwall of the Peralta frontal thrust (Díaz de Neira & Solé Pont, 2002). As documented in the present work, these coarse-grained continental deposits were folded and thrust in the footwall of the San Juan-Pozos fault zone, current frontal thrust of the PB.

After a sedimentary hiatus, uplift and erosion of the resulting relief fed several staircase alluvial fan systems, developed at different topographic levels on the southern slopes of the Cordillera Central probably since the Early Pleistocene (Díaz de Neira, 2000; Pérez-Valera, 2010). The ages obtained by optically stimulated luminescence geochronology between 43.8 ± 8.3 ka and 5.9 ± 0.6 ka for the intermediate and young alluvial fan systems indicate the uplift continued, at least, during the Late Pleistocene to the Holocene (Escuder-Viruete et al., 2023). The older alluvial fan is not yet been dated, but probably also records uplift and erosion during the Middle Pleistocene.

In both the eastern and western sectors of the Ocoa Bay, these alluvial fan systems unconformably overlie a fossil coral reef terrace developed during the MIS 5e (118–128 ka) and 5c (~105 ka) stages in the Last Interglacial. Therefore, the fluvial incision and the progradation/aggradation of the intermediate and young alluvial fans were also controlled by the global sea level fall and its variations during the Last Glacial. The coral terrace also includes

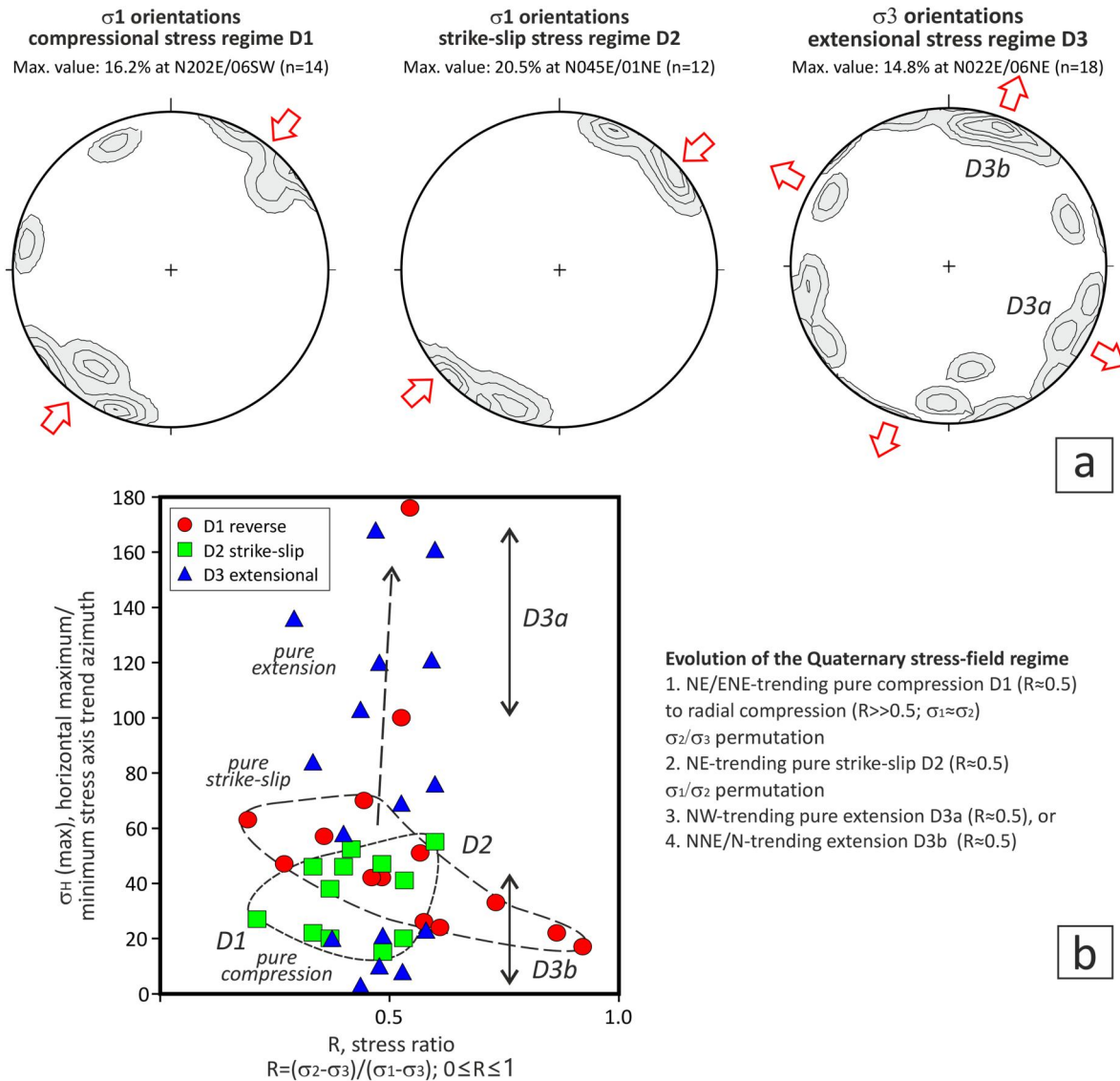


Figure 15. (a) Stereoplots of the principal stress-axes obtained from fault-slip data inversion grouped by deformation events and (b) their classification according to its kinematic regime (see Table S6). The orientation of σ_1 has been restored at sites that have undergone a post-D1 rotation. Contours in stereoplots at 1.0%, 5.0%, 10.0%, 15.0%, 20.0%, and 25.0%. Computed mean stress axes for each deformation event are expressed in % and trend/plunge angles.

reworked corals grown during MIS 7 and 9 stages. However, no remains have been found of coral terraces built during these stages in the Ocoa Bay, so erosion might eliminated them.

On the other hand, the Quaternary coral reef terrace and the alluvial fans unconformably overlie the D1 large-scale structure of NW-trending and SW-verging folds and thrusts that affect the NE margin of the Azua basin. Therefore, the regional pervasive D1 deformation ends, at least in southern central Hispaniola, during the Lower Pleistocene. Late Pleistocene to Holocene alluvial fan and pediment deposits are all offset by strike-slip faults of the D2 event, implying that the more recent tectonic activity is mainly partitioned in the Ocoa-Bonao and Beata Ridge fault zones, as well as by faulting in related structures. Finally, both the coral reef terraces of the MIS 5e and 5c stages and the overlapping alluvial fan systems of Late Pleistocene to Holocene age appear deformed by the normal faults of the D3 event in the Ocoa Bay sector.

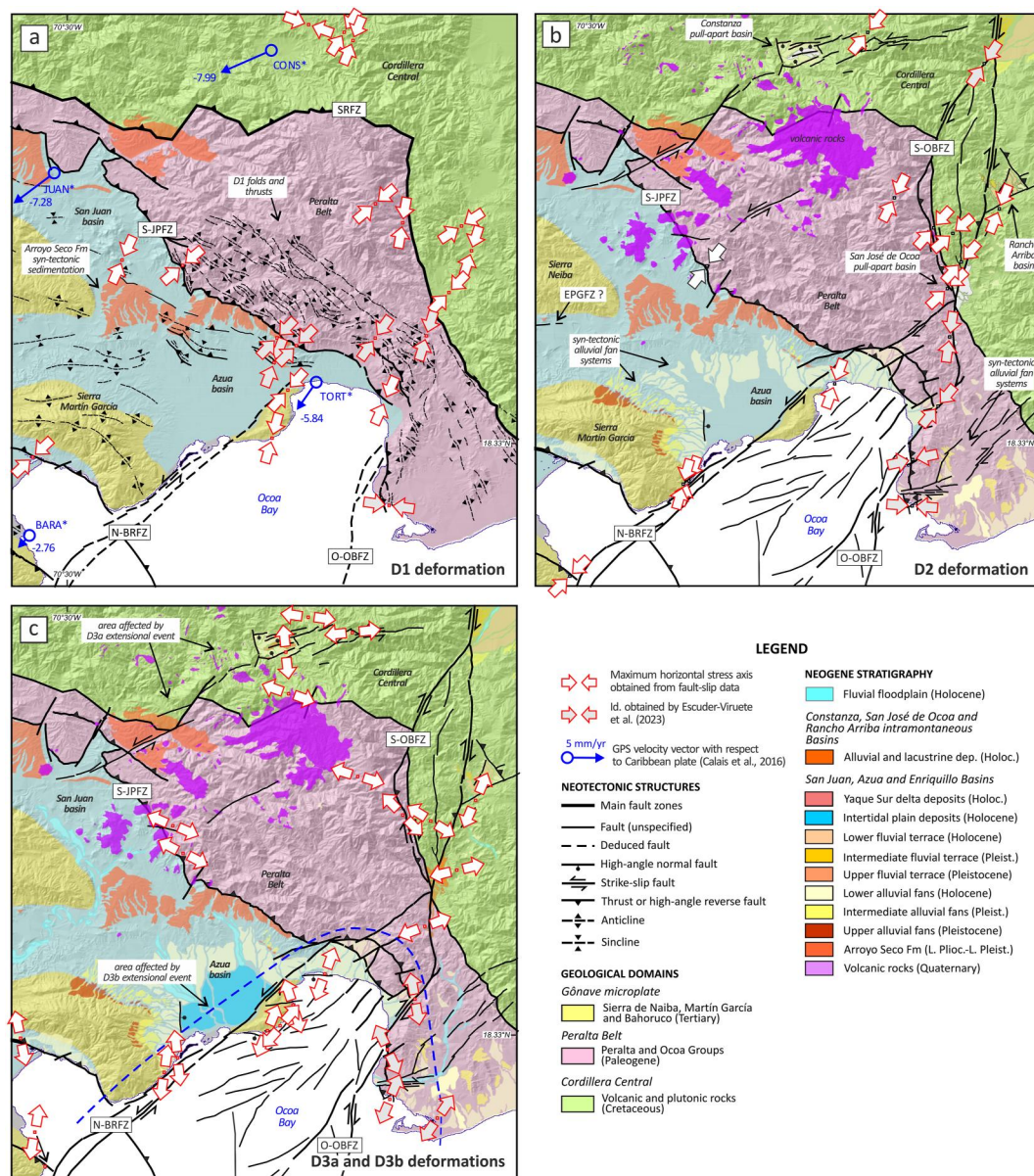


Figure 16. Neotectonic diagrams showing the evolution of the Quaternary stress regime in southern central Hispaniola set up for (a) D1 reverse, (b) D2 strike-slip, and (c) D3 extensional events (Table 1). Maximum horizontal stress axis trends were derived from fault-slip data inversion. Shaded relief in grayscale has been made as in Figure 3, indicating the overlay color different geological domains: green, the Cretaceous basement of the Cordillera Central; pink, the middle Eocene-lower Miocene Peralta fold-and-thrust belt and the overlying uplifted forearc basin; yellow, the Tertiary limestones of the Sierras de Naiba, Martín García y Bahoruco; and pale blue, the Neogene San Juan-Azua Basin. Vectors of GPS velocities relative to the Caribbean plate at stations located in the study area are from Symithe et al. (2015), Calais et al. (2016), and UNAVCO (<https://coconet.unavco.org>). Acronyms as in Figure 3. See text for explanation.

6.2. Evolution of the Quaternary Stress Regime in Southern Central Hispaniola

The geometric characteristics of the faults at all scales, the striae sets in their planes, the compatible stress tensors and their chronological succession, constrained by offset relations with dated lithostratigraphic units, define three types of neotectonic fault kinematics in southern central Hispaniola (Table 1). These types are: thrust and reverse faulting with horizontal σ_1 and σ_2 ; strike-slip faulting with horizontal σ_1 and σ_3 ; and extensional faulting with vertical σ_1 (Figure 15; see also Table S6). Each type of fault kinematics is related to a different deformation event,

characterized by a specific state of stress, whose development changes geographically throughout southern central Hispaniola (Figure 16).

Throughout the Cordillera Central domain, Sierra Martín García and San Juan-Azua basin there is evidence of slip on thrust and reverse faults related to a NNE to NE-trending compressional D1 stress regime (Figure 16). These NW-trending D1 structures deform the middle Eocene-lower Miocene sedimentary rocks of the Rfo Ocoa Group, as well as its substrate of the PB accretionary prism, the early/middle Miocene to middle Pliocene marine turbiditic and platform sediments of the San Juan-Azua foreland basin, and the upper Pliocene to Early Pleistocene clastic continental deposits of the Arroyo Seco Formation (Díaz de Neira & Solé Pont, 2002; Heubeck & Mann, 1991; Hernáiz Huerta & Pérez-Estaún, 2002; among others). A similar structural relationship has been described along the southern border of the Chaîne des Matheux in Haiti, where SW-directed thrusts deform rocks of middle to upper Miocene age (Pubellier et al., 2000). Upper Miocene to lower Pliocene onset of uplift in the Cordillera Central is simultaneous with uplift in the Sierra de Neiba, with both ranges providing the clastic sedimentary source for the eastern San Juan and Azua (piggyback) basins. The pre-Early Pleistocene folding and thrusting D1 event has been related to the collision between CLIP-related units of the Southern Hispaniola Peninsula and the island-arc crust of the Cordillera Central (Heubeck & Mann, 1991; Mann, McLaughlin, & Cooper, 1991).

Stress tensors obtained for D1 event indicate a general NE-trending σ_1 axis, ranging between N017°E and N070°E directions, with a relatively well-constrained maximum value in the count-contours stereoplot at N202°E, plunging 06° to the SW (Figure 15). A similar NE to ENE-directed shortening was obtained by Ramírez (1995) from the analysis of the faults that deform the Arroyo Blanco Fm. In the calculations, the orientation of σ_1 has been restored at sites in the eastern Ocoa Bay that have undergone a post-D1 clockwise rotation. The vertical arrangement of σ_3 axis in the computed stress tensors is consistent with deformation by thrusting. The R stress ratio has values of 0.50 ± 0.25 , indicating stress tensors close to pure compression. Therefore, the regional D1 stress regime consisted of a NE-trending subhorizontal compression. However, R ratio presents some values of 0.87 and 0.92 (21JE73 and 21JE79 sites), which means that the maximum and minimum σ_H axes are close in magnitude and higher than σ_V ($\sigma_1 \approx \sigma_2$). These R values suggest that a D1 deformation locally characterized by a radial compression regime. On the other hand, the WSW-directed GPS motions measured in JUAN, CONS and BARA stations, located away from important D2 structures, are suborthogonal to the strike of the San Juan-Pozos and Barahona fault zones, as well as the thrust structures in the Cordillera Central and PB domains. Therefore, present-day reverse faulting dominates active D1 structures (Figure 16). This argument agrees with thrust kinematics and reverse stress regime obtained for D1 from field permanent deformation.

The NNE to NE-trending strike-slip D2 stress regime has been deduced near the Ocoa-Bonao-La Guácara fault zone, particularly in the eastern sector of the Ocoa Bay and in the margins of the San José de Ocoa and Rancho Arriba intramountain basins (Figure 16). This strike-slip deformation has also been observed in the vicinity of the BRZ, in the western sector of the Ocoa Bay, and in relation to NE to ENE-striking left-hand strike-slip faults that cut and displace D1 thrusts in the Cordillera Central. Therefore, D2 strike-slip faults cut and displace the D1 fold-and-thrust structures, as described in previous works (Hernáiz Huerta & Pérez-Estaún, 2002; Pérez-Valera, 2010; Ramírez, 1995).

D2 strike-slip faults deform the Quaternary deposits in several places, as the fossil coral reef terrace built during the MIS 5e and 5c stages in the SW and NE flanks of the Sierra Martín García and Bahoruco. Recent field-data collected in the eastern sector of Ocoa Bay (Escuder-Viruet et al., 2023), indicate that D2 strike-slip faults subparallel to the O-OBZ segment deform an alluvial fan of latest Pleistocene age, but are locally fossilized by a younger alluvial fan of Holocene age. Nonetheless, the Ocoa-Bonao-La Guácara fault zone cuts geomorphic features along its path, such as Late Pleistocene-Holocene alluvial fans, fluvial terraces and streams in the San José de Ocoa and Rancho Arriba intramountain basins, which collectively evidence active D2 deformation. Therefore, the D2 stress-field continues through the latest Pleistocene and most likely today. This interpretation is consistent with the moment tensor solutions of strike-slip faulting calculated for the 1977 and 1988 earthquakes (CMT catalogue; Ekström et al., 2012), whose epicenters are located very close to the OBZ trace.

The change from a D1 compressional to a D2 strike-slip stress regimes took place during the Early and Middle Pleistocene (or sometime in the Early Pleistocene). This change could be related to the indentation of the eastern sector of the Beata Ridge in southern Hispaniola, as part of the Caribbean oceanic plateau collision in the back-arc region of the Hispaniola microplate. This processes could produced the large-scale drag of the pre-existing D1

structures in the eastern Ocoa Bay and generated large-scale conjugate D2 strike-slip faults on the margins of the aseismic ridge indenter. In this sense, the geometric characteristics of the D2 deformation, such as landward deflection of the Muertos trench axis and development of conjugate strike-slip faults and back-thrusts, are analogous to those produced above a subducted conical seamount or submarine aseismic ridge (Gardner et al., 2013; Ranero & von Huene, 2000; Sak et al., 2009), as it has been faithfully reproduced by sandbox analog models of such convergent margins (Dominguez et al., 2000).

Stress tensors of D2 event indicate a general NE-trending σ_1 axis, comprised between N015°E and N055°E directions, with a relatively well-constrained maximum value at N045°E, plunging 01° to the NE (Figure 15). The dispersion of σ_1 axes is due to fault-slip measures in sites located in the San José de Ocoa Basin, where the S-OBFZ trends N-S, or probably due to the reorientation of the regional stress field that occurs around this large-scale strike-slip fault. The subvertical arrangement of the σ_2 axes indicates that the D2 deformation took place in a strike-slip regime, characterized by a NE-trending subhorizontal shortening for R-values ranging between 0.21 and 0.60, with prevalence of values close to 0.5. These R-values suggest a deformation mode close to pure strike-slip, consistent with the low-pitch angle of the displacement vectors observed in D2 strike-slip faults and some focal mechanism solutions. Note that the SW-directed GPS motion measured in the TORT station is parallel to the NE-SW strike of the nearby Beata Ridge fault segment, implying a present-day pure strike-slip faulting along this D2 structure (Figure 16).

D3 faults can be grouped into two geometric families: D3a and D3b. The first family includes NE-SW to NNE-SSW trending normal and oblique normal D3a faults. Although the number of computed stress tensors is limited, inversion of fault-slip data establishes a general NW-SE trending extensional stress regime D3a (Figure 15). This extensional stress regime has only been detected in the western Cordillera Central-Peralta Belt domains and in sectors close to the S-OBFZ segment, as the San José de Ocoa and Rancho Arriba intramountain basins (Figure 16). The orientation of σ_3 axes has a high dispersion, ranging between N103°E and N168°E, for values of the R ratio very close to 0.5, establishing stress tensors of pure extension. The age of the D3a event could not be precisely established. However, these normal faults affect the volcanic rocks of Pleistocene age of the Valle Nuevo area whose K-Ar ages are 0.5 ± 0.3 and 0.3 ± 0.2 Ma (Kamenov et al., 2011; Vespucci, 1988; and references herein) and, therefore, its age is at least post-Middle Pleistocene. The alignment of the emissive centers of the Quaternary calc-alkaline to mafic alkaline volcanism in the region follows a NE-SW strike (Figure 16), so the NW-directed extension during D3a could have favored the opening of NE-SW striking planes and the rise of magmas. Alternatively, the rise of magmas could have taken place in favor of releasing bends formed during D2 deformation. Hot springs and associated travertine deposits in the volcanic region indicate that geothermal activity continues today.

The second family includes WNW to W-striking dip-slip normal faults that established an N to NNE-trending extensional D3b stress regime. Its development is geographically limited to the surroundings of Ocoa Bay (Figure 16). D3b normal faults deform the coral reef terraces of the MIS 5e and 5c stages (22JE26, Playa Azul; 21JE126, Playa Las Caobitas; and 20JE04, Palmar de Ocoa sites) and the overlapping alluvial fan of Late Pleistocene to Holocene? age (21JE127 and 22JE15 sites). Inversion of 12 fault-slip data sets gives rise to NNE-trending σ_3 axes, comprised between N003°E and N023°E directions, with a relatively well-constrained maximum value at N022°E, plunging 6° to the NE (Figure 15). The subvertical arrangement of the σ_1 axes and the obtained R-values close to 0.5 indicate stress tensors close to pure extension.

In summary, a relatively constant NE-trending horizontal shortening, parallel to the current direction of plate convergence established by GPS measurements, controlled the evolution of the Quaternary stress tensor in southern central Hispaniola. This evolution included a D1 event of compression followed by a D2 near pure strike-slip event, which was locally coeval by a more heterogeneous and geographically localized D3 regime of pure extension. The successive changes in the stress regime were related to a permutation of σ_3 by σ_2 vertical stress between D1 and D2 events, and to a permutation of σ_2 by σ_1 vertical stress between D2 and D3 events (Figure 15).

6.3. Origin of the Extensional Tectonics Localized in the Ocoa Bay

Figure 13 shows the coast of southern central Hispaniola intermittently covered by the fossil coral reef terrace that grew as a fringing reef during MIS 5e/5c stage and currently ranges in elevation from 0 to 20 m above sea level. The MIS 5e stage corresponds to a relatively long period of high-sea level that took place during the 118–128 ka

interval in the Last Interglacial, when the sea level was between 2 and 6 m above the current level (e.g., Schellmann & Radtke, 2004). The existence of coral reef terraces of the MIS 5e/5c stage at elevations between 1 and 25 m above the current sea level can be explained by active tectonics that has uplifted in variable amounts the southeastern margin of Cordillera Central, the Sierra Martín García and the Sierra Bahoruco. Assuming a *Diploria* sp. growth depth of ~ 2 m and an average sea level height during the MIS 5e of +2.0 m (see details in Escuder-Viruete et al. (2020)), the minimum uplift rates for the terrace range between 0.01 and 0.22 m/ka. The absence of the coral terrace, as well as of other coral terraces presumably built up during older MIS stages, can be explained as due to erosion or to being located at elevations below present sea level as a consequence of later subsidence. In our case, the absence of the coral terrace of the MIS 5c/5e stage coincides with the reentrant of the Ocoa Bay affected by D3b extensional tectonics.

Figure 13 also shows two outcrops of the modern fringing reef raised between 0.5 and 3 m above sea level, which are currently subjected to strong marine erosion. An specimen of coral *Diploria* sp. collected in the uppermost levels of the terrace at Playa Caracoles (21JE124 site) have provided an U-Th ages of 0.730 ± 0.01 ka. This age indicates growth of the coral terrace during MIS 1 stage in the Middle Holocene. The calculated minimum uplift rate for the terrace is 4.11 m/ka.

Thus, the spatial distribution of the topography in the Ocoa Bay, the D3b extensional deformation, outcrops of the coral reef terraces and uplift rates are, to the first order, controlled by the subducting Beata Ridge of the Caribbean plate. This is because the Muertos accretionary prism that makes up the margin wedge on the Ocoa Bay must deform around this indenting bathymetric feature. The topographically low area of the Ocoa Bay lines up along the relative plate motion vector with the Beata Ridge indenter. The highest uplift rates are recorded along the central northern coast of the Ocoa Bay and decrease parallel to the trench and perpendicular to the Beata Ridge to the E (southeast coast of the Cordillera Central) and the W (Sierra Martín García).

This pattern in the distribution of the D3b deformation and vertical motions can be interpreted as a wave of rapid uplift followed by subsidence that propagates parallel to the current plate motion vector in the Ocoa Bay, as a response to the subduction of bathymetric irregularities in the Beata Ridge. Following the deformation mechanism proposed for seamount subduction in the New Hebrides and Solomon Arcs (e.g., Taylor et al., 2005), the passage of a subducting bathymetric high produces a history of rapid uplift and subsequent collapse and subsidence in a block of similar dimensions of the upper plate.

Along the Ocoa Bay, where the Beata Ridge indenter currently entering the Muertos Trench, macroscale WNW to W-striking dip-slip normal faults and mesoscale fault-slip data, are consistent with SSW to S-directed extension perpendicular to the margin (Figure 16). These steeply dipping normal faults may be a consequence of the collapse of the margin, constituted by relatively soft sedimentary rocks of the Muertos accretionary prism, in the wake of the stronger mafic igneous rocks of the subducting Beata Ridge that produce a basal erosion of the upper plate (Gardner et al., 2013; Ranero & von Huene, 2000; Sak et al., 2009; Vannucchi et al., 2013). The subvertical and NE-striking faults formed during D2, such as the N-BRFZ and O-OBFZ segments, are arranged at high angles to the margin and may have accommodated differential displacements during D3, acting as transfer faults. Ocoa Bay would therefore be an embayment of ~ 20 km wide and ~ 25 km length, formed by the passage of a bathymetric high in the subducting Beata Ridge. A similar mechanism has been proposed along the northern Hispaniola-Puerto Rico margin, where subduction/collision of bathymetric highs built on the Atlantic oceanic crust has resulted to basal erosion in the upper plate and forearc collapse (Escuder-Viruete and Pérez, 2020; Grindlay et al., 2005).

This interpretation is favored by the absence of the coral terrace of the MIS 5e/5c inboard of the Beata indenter (Figure 13), which must have been uplifted and eroded or sunk by D3b extensional tectonics. In turn, the gravimetric and magnetic anomaly produced by the CLIP magnetic basalts that characterizes the surroundings of Ocoa Bay (Figure 4) suggests a thinning of the upper plate wedge in the submarine portion of the margin. In this tectonic context, the high uplift rates detected in the uplifted modern coral terrace indicate a new episode of rapid uplift and future subsidence of the margin during continued subduction of the Beata Ridge.

Although the role of seamounts/aseismic ridge subduction in the plate-margin seismicity is disputed, for example, enhancing seismic coupling (e.g., Bangs et al., 2015) versus decreasing the degree of coupling and limiting the lateral propagation of megathrust-earthquake rupture planes (e.g., Bonnet et al., 2019), the 1751 earthquake occurred in the vicinity of the Ocoa Bay and destroyed the city of Azua. The presence of the subducting Beata

Table 2
Characteristics of the Main Seismotectonic Structures in Southern Central Hispaniola

Code	Fault/segment name	Deformation mechanism	Maximum estimated magnitude (M_w)	Major known earthquake and magnitude (M_w)	Estimated displacement rate ^a	Length ^b	Azimuth and dip of fault zone ^b	Width of fault zone ^b (km)
S-OBFZ	Southern Ocoa-Bonao-La Guacara Fault Zone	Right-lateral strike-slip	M_{max} 6,5 ($\pm 0,5$)	Unknown	0.4 (± 0.2) mm/yr	60 (± 10) km	N010°E to N030° E, subvertical dip	10 \pm 5
C-OBFZ	Central Ocoa-Bonao-La Guacara Fault Zone	Oblique reverse	M_{max} 6,5 ($\pm 0,5$)	Unknown	0.4 (± 0.2) mm/yr	50 (± 10) km	N160°E to N010° E, subvertical dip to 40° (± 15) W	10 \pm 5
W-OBFZ	Western Ocoa-Bonao-La Guacara Fault Zone	Left-lateral oblique reverse to strike-slip	M_{max} 6,0 ($\pm 1,0$)	1562 earthquake?	0.2 (± 0.1) mm/yr	90–120 km	N100°E to N150° E, 45° (± 15) SW to subvertical dip	5 \pm 2
S-HFZ	Southern Hispaniola Fault Zone	Right-lateral strike-slip?	M_{max} 7.1 (± 0.3)	Unknown	<0.2 mm/yr	50–70 km	N140°E (± 15), subvertical dip	10 \pm 5
E-MAFZ	Eastern Sierra de Neiba-Matheux thrust	Left-lateral oblique reverse to thrust	M_{max} 5.8 (± 0.3)	1942 (M_w 5.8)	0.2 mm/yr	segments of 30 (± 5) km	N120°S (± 15), 65° (± 10) N	15 \pm 5
S-JPFZ	Southern San Juan—Pozos Fault Zone	Left-lateral oblique reverse to thrust	M_{max} 6.5 (± 0.5)	1911 (M_w 6.7)	1.5 (± 1.5) mm/yr	>250 km, including segments and imbrications	N130°E (± 15), 45° (± 15) NE	7 \pm 5
BAFZ	Bahoruco Fault Zone or Barahona Thrust	Reverse	M_{max} 7.0 (± 0.6)	1963, M_w 5.7; FD 9 km	0.2 mm/yr	50–85 km, including segments and imbrications	N100°E (± 15), 50° (± 15) S	7 \pm 5
E-EPGFZ	Eastern Enriquillo-Plantain Garden Fault Zone	Left-lateral strike-slip to oblique reverse	M_{max} 7.3 (± 0.3)	1751 (M_w 7.5)?, 2010 (M_w 7.0)	8.3 (± 2.0) mm/yr	80 (± 10) km	N080°E (± 10), subvertical dip	10 \pm 5
N-BRFZ	Northern Beata Ridge Fault Zone	Left-lateral strike-slip to reverse	M_{max} 6.5 (± 0.1), recorded: 4.3 (12/09/2005) and 4.1 (12/10/2013)	1751 (M_w 7.5–8.0)?, 1691?	0.2 mm/yr, probably	60 (± 5) km	N040°E (± 10), subvertical dip	10 \pm 5
C-BRFZ	Central Beata Ridge Fault Zone	Left-lateral strike-slip to normal dip-slip	M_{max} 6.5 (± 0.1), recorded: 4.3 (12/09/2005) and 4.1 (12/10/2013)	1751 (M_w 7.5–8.0)?, 1691?	0.2 mm/yr, probably	100 (± 5) km	N030°E (± 10), 70° (± 15) E to subvertical dip	10 \pm 5
W-MT	Western Muertos Trough	Reverse to oblique reverse	M_{max} 7.5 (± 0.5)	1673 (M_w 7.3)?; 1691 (M_w 7.7)?; 1751 (M_w 7.5–8.0)?	6.2 (± 1.0) mm/yr	170 km	N100°E (± 5), 12° (± 5) northward dip	20 \pm 15
W-DEEP-MT	Western Muertos Trough, deep part	Reverse to oblique reverse	M_{max} 7.5 (± 0.5)	1673 (M_w 7.3)?; 1691 (M_w 7.7)?; 1751 (M_w 7.5–8.0)?	6.2 (± 1.0) mm/yr	170 km	N100°E (± 5), 40° (± 5) northward dip	20 \pm 15
O-MT	Muertos Trough, Ocoa Bay part	Reverse to oblique reverse	M_{max} 7.5 (± 0.5)	1751 (M_w 7.5–8.0)?	6.2 (± 1.0) mm/yr	40 km	N135°E (± 5), 15° (± 5) northward dip	20 \pm 15

^aDerived from geological mapping (SYSMIN Project, 2010; Escuder-Viruete, 2022; this work), geodetic GPS measurements (Calais et al., 2002; Manaker et al., 2008) and empirical relationships (e.g., Wells & Coppersmith, 1994). ^bDerived from geological mapping (Bertil et al., 2015; Escuder-Viruete, 2022; Escuder-Viruete et al., 2023; SYSMIN Project, 2010; Terrier-Sedan & Bertil, 2021; this work).

Ridge in high-resolution bathymetric swath maps of the Caribbean-Hispaniola plate boundary region and in seismic reflection profiles across the Muertos Trench (e.g., Granja Bruña et al., 2014), together with the proposed location of the Azua earthquake intensity center in the Ocoa Bay (Bakun et al., 2012), suggest that this $M_w = 7.5$ event may have resulted from the rupture of a ridge asperity in the subduction and can therefore be repeated in the future.

6.4. Definition of Seismotectonic Structures in Southern Central Hispaniola

The characterization of seismotectonic structures has been previously carried out in some sectors of Hispaniola Island (Bertil et al., 2015; Escuder-Virueite et al., 2020; Frankel et al., 2011; Terrier-Sedan & Bertil, 2021). Used criteria in the definition were: geodynamic situation; geological, stratigraphic and/or tectonic evidence of recent activity; kinematic type of fault and rate of displacement; and associated historical and/or instrumental seismicity. The definition of these large-scale active structures is critical since it allows for establishing seismotectonic zonation models of the area under consideration, which is fundamental for the quantitative seismic hazard assessment. However, this approach requires updating the inventory of active structures as tectonic and seismological knowledge increases.

The previous works and the new data presented in this work allow updating the main seismotectonic fault zones structures in southern central Hispaniola, including its adjacent offshore sector. They are: San Juan-Pozos (Mann, Draper, & Lewis, 1991); Matheux-Sierra de Neiba (MAFZ, Hernáiz-Huerta et al., 2007a, 2007b); Bahoruco (BAFZ or Barahona Thrust; Rodríguez et al., 2018); Beata Ridge (Mauffret & Leroy, 1999); MT (Granja Bruña et al., 2009, 2014); Ocoa-Bonao-La Guacara (Escuder-Virueite et al., 2023; Pérez-Estaún et al., 2007); and probably the eastern end of the Enriquillo-Plantain Garden (EPGFZ; Mann et al., 1995).

The attribute compilation of these seismotectonic structures is outlined in Table 2, including the fault or segment name, deformation mechanism, estimated maximum magnitude (M_w), known biggest earthquake (magnitude in M_w), estimated displacement rate, length, strike and dip, and width of the fault zone. Following Bertil et al. (2015), the maximum magnitude of rupture for each fault/segment was estimated using the major recorded historical earthquake (Terrier-Sedan & Bertil, 2021), or its geometric parameters (e.g., Wells & Copper-smith, 1994), taking into account its degree of uncertainty. Displacement rates for each seismogenic structure were derived from geological mapping (Escuder-Virueite, 2022; Escuder-Virueite et al., 2023; SYSMIN Project; this work), geodetic GPS measurements (Calais et al., 2002; Manaker et al., 2008), or calculated in the present study through empirical relationships (e.g., Wells & Coppersmith, 1994).

From this information, a simplified seismotectonic model was built that considers two types of seismic sources: subduction and strike-slip fault zones in which the seismicity of greater magnitude is concentrated; and superficial/upper crustal areas located between them where the seismicity is of moderate to low magnitude and is more homogeneously distributed. This seismotectonic model is the starting point for the seismic hazard assessment in southern central Hispaniola presented below.

6.5. Seismic Hazard Assessment in Southern Central Hispaniola

The seismic hazard assessment carried out in this work follows a probabilistic approach. Following the Cornell-McGuire methodology, the R-CRISIS calculation code (Ordaz et al., 2014) builds a probabilistic model that takes into account the spatial distribution of seismogenic sources, the occurrence and magnitude of earthquakes in time, and the attenuation characteristics of the strong motion in the ground. Thus, the R-CRISIS code computes the seismic hazard in terms of the probability of exceeding a PGA value for a specific site in a given period.

For the seismic hazard assessment in southern Central Hispaniola, the previously described seismotectonic zonation model composed of subduction zones, main strike-slip fault zones and diffuse seismogenic zones located between them, was geometrically built as simplified 3-D polygonal surfaces of specific width. In these seismic sources, earthquakes can occur at any point of the source with equal probability (Ordaz et al., 2014). Functions selected to describe the attenuation of the ground motion acceleration with distance from the source are the same as those used by Frankel et al. (2011) and Benito et al. (2012) to evaluate the seismic hazard in Haiti after the 12 October 2010 earthquake. Parameters used to establish the seismic activity of each source and their uncertainties are included in Escuder-Virueite et al. (2020). The hazard analysis performed in this work did not take into account possible amplifications of the seismic parameters by site effects. Seismic hazard was computed in a rectangular

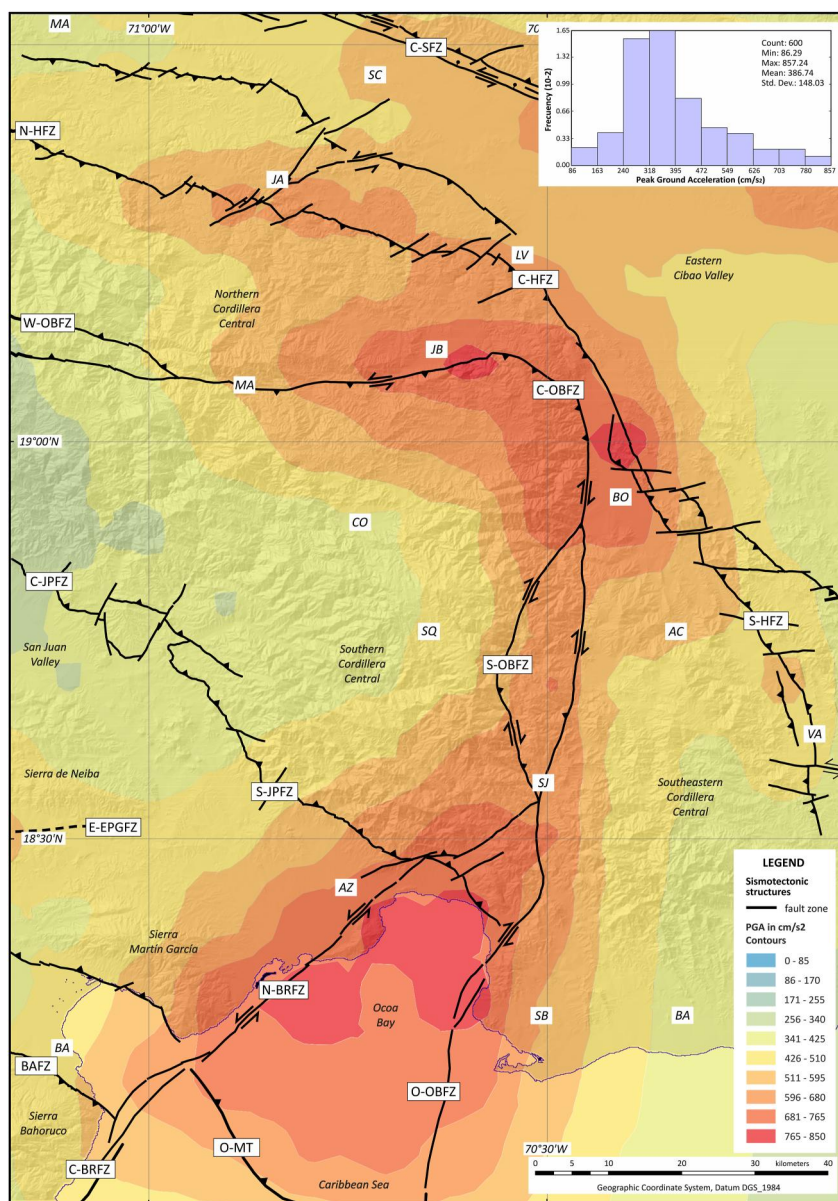


Figure 17. Result of the probabilistic seismic hazard modeling in southern central Hispaniola, as well as adjacent offshore sectors of the Ocoa Bay, expressed as iso-peak ground acceleration zones (in cm/s^2) for a return period of 475 years (i.e., an exceedance probability of 10% in 50 years). The modelled area is the same of Figure 3 and framed by a discontinuous red box in Figure 2. Figure also includes the trace of the main seismogenic structures described in Table 2. MDT. Shaded relief and acronyms as in Figure 3. See text for explanation.

point grid, framed by the coordinates: 17.960° and 18.835°N of latitude; -70.175° and -71.250°W of longitude (WGS-84 projection system), with a point spacing of 0.025° in both directions. Results were converted in a continuous surface using an inverse distance squared weighted interpolation algorithm.

Figure 17 includes the results of the seismic hazard assessment in southern central Hispaniola, expressed as PGA intervals (values in cm/s^2) and for a return period of 475 years (i.e., for a probability of exceedance of 10% in 50 years). Modeled minimum and maximum PGA values are 86 and 857 cm/s^2 , respectively, with a mean (and standard deviation) of 386.7 (148.0). Therefore, the regional seismic hazard values range from low to very high. PGA zoning defines an elongated pattern sub-parallel to the main fault zones. Seismic hazard is higher in the Ocoa Bay, along the San José de Ocoa valley in the southern Cordillera Central, and in the topographic transition between the northern Cordillera Central and the eastern Cibao Valley. It decreases toward the NW and SE regions.

This seismic hazard zoning contrasts with the previously proposed by Frankel et al. (2011), Benito et al. (2012), and Bertil et al. (2010, 2015), which did not take into account all the seismic sources included in the present work, particularly the Ocoa-Bonao-La Guácara fault zone.

With this seismotectonic model, the highest PGA values ($>600 \text{ cm/s}^2$) are associated with the N-BRFZ, O-OBZF and C-OBZF segments. Branches of the S-OBZF segment set intermediate to high values ($500\text{--}650 \text{ cm/s}^2$). The C-OBZF segment also has associated high PGA values ($>650 \text{ cm/s}^2$), which decrease to intermediate and low values westward along the W-OBZF segment ($250\text{--}450 \text{ cm/s}^2$). The superficial trace of the O-MT segment of the MT also has associated high PGA values (600 cm/s^2), which extend into depth following the subduction interface. The BAFZ has associated intermediate PGA values in its connection to the BRFZ, which also decrease westward. The S-JPFZ presents high PGA values at its SE end ($500\text{--}700 \text{ cm/s}^2$), where it is displaced by the N-BRFZ, decreasing toward the NW. The HFZ has also been included in the modeling, giving rise to intermediate values of the PGA that become high in its central segment. The E-EPGFZ segment also has associated intermediate to low PGA values ($400\text{--}500 \text{ cm/s}^2$).

In summary, the highest PGA values in southern central Hispaniola are associated with N-BRFZ, O-OBGFZ and A-MT segments, whose traces frame a triangular zone centered on Ocoa Bay where the seismic hazard is very high. As described, this sector includes the intensity center estimated for the 1751 Azua earthquake (M_w 7.5), which according to some historical accounts gave rise to a tsunami in the bay. For Bakun et al. (2012), this event could be produced by the Enriquillo-Platain Garden fault zone or, as an alternative source, the Muertos deformation belt. The results of the PGA modeling rule out the EPGFZ as a source and indicate that the BRFZ, the O-MT and, less likely, the O-OBZF, could have generated this earthquake.

Historical records indicate that the greatest effects of the 1615, 1684, 1691 and 1911 earthquakes (M_w from 6.0 to 7.5) were in the southern sector of the Central Cordillera. However, the determination of its seismic source could not be confidently established with the available data, since these strong earthquakes did not produce known surface ruptures. Future neotectonic and paleoseismological studies, together with the seismic hazard modeling, may shed light on the active fault zones that generated large earthquakes in the region and therefore allow updating the spatial distribution of the seismic hazard.

7. Conclusions

The characterization of active tectonics and the main seismotectonic faults in southern central Hispaniola was developed from tectonic and geomorphologic field observations, the regional gravimetric and magnetic data interpretation, and the inversion of fault-slip data. The main conclusions of this work are:

1. A relatively constant NE-directed shortening controlled the geometry and kinematics of main active faults in central southern Hispaniola, as well as the evolution of the Quaternary stress regime.
2. Quaternary stress regime evolution includes a compressional D1 event, which gave rise to the large-scale fold and thrust structure in the Cordillera Central, PB, Sierra Martín García and San Juan-Azua basin.
3. D1 was followed by a strike-slip D2 stress regime, partitioned into the N-S to NE-SW transverse Ocoa-Bonao-La Guácara and Beata Ridge fault zones, which are related to indentation of the Beata Ridge in southern Hispaniola from the Early to Middle Pleistocene and continues today.
4. D2 was coeval by a more heterogeneous and geographically localized D3 extensional deformation.
5. Several seismotectonic fault zones divide the region into a set of simplified seismogenic zones.
6. Modeled highest PGA values establish a very high seismic hazard. in the Ocoa Bay.

Data Availability Statement

The data for this paper are contained in the text, figures, and the Supporting Information, and can also be found in the data repository DIGITAL.CSIC, which is the institutional repository of the Spanish National Research Council (Escuder-Viruet et al., 2024, <https://doi.org/10.20350/digitalCSIC/16112>).

References

- Alonso, J. L., Marcos, A., Villa, E., Suárez, A., Merino-Tomé, O. A., & Fernández, L. P. (2014). Mélanges and other types of block-in-matrix formations in the Cantabrian Zone (Variscan Orogen, northwest Spain): Origin and significance. *International Geology Review*, 57(5–8), 563–580. <https://doi.org/10.1080/00206814.2014.950608>

Acknowledgments

We would like to thank the support and infrastructures provided by the Servicio Geológico Nacional of the Dominican Republic, particularly to Yésica Pérez-Alejandro, María Betania Roque-Quezada and Edwin García. Detailed and constructive reviews made by Grenville Draper and Mark B. Gordon, as well as the editorial work by Yamirka Rojas-Agramonte and Claudio Faccenna, significantly improved the manuscript. The research was funded through PID2019-105625RB-C22 project of the MCIN/AEI/10.13039/501100011033 of the Spanish Government. Some works also received funding from the DR-T 1190 Project of the Banco Interamericano de Desarrollo (World Bank) and the FONDOCYT project 2015-1b3-118 of the MESCYT of the Dominican Republic Government.

- Alvarez, L., Chuy, T., García, J., Moreno, B., Álvarez, H., Blanco, M., et al. (1999). *An earthquake catalogue of Cuba and neighboring areas*. Internal Report IC/IE/99/1 (p. 62). The Abdus Salam International Centre for Theoretical Physics.
- Angelier, J. (1994). Fault slip analysis and paleostress reconstruction. In P. Hancock (Ed.), *Continental deformation* (pp. 53–100). Pergamon Press.
- Ayala, C., García-Lobón, J. L., Escuder-Viruet, J., Rey-Moral, C., Pérez-Estaún, A., & Padín-Debén, A. (2017). High-resolution magnetic, regional gravity and petrophysical characterization of the Dominican Republic tectonic domains with special focus on the Central Cordillera. *Boletín Geológico y Minero*, 128(3), 611–631. <https://doi.org/10.21701/bolgeomin.128.3.005>
- Bakun, W. H., Flores, C. H., & Uri, S. (2012). Significant earthquakes on the Enriquillo fault system, Hispaniola, 1500–2010: Implications for seismic hazard. *Bulletin of the Seismological Society of America*, 102(1), 18–30. <https://doi.org/10.1785/0120110077>
- Bangs, N. L., McIntosh, K. D., Silver, E. A., Kluesner, J. W., & Ranero, C. R. (2015). Fluid accumulation along the Costa Rica subduction thrust and development of the seismogenic zone. *Journal of Geophysical Research: Solid Earth*, 120(1), 67–86. <https://doi.org/10.1002/2014jb011265>
- Benford, B., Demets, C., & Calais, E. (2012). GPS estimates of microplate motions, northern Caribbean: Evidence for a Hispaniola microplate and implications for earthquake hazard. *Geophysical Journal International*, 191(2), 481–490. <https://doi.org/10.1111/j.1365-246x.2012.05662.x>
- Benito, O. B., Cervera, B. J., Molina, P. S., Navarro, B. M., Doblas, L. M., Martínez, D. J., & others (2012). *Évaluation de l'âge et du risque sismique en Haïti dirigée vers la conception parasismique*. Monografía ETSI en Topografía, Geodesia y Cartografía (p. 137). Universidad Politécnica de Madrid. Retrieved from <http://oa.upm.es/view/finstitucion/Topografia/>
- Bertil, D., Lemoine, A., Winter, T., & Belvaux, M. (2010). *Microzonificación sísmica de Santiago – República Dominicana. Amenaza regional*. Informe final, BRGM/RC-59107-FR (p. 100). Bureau de Recherches Géologiques et Minières.
- Bertil, D., Terrier, M., & Belvaux, M. (2015). *Análisis de las fuentes sísmicas y evaluación de la amenaza sísmica regional del gran Santo Domingo. Estudio de la amenaza sísmica y vulnerabilidad física del Gran Santo Domingo*. Informe Actividad, BRGM/RP-65305-FR (p. 149). Bureau de Recherches Géologiques et Minières.
- Bonnet, G., Agard, P., Angiboust, S., Fournier, M., & Omrani, J. (2019). No large earthquakes in fully exposed subducted seamount. *Geology*, 47(5), 407–410. <https://doi.org/10.1130/g45564.1>
- Byrne, D. B., Suarez, G., & McCann, W. R. (1985). Muertos Trough subduction, microplate tectonics in the northern Caribbean? *Nature*, 317(6036), 420–421. <https://doi.org/10.1038/317420a0>
- Calais, E., Freed, A., Mattioli, G., Amelung, F., Jonsson, S., Jansma, P., et al. (2010). Transpressional rupture of an unmapped fault during the 2010 Haiti earthquake. *Nature Geoscience*, 3(11), 1–6. <https://doi.org/10.1038/ngeo992>
- Calais, E., Mazabraud, Y., de Lépinay, M., Mann, P., Mattioli, G., & Jansma, P. (2002). Strain partitioning and fault slip rates in the northeastern Caribbean from GPS measurements. *Geophysical Research Letters*, 29(18), 1856. <https://doi.org/10.1029/2002gl015397>
- Calais, E., Smithe, S., Mercier de Lépinay, B. M., & Prépetit, C. (2016). Plate boundary segmentation in the northeastern Caribbean from geodetic measurements and Neogene geological observations. *Comptes Rendus Geoscience*, 348(1), 42–51. <https://doi.org/10.1016/j.crte.2015.10.007>
- Célérier, B., Etchecopar, A., Bergerat, F., Vergely, P., Arthaud, F., & Laurent, P. (2012). Inferring stress from faulting: From early concepts to inverse methods. *Tectonophysics*, 581, 206–219. <https://doi.org/10.1016/j.tecto.2012.02.009>
- Cheng, H., Edwards, R. L., Hoff, J., Gallup, C. D., Richardsm, D. A., & Asmerom, Y. (2000). The half-lives of uranium-234 and thorium-230. *Chemical Geology*, 169(1–2), 17–33. [https://doi.org/10.1016/s0009-2541\(99\)00157-6](https://doi.org/10.1016/s0009-2541(99)00157-6)
- Corbeau, J., Gonzalez, O. L., Clouard, V., Rolandone, F., Leroy, S., Keir, D., et al. (2019). Is the local seismicity in western Hispaniola (Haiti) capable of imaging northern Caribbean subduction? *Geosphere*, 15(6), 1738–1750. <https://doi.org/10.1130/GES02083.1>
- Corbeau, J., Rolandone, F., Leroy, S., de Lépinay, B. M., Meyer, B., Ellouz-Zimmermann, N., & Momplaisir, R. (2016). The northern Caribbean plate boundary in the Jamaica Passage: Structure and seismic stratigraphy. *Tectonophysics*, 675, 209–226. <https://doi.org/10.1016/j.tecto.2016.03.022>
- Corbeau, J., Rolandone, F., Leroy, S., Guerrier, K., Keir, D., Stuart, G., et al. (2017). Crustal structure of the western Hispaniola (Haiti) from teleseismic receiver function study. *Tectonophysics*, 709, 9–19. <https://doi.org/10.1016/j.tecto.2017.04.029>
- Díaz de Neira, J. A. (2000). Evolución geomorfológica del Llano de Azua (Sur de la República Dominicana). *Acta Geológica Hispánica*, 37, 207–227.
- Díaz de Neira, J. A. (2004). *Mapa Geológico de la Hoja a E. 1:50.000 n° 5970-1 (Barahona)* (p. 68). Dirección General de Minería. Retrieved from <https://www.sgn.gob.do>
- Díaz de Neira, J. A., & Solé Pont, F. J. (2002). Precisiones estratigráficas sobre el Neógeno de la cuenca de Azua (República Dominicana). *Acta Geologica Hispanica*, 37, 163–181.
- Dolan, J., Mann, P., De Zoeten, R., Heubeck, C., & Shiroma, J. (1991). Sedimentologic, stratigraphic, and tectonic synthesis of Eocene-Miocene sedimentary basins, Hispaniola and Puerto Rico. In P. Mann, G. Draper, & J. F. Lewis (Eds.), *Geologic and Tectonic Development of the North America-Caribbean Plate Boundary in Hispaniola* (Vol. 262, pp. 17–26). Geological Society of America Special Paper.
- Dolan, J. F., Mullins, H. T., & Wald, D. J. (1998). Active tectonics of the north-central Caribbean region: Oblique collision, strain partitioning and opposing slabs. In J. Dolan & P. Mann (Eds.), *Active Strike-Slip and Collisional Tectonics of the Northern Caribbean Plate Boundary in Hispaniola* (Vol. 326, pp. 1–61). Geological Society America Special Paper.
- Dominguez, S., Malavieille, J., & Lallemand, S. E. (2000). Deformation of accretionary wedges in response to seamount subduction: Insights from sandbox experiments. *Tectonics*, 19(1), 182–196. <https://doi.org/10.1029/1999tc000055>
- Draper, G., Mann, P., & Lewis, J. F. (1994). Hispaniola. In S. K. Donovan & T. A. Jackson (Eds.), *Caribbean Geology: An introduction*. Jamaica (pp. 129–150). University of the West Indies Publishers Association.
- Driscoll, N. W., & Diebold, J. B. (1998). Deformation of the Caribbean region: One plate or two? *Geology*, 26(11), 1043–1046. [https://doi.org/10.1130/0091-7613\(1998\)026<1043:dotcro>2.3.co;2](https://doi.org/10.1130/0091-7613(1998)026<1043:dotcro>2.3.co;2)
- Dürkefelden, A., Hoernle, K., Hauff, F., Wartho, J. A., van den Bogaard, P., & Werner, R. (2019). Age and geochemistry of the Beata Ridge: Primary formation during the main phase (~89 Ma) of the Caribbean Large Igneous Province. *Lithos*, 328–329, 69–87. <https://doi.org/10.1016/j.lithos.2018.12.021>
- Ekström, G., Nettles, M., & Dziewonski, A. M. (2012). The global CMT project 2004–2010: Centroid-moment tensors for 13,017 earthquakes. *Physics of the Earth and Planetary Interiors*, 200–201, 1–9. <https://doi.org/10.1016/j.pepi.2012.04.002>
- Escuder Viruete, J. (2022). *Microzonificación sísmica y escenario de daños en los cascos urbanos de Barahona y Jimaní: Neotectónica, Sismotectónica y Modelización de la Amenaza Sísmica*. Fortalecimiento del Sistema Nacional de la Gestión de Riesgo de Desastre (DR-T 1190), República Dominicana. Informe Final (p. 153). Banco Interamericano de Desarrollo, World Bank. 6 Anexos.
- Escuder-Viruet, J., & Baumgartner, P. O. (2014). Structural evolution and deformation kinematics of a subduction-related serpentinite-matrix mélange, Santa Elena Peninsula, northwest Costa Rica. *Journal of Structural Geology*, 66, 356–381. <https://doi.org/10.1016/j.jsg.2014.06.003>

- Escuder Viruete, J., Beranoaguirre, A., Valverde-Vaquero, P., & McDermott, F. (2020). Quaternary deformation and uplift of coral reef terraces produced by oblique subduction and underthrusting of the Bahama Platform below the northern Hispaniola forearc. *Tectonophysics*, *796*, 228631. <https://doi.org/10.1016/j.tecto.2020.228631>
- Escuder-Viruete, J., Fernández, F. J., Pérez Valera, F., & McDermott, F. (2024). Active tectonics, Quaternary stress regime evolution and seismotectonic faults in southern central Hispaniola: Implications for the quantitative seismic hazard assessment [Dataset]. DIGITAL.CSIC repository. <https://doi.org/10.20350/digitalCSIC/16112>
- Escuder-Viruete, J., Fernández, F. J., Pérez Valera, F., & Medialdea, A. (2023). Present-day accommodation of Caribbean-North American oblique plate convergence through the Ocoa-Bonao-La Guacara fault zone, southern central Hispaniola: A transition zone between oceanic subduction and arc-oceanic plateau collision. *Tectonics*, *42*(4), e2022TC007618. <https://doi.org/10.1029/2022TC007618>
- Escuder-Viruete, J., Joubert, M., Abad, M., Pérez-Valera, F., & Gabites, J. (2016). The basaltic volcanism of the Dumisseau Formation in the Sierra de Bahoruco, SW Dominican Republic: A record of the mantle plume-related magmatism of the Caribbean large Igneous Province. *Lithos*, *254–255*, 67–83. <https://doi.org/10.1016/j.lithos.2016.03.013>
- Escuder-Viruete, J., Joubert, M., Urien, P., Friedman, R., Weis, D., Ullrich, T., & Pérez-Estaún, A. (2008). Caribbean island-arc rifting and back-arc basin development in the Late Cretaceous: Geochemical, isotopic and geochronological evidence from Central Hispaniola. *Lithos*, *104*(1–4), 378–404. <https://doi.org/10.1016/j.lithos.2008.01.003>
- Escuder-Viruete, J., & Pérez, Y. (2020). Neotectonic structures and stress fields associated with oblique collision and forearc sliver formation in northern Hispaniola: Implications for the seismic hazard assessment. *Tectonophysics*, *784*, 228452. <https://doi.org/10.1016/j.tecto.2020.228452>
- Escuder-Viruete, J., Pérez-Estaún, A., Booth-Rea, G., & Valverde-Vaquero, P. (2011). Tectonometamorphic evolution of the Samaná complex, northern Hispaniola: Implications for the burial and exhumation of high-pressure rocks in a collisional accretionary wedge. *Lithos*, *125*(1–2), 190–210. <https://doi.org/10.1016/j.lithos.2011.02.006>
- Escuder-Viruete, J., Pérez-Estaún, A., Gabites, J., & Suárez-Rodríguez, Á. (2011). Structural development of a high-pressure collisional accretionary wedge: The Samaná complex, northern Hispaniola. *Journal of Structural Geology*, *33*(5), 928–950. <https://doi.org/10.1016/j.jsg.2011.02.006>
- Escuder-Viruete, J., Suárez, A., Gabites, J., & Pérez-Estaún, A. (2016). The Imbert Formation of northern Hispaniola: A tectono-sedimentary record of arc-continent collision and ophiolite emplacement in the northern Caribbean accretionary prism. *Solid Earth Discussions*, *6*, 1–50.
- Escuder-Viruete, J., Valverde-Vaquero, P., Rojas-Agramonte, Y., Gabites, J., & Pérez-Estaún, A. (2013). From intra-oceanic subduction to arc accretion and arc-continent collision: Insights from the structural evolution of the Río San Juan metamorphic complex, northern Hispaniola. *Journal of Structural Geology*, *46*, 34–56. <https://doi.org/10.1016/j.jsg.2012.10.008>
- Fankhauser, A., McDermott, F., & Fleitmann, D. (2016). Episodic speleothem deposition tracks the terrestrial impact of millennial-scale last glacial climate variability in SW Ireland. *Quaternary Science Review*, *152*, 104–117. <https://doi.org/10.1016/j.quascirev.2016.09.019>
- Flores, C. H., ten Brink, U. S., & Bakun, W. H. (2011). Accounts of damage from historical earthquakes in the northeastern Caribbean, to aid in the determination of their location and intensity magnitudes. *U.S. Geological Survey Open File Report 2011–1133* (p. 226).
- Frankel, A., Harmsen, S., Mueller, C., Calais, E., & Haase, J. (2011). Seismic hazard maps for Haiti. *Earthquake Spectra*, *27*(S1), S23–S41. <https://doi.org/10.1193/1.3631016>
- García-Lobón, J. L., & Ayala, C. (2007). Cartografía geofísica de la República Dominicana: Datos de densidad, susceptibilidad magnética y magnetización remanente. *Boletín Geológico y Minero*, *118*(2), 175–194.
- García Lobón, J. L., & Rey Moral, C. (2004). Magnetismo y radiación gamma natural de la República Dominicana. *Boletín Geológico y Minero*, *115*(1), 153–168.
- Gardner, T. W., Fisher, D. M., Morell, K. D., & Cupper, M. L. (2013). Upper-plate deformation in response to flat slab subduction inboard of the aseismic Cocos Ridge, Osa Peninsula, Costa Rica. *Lithosphere*, *5*(3), 247–264. <https://doi.org/10.1130/L251.1>
- Granja Bruña, J. L., Carbó-Gorosabel, A., Llanes Estrada, P., Muñoz-Martín, A., ten Brink, U. S., Gómez Ballesteros, M., et al. (2014). Morphostructure at the junction between the Beata ridge and the Greater Antilles island arc (offshore Hispaniola southern slope). *Tectonophysics*, *618*, 138–163. <https://doi.org/10.1016/j.tecto.2014.02.001>
- Granja Bruña, J. L., ten Brink, U. S., Carbó-Gorosabel, A., Muñoz-Martín, A., & Gómez Ballesteros, M. (2009). Morphotectonics of the central Muertos thrust belt and Muertos Trough (northeastern Caribbean). *Marine Geology*, *263*(1–4), 7–33. <https://doi.org/10.1016/j.margeo.2009.03.010>
- Grindlay, N. R., Mann, P., Dolan, J. F., & van Gestel, J. P. (2005). Neotectonics and subsidence of the northern Puerto Rico–Virgin Islands margin in response to the oblique subduction of high-standing ridges. *Geological Society American Special Paper*, *385*, 31–60.
- Hernández-Huerta, P. P., Díaz de Neira, J. A., García Senz, J., Deschamps, I., Genna, A., Nicole, N., et al. (2007a). La estructura de la sierra de Neiba, margen norte de la sierra de Bahoruco, Sierra de Martín García y cuenca de Enriquillo de la República Dominicana: Un ejemplo de deformación transpresiva. *Boletín Geológico y Minero*, *118*, 337–357.
- Hernández-Huerta, P. P., Díaz de Neira, J. A., García Senz, J., Deschamps, I., Lopera, E., Escuder Viruete, J., et al. (2007b). La estratigrafía de la Sierra de Neiba, República Dominicana. *Boletín Geológico y Minero*, *118*, 313–336.
- Hernández Huerta, P. P., & Pérez-Estaún, A. (2002). Estructura del cinturón de pliegues y cabalgamientos de Peralta, República Dominicana. *Acta Geológica Hispánica*, *37*, 183–205.
- Heubeck, C., & Mann, P. (1991). Structural geology and Cenozoic tectonic history of the southeastern termination of the Cordillera Central, Dominican Republic. In P. Mann, G. Draper, & J. F. Lewis (Eds.), *Geologic and Tectonic Development of the North America-Caribbean Plate Boundary in Hispaniola* (Vol. 262, pp. 315–336). Geological Society of America Special Paper.
- Heubeck, C., Mann, P., Dolan, J., & Monechi, S. (1991). Diachronous uplift and recycling of sedimentary basins during Cenozoic tectonic transpression, northeastern Caribbean plate margin. *Sedimentary Geology*, *70*, 1–32. [https://doi.org/10.1016/0037-0738\(91\)90063-j](https://doi.org/10.1016/0037-0738(91)90063-j)
- Hibbert, F. D., Rohling, E. J., Dutton, A., Williams, F. H., Chutcharavan, P. M., Mark, C. Z., & Tamisiea, E. (2016). Coral indicators of past sea-level change: A global repository of U-series dated benchmarks. *Quaternary Science Reviews*, *145*, 1–56. <https://doi.org/10.1016/j.quascirev.2016.04.019>
- Jaffey, A. H., Flynn, K. F., Glendenin, L. E., Bentley, W. C., & Essling, A. M. (1971). Precision measurement of half-lives and specific activities of ^{235}U and ^{238}U . *Physical Reviews*, *C*, *4*(5), 1889–1906. <https://doi.org/10.1103/physrevc.4.1889>
- Kamenov, G., Perfit, M., Lewis, J., Goss, A. R., Arévalo, R., & Shuster, R. D. (2011). Ancient lithospheric source for Quaternary lavas in Hispaniola. *Nature Geoscience*, *4*(8), 554–557. <https://doi.org/10.1038/ngeo1203>
- Kroehler, M. E., Mann, P., Escalona, E., & Christeson, G. L. (2011). Late Cretaceous-Miocene diachronous onset of back thrusting along the South Caribbean deformed belt and its importance for understanding processes of arc collision and crustal growth. *Tectonics*, *30*(6), TC6003. <https://doi.org/10.1029/2011tc002918>

- Kumar, S., Agrawal, M., Pulliam, J., Polanco Rivera, E., & Huérfano, V. A. (2020). Crustal thickness and bulk Poisson ratios in the Dominican Republic from receiver function analysis. *Tectonophysics*, 775, 228308. <https://doi.org/10.1016/j.tecto.2019.228308>
- Manaker, D. M., Calais, E., Freed, A. M., Ali, S. T., Przybylski, P., Mattioli, G., et al. (2008). Interseismic plate coupling and strain partitioning in the Northeastern Caribbean. *Geophysical Journal International*, 174(3), 889–903. <https://doi.org/10.1111/j.1365-246x.2008.03819.x>
- Mann, P., Calais, E., Ruegg, J. C., Demets, C., Jansma, P. E., & Mattioli, G. S. (2002). Oblique collision in the northeastern Caribbean from GPS measurements and geological observations. *Tectonics*, 21(6), 1–23. <https://doi.org/10.1029/2001tc001304>
- Mann, P., Draper, G., & Lewis, J. F. (1991). An overview of the geologic and tectonic development of Española. In P. Mann, G. Draper, & J. F. Lewis (Eds.), *Geologic and Tectonic Development of the North America-Caribbean Plate Boundary in Hispaniola* (Vol. 262, pp. 1–28). Geological Society of America Special Paper.
- Mann, P., McLaughlin, P. P., Jr., & Cooper, J. C. (1991). Geology of the Enriquillo-Azua basins, Dominican Republic, 2. Structure and tectonics. In P. Mann, G. Draper, & J. F. Lewis (Eds.), *Geologic and Tectonic Development of the North America-Caribbean Plate Boundary in Hispaniola* (Vol. 262, pp. 367–389). Geological Society of America Special Paper.
- Mann, P., Rogers, R., & Gahagan, L. (2007). Overview of plate tectonic history and its unresolved tectonic problems. In J. Bundschuh & G. E. Alvarado (Eds.), *Central America: Geology, Resources and Hazards* (Vol. 1, pp. 201–237). Taylor and Francis/Balkema.
- Mann, P., Taylor, F. W., Edwards, R. L., & Ku, T. L. (1995). Actively evolving microplate formation by oblique collision and sideways motion along strike-slip faults: An example from the northeastern Caribbean plate margin. *Tectonophysics*, 246(1–3), 1–69. [https://doi.org/10.1016/0040-1951\(94\)00268-e](https://doi.org/10.1016/0040-1951(94)00268-e)
- Mauffret, A., & Leroy, S. (1999). Neogene intraplate deformation of the Caribbean plate at the Beata Ridge. In P. Mann (Ed.), *Sedimentary Basins of the World, Caribbean Basins* (Vol. 4, pp. 627–669). Elsevier Science.
- Mauffret, A., Leroy, S., Vila, J. M., Hallot, E., Mercier de Lépinay, B., & Duncan, R. A. (2001). Prolonged magmatic and tectonic development of the Caribbean Igneous Province revealed by a diving submersible survey. *Marine Geophysical Research*, 22(1), 17–45. <https://doi.org/10.1023/a:1004873905885>
- McCann, W. R., Feldman, L., & McCann, M. (2011). Catalog of felt earthquakes for Puerto Rico and neighboring islands 1492–1899 with additional information for some 20th century earthquakes. *Revista Geofísica*, 62, 141–293.
- McLaughlin, P. P., van den Bold, W. A., & Mann, P. (1991). Geology of the Azua and Enriquillo basins, Dominican Republic; 1. Neogene lithofacies, biostratigraphy, biofacies, and paleogeography. In P. Mann, G. Draper, & J. F. Lewis (Eds.), *Geologic and Tectonic Development of the North America-Caribbean Plate Boundary in Hispaniola* (Vol. 262, pp. 337–366). Geological Society of America Special Paper.
- Mercier de Lépinay, B. (1987). *L'évolution géologique de la bordure nord-caribéenne: L'exemple de la transversale de l'île d'Hispaniola (Grandes Antilles)* (Thèse d'Etat) (p. 366). Université Pierre et Marie Curie.
- Mercier de Lépinay, B., Deschamps, A., Klingelhoefer, F., Mazabraud, Y., Delouis, B., Clouard, V., et al. (2011). The 2010 Haiti earthquake: A complex fault pattern constrained by seismologic and tectonic observations. *Geophysical Research Letters*, 38(22), L22305. <https://doi.org/10.1029/2011GL049799>
- Müller, R. D., Cannon, J., Qin, X., Watson, R. J., Gurnis, M., Williams, S., et al. (2018). GPlates: Building a virtual Earth through deep time. *Geochemistry, Geophysics, Geosystems*, 19(7), 2243–2261. <https://doi.org/10.1029/2018GC007584>
- Núñez, D., Córdoba, D., & Kissling, E. (2019). Seismic structure of the crust in the western Dominican Republic. *Tectonophysics*, 773, 228224. <https://doi.org/10.1016/j.tecto.2019.228224>
- Ordaz, M., Cardona, O., Salgado-Gálvez, M. A., Bernal, G., Singh, K., & Zuloaga, D. (2014). Probabilistic seismic hazard assessment at global level. *International Journal of Disaster Risk Reduction*, 10, 419–427. <https://doi.org/10.1016/j.ijdr.2014.05.004>
- Ortner, H., Reiter, F., & Acs, P. (2002). Easy handling of tectonic data: The programs TectonicVB for Mac and TectonicsFP for Window. *Computers & Geosciences*, 28(10), 1193–1200. [https://doi.org/10.1016/s0098-3004\(02\)00038-9](https://doi.org/10.1016/s0098-3004(02)00038-9)
- Pérez-Estaún, A., Hernaiz Huerta, P. P., Lopera, E., Joubert, M., Escuder Viruete, J., Díaz de Neira, A., et al. (2007). Geología de la República Dominicana: De la construcción de arco-isla a la colisión arco-continente. *Boletín Geológico y Minero*, 118, 157–174.
- Pérez-Valera, F. (2010). *Mapa Geológico de la Hoja a E. 1:50.000 n° 6070-I (Sabana Buey)* (p. 96). Dirección General de Minería. Retrieved from <https://www.sgn.gob.do>
- Pindell, J., & Kennan, L. (2009). Tectonic evolution of the Gulf of Mexico, Caribbean and northern South America in the mantle reference frame: An update. In K. James, M. A. Lorente, & J. Pindell (Eds.), *The geology and evolution of the region between North and South America* (Vol. 328, pp. 1–55). Geological Society of London Special Publication.
- Prentice, C. S., Mann, P., Crone, A. J., Gold, R. D., Hudnut, K. W., Briggs, R. W., et al. (2010). Seismic hazard of the Enriquillo–Plantain Garden fault in Haiti inferred from palaeoseismology. *Nature Geoscience*, 3(11), 789–793. <https://doi.org/10.1038/ngeo991>
- Pubellier, M., Mauffret, A., Leroy, S., Vila, J. M., & Amilcar, H. (2000). Plate boundary readjustment in oblique convergence: Example of the Neogene of Hispaniola, Greater Antilles. *Tectonics*, 19(4), 630–648. <https://doi.org/10.1029/2000tc90007>
- Ramírez, M. I. (1995). *Neotectonic structures and paleostress in the Azua region, south-central Hispaniola*. In *Master of Science in Geology* (p. 144). Florida International University.
- Ranero, C. R., & von Huene, R. (2000). Subduction erosion along the Middle America convergent margin. *Nature*, 404(6779), 748–752. <https://doi.org/10.1038/35008046>
- Reiter, F., & Acs, P. (2000). TectonicsFP 1.6 [Software]. Computer Software for Structural Geology. Operating Manual, 48. <https://github.com/freiter/TectonicsFP/blob/master/Tectfp32.dsk>
- Révilion, S., Hallot, E., Arndt, N., Chauvel, C., & Duncan, R. A. (2000). A complex history for the Caribbean Plateau: Petrology, geochemistry, and geochronology of the Beata Ridge, South Hispaniola. *Journal of Geology*, 108(6), 641–661. <https://doi.org/10.1086/317953>
- Rodríguez, J., Havskov, J., Botter Sorebseb, M., & Santos, L. F. (2018). Seismotectonics of south-west Dominican Republic using recent data. *Journal of Seismology*, 22(4), 883–896. <https://doi.org/10.1007/s10950-018-9738-9>
- Rodríguez-Zurrero, A., Granja-Bruña, J. L., Carbó-Gorosabel, A., Muñoz-Martín, A., Gorosabel-Araus, J. M., Gómez de la Peña, L., et al. (2019). Submarine morpho-structure and active processes along the North American-Caribbean plate boundary (Dominican Republic sector). *Marine Geology*, 407, 121–147. <https://doi.org/10.1016/j.margeo.2018.10.010>
- Russo, R. M., & Villaseñor, A. (1995). The 1946 Hispaniola earthquake and the tectonics of the North America Caribbean plate boundary, northeastern Hispaniola. *Journal of Geophysical Research*, 100(B4), 6265–6280. <https://doi.org/10.1029/94jb02599>
- Ryan, W. B. F., Carbotte, S. M., Coplan, J., O'Hara, S., Melkonian, A., Arko, R., et al. (2009). Global Multi-Resolution Topography (GMRT) synthesis data set. *Geochemistry, Geophysics, Geosystems*, 10(3), Q03014. <https://doi.org/10.1029/2008GC002332>
- Saint Fleur, N., Feuillet, N., & Klinger, Y. (2019). Active tectonics along the Cul-de-Sac—Enriquillo plain and seismic hazard for Port-au-Prince, Haiti. *Tectonophysics*, 771, 228235. <https://doi.org/10.1016/j.tecto.2019.228235>

- Sak, P. B., Fisher, D. M., Gardner, T. W., Marshall, J. S., & LaFemina, P. C. (2009). Rough crust subduction, forearc kinematics, and Quaternary uplift rates, Costa Rican segment of the Middle American Trench. *Geological Society America Bulletin*, 121(7–8), 992–1012. <https://doi.org/10.1130/b26237.1>
- Schellmann, G., & Radtke, U. (2004). A revised morpho- and chronostratigraphy of the late and middle Pleistocene coral reef terraces on Southern Barbados (West Indies). *Earth-Science Reviews*, 64(3–4), 157–187. [https://doi.org/10.1016/s0012-8252\(03\)00043-6](https://doi.org/10.1016/s0012-8252(03)00043-6)
- Sinton, C. W., Duncan, R. A., Storey, M., Lewis, J., & Estrada, J. J. (1998). An oceanic flood basalt province within the Caribbean plate. *Earth and Planetary Science Letters*, 155(3–4), 221–235. [https://doi.org/10.1016/s0012-821x\(97\)00214-8](https://doi.org/10.1016/s0012-821x(97)00214-8)
- SISFRANCE-Antilles. (2009). *Sismicité historique de la France Antilles-Guyane-Mer des Caraïbes*. Bureau de Recherches Géologiques et Minières. Retrieved from <https://sisfrance.irsrn.fr/Antilles/>
- Suárez-Rodríguez, Á., Escuder-Virueite, J., & Colmenero-Hidalgo, E. (2017). La mezcla de San Marcos, Cordillera Septentrional de la República Dominicana. Significado, origen y edad. *Boletín Geológico y Minero*, 128(3), 633–656. <https://doi.org/10.21701/bolgeomin.128.3.006>
- Symithe, S., Calais, E., de Chabalière, J. B., Robertson, R., & Higgins, M. (2015). Current block motions and strain accumulation on active faults in the Caribbean. *Journal of Geophysical Research: Solid Earth*, 120(5), 3748–3774. <https://doi.org/10.1002/2014jb011779>
- Takaku, J., Tadono, T., Doutsu, M., Ohgushi, F., & Kai, H. (2020). Updates of 'AW3D30' ALOS Global Digital Surface Model with Other Open Access Datasets. *The International Archives of the Photogrammetry, Remote Sensing and Spatial Information Sciences, ISPRS, XLIII-B4–2020*, 183–189. <https://doi.org/10.5194/isprs-archives-xliii-b4-2020-183-2020>
- Tanner, J. G., & Shepherd, J. B. (1997). *Seismic hazard in Latin America and the Caribbean, Final Report. Volume I: Project Catalogue and Seismic Hazard Maps* (p. 143). Instituto Panamericano de Geografía y Historia (IPGH). Project n°89-0190. International Development Research Centre.
- Taylor, F. W., Mann, P., Bevis, M. G., Edwards, R. L., Cheng, H., Cutler, K. B., et al. (2005). Rapid forearc uplift and subsidence caused by impinging bathymetric features: Examples from the New Hebrides and Solomon arcs. *Tectonics*, 24, 6. <https://doi.org/10.1029/2004tc001650>
- ten Brink, U. S., Bakun, W. H., & Flores, C. H. (2011). Historical perspective on seismic hazard to Hispaniola and the northeast Caribbean region. *Journal of Geophysical Research*, 116(B12), b12318. <https://doi.org/10.1029/2011jb008497>
- Terrier-Sedan, M., & Bertil, D. (2021). Active fault characterization and seismotectonic zoning of the Hispaniola island. *Journal of Seismology*, 25(2), 499–520. <https://doi.org/10.1007/s10950-021-09985-0>
- Tozer, B., Sandwell, D. T., Smith, W. H. F., Olson, C., Beale, J. R., & Wessel, P. (2019). Global bathymetry and topography at 15 Arc Sec: SRTM15+. *Earth and Space Science*, 6(10), 1847–1864. <https://doi.org/10.1029/2019EA000658>
- Twiss, R. J., & Unruh, J. R. (1998). Analysis of fault slip inversions: Do they constrain stress or strain rate? *Journal of Geophysical Research*, 103(6), 12205–12222. <https://doi.org/10.1029/98jb00612>
- Vannucchi, P., Sak, P. B., Morgan, J. P., Ohkushi, K., & Ujiie, K. (2013). Rapid pulses of uplift, subsidence, and subduction erosion offshore Central America: Implications for building the rock record of convergent margins. *Geology*, 41(9), 995–998. <https://doi.org/10.1130/g34355.1>
- Vespucchi, R. M. (1988). *Petrology and Geochemistry of Late Cenozoic Volcanic Rocks of the Dominican Republic* (PhD thesis) (p. 378). George Washington University.
- Wang, J., Mann, P., & Stewart, R. R. (2018). Late Holocene structural style and seismicity of highly transpressional faults in southern Haiti. *Tectonics*, 37(10), 3834–3852. <https://doi.org/10.1029/2017TC004920>
- Wells, D. L., & Coppersmith, K. J. (1994). New empirical relationships among magnitude, rupture length, rupture width, rupture area, and surface displacement. *Bulletin of the Seismological Society of America*, 84(4), 974–1002. <https://doi.org/10.1785/bssa0840040974>
- Witschard, M., & Dolan, J. F. (1990). Contrasting structural styles in siliciclastic and carbonate rocks of an offscraped sequence: The Peralta accretionary prism, Hispaniola. *Geological Society of America Bulletin*, 102(6), 792–806. [https://doi.org/10.1130/0016-7606\(1990\)102<0792:cssisa>2.3.co;2](https://doi.org/10.1130/0016-7606(1990)102<0792:cssisa>2.3.co;2)

References From the Supporting Information

- André, A. S., Sausse, J., & Lespinasse, M. (2001). New approach for the quantification of paleostress magnitudes: Application to the Soultz vein system (Rhine graben, France). *Tectonophysics*, 336(1–4), 215–231. [https://doi.org/10.1016/s0040-1951\(01\)00103-2](https://doi.org/10.1016/s0040-1951(01)00103-2)
- Angelier, J., & Goguel, J. (1979). Sur une method simple de determination des axes princepaux des contraintes pour une population de failles. *Comptes Rendus Hebdomadaires des Seances de l'Academie des Sciences, Serie D: Sciences Naturelles*, 288(3), 307–310.
- Angelier, J., & Mechler, P. (1977). Sur une méthode graphique de recherche des contraintes principales également utilisable en tectonique et en séismologie: La méthode des dièdres driots. *Bulletin de la Société Géologique de France*, 7(6), 1309–1318. <https://doi.org/10.2113/gssgfbull.s7-xix.6.1309>
- Bott, M. H. P. (1959). The mechanics of oblique slip faulting. *Geological Magazine*, 96(2), 109–117. <https://doi.org/10.1017/s0016756800059987>
- Montaggioni, L. F., & Braithwaite, C. J. R. (2009). *Quaternary coral reef systems: History, development processes and controlling Factors* (Vol. 5, p. 532). Elsevier.
- Muhs, D. R., Pandolfi, J. M., Simmons, K. R., & Schumann, R. R. (2012). Sea-level history of past interglacial periods from uranium-series dating of corals, Curaçao, Leeward Antilles islands. *Quaternary Research*, 78(2), 157–169. <https://doi.org/10.1016/j.yqres.2012.05.008>
- Sperner, B., & Zweigel, P. (2010). A plea for more caution in fault-slip analysis. *Tectonophysics*, 482(1–4), 29–41. <https://doi.org/10.1016/j.tecto.2009.07.019>
- Turner, F. J. (1953). Nature and dynamic interpretation of deformation lamellae in calcite of three marbles. *American Journal of Science*, 251(4), 276–298. <https://doi.org/10.2475/ajs.251.4.276>
- Woodroffe, C. D., & Webster, J. M. (2014). Coral reefs and sea-level change. *Marine Geology*, 352, 248–267. <https://doi.org/10.1016/j.margeo.2013.12.006>